



NTNU – Trondheim
Norwegian University of
Science and Technology

Multifunctional Gold nanoparticles for targeted drug delivery

Elena Moran-Rico

Master of Chemical Engineering

Submission date: March 2012

Supervisor: Wilhelm Robert Glomm, IKP

Norwegian University of Science and Technology
Department of Chemical Engineering



NTNU
Norwegian University of
Science and Technology

Multifunctional Gold nanoparticles for targeted drug delivery

Elena Morán Rico

Master Thesis

Submission date: 25th March 2012

Supervisor: Wilhelm R. Glomm

Co-supervisor: Sondre Volden, Sina M. Lystvet, and Sabina Strand

Norwegian University of Science and Technology

Preface

This thesis was carried out at the Department of Chemical Engineering at the Norwegian University of Science and Technology (NTNU) during the period from September 2011 to March 2012.

I wish to express my gratitude to my supervisor Professor Wilhelm Glomm for his invaluable motivation, assistance, and continuous guidance. This thesis gave me the opportunity of entry in a interesting field totally unknown for me.

I would also give special thanks to Dr. Sondre Volden and PhD. Sina Maria Lystvet for their suggestions and continuous support I cannot imagine this work finished without them. I cannot forget to be grateful to her for making sweet meetings.

I would like to thank Dr. Sabina Strand for providing chitosan and siRNA samples and her disposition to answer any question about them. Gratitude is also given to Dr. Gurvinder Singh for proving magnetic gold nanoparticles.

Special thanks for all friends meet in Trondheim because they are awesome. Not only they have support me the whole period of thesis research and writing but also they make me feel like at home.

I cannot forget my university friends because I am grateful for known they have been my family in Valencia. Especially thanks for Ivan for being something complicated for me, and Mimi because I cannot conceive the end of my studies without my UPV twin.

I am grateful for the moral support to my friends always ready to cheer me up. Especially to Avi because of all moments lived in Albocàsser in my student period.

Finally but the most important, I would also thanks to my family, and overall for my parents and my sister because everything of this is possible thanks to them and their unconditional support.

Trondheim, March 25th

Elena Morán Rico

Abstract

The combination of nanoparticles with pharmaceutically compounds such as small drug molecules, peptides, enzymes, and antibodies, allows the promising development of delivery vectors with superior performance and selectivity. Metal nanoparticles, specifically gold nanoparticles (AuNP), have emerged recently as a suitable material in diverse applications due to their exceptional properties associated with the nanometric scale.

The main aim of this thesis was the synthesis of a new selective drug delivery vector based on the properties of gold nanoparticles. Specifically, the objective of this nanocarrier was the siRNA delivery with the objective to trigger the gene-silencing of the gene therapy. The design of this nanoparticles was established as a gold nanoparticle core covered with chitosan, a biocompatible cationic polysaccharide able to be bound to the gold nanoparticle (AuNP) by charge reversal. Gold nanoparticles were synthesized in different ways and characterized before and after the covering with different samples with the aim of finding the type with the best relation between quickness and strength. Once the AuNP/Chitosan nanoparticles were accomplished, the siRNA covering was attempted to complete the vector. The failure in the adsorption of this siRNA into the chitosan surface was the promoter to try other options to solve this problem.

Second option was the use of hexadecyltrimethylammonium bromide ($C_{16}TAB$), a cationic surfactant, instead of the chitosan. The vector in this case was established as AuNP/ $C_{16}TAB$ /siRNA and was analysed following the same procedure. $C_{16}TAB$ was adsorbed successfully into the gold surface but the siRNA binding failed.

The last attempt in this research was to come back to the original idea of covering with chitosan to take advantage of its properties. In this case, N-(3-Dimethylaminopropyl)-N-ethylcarbodiimide hydrochloride (EDAC) was used to crosslink the chitosan to the gold surface. This study was carried out with different chitosan samples to characterize the quickness and the strength. The successful attachment allowed the study of several gold nanoparticles sizes and EDAC concentrations.

Table of contents

Introduction	1
Theory	3
2.1 Gold nanoparticles.....	3
2.1.1 Properties	4
2.1.1.1 Optical properties.....	4
2.1.1.2 Biological properties	6
2.1.1.3 Adsorption.....	7
2.1.1.4 Stability: zeta potential.....	7
2.1.2 Synthesis.....	9
2.1.2.1 Turkevich method	10
2.1.2.2 Brust method	10
2.1.2.3 Ascorbic acid reduction in a single reduction/stabilizing step	11
2.1.2.4 Sodium borohydride reduction with MUA as stabilizer	12
2.1.2.5 Perrault method	12
2.1.2.6 Martin method	13
2.1.3 Surface modifications and coatings	13
2.1.4 Applications	14
2.1.4.1 Gold nanoparticles as vector for drug delivery	14
2.1.4.2 Gold nanoparticles for labelling in biological imaging	17
2.1.4.3 Gold nanoparticles as a heat source	17
2.1.4.4 Gold nanoparticles in environmental applications	17
2.2 Chitosan.....	18
2.2.1 Source and structure of chitosan	18
2.2.2 Physicochemical and biological properties of chitosan.....	19
2.2.3 Preparation of chitosan.....	20
2.2.4 Chitosan modifications.....	20
2.2.5 Chitosan applications.....	21
2.3 siRNA	22
2.3.1 Small interfering RNA.....	22
2.3.2 RNAi gene-silencing mechanism.....	23
2.3.3 siRNA delivery	24
2.3.4 siRNAs generation and chemical modification.....	24
2.3.5 Therapeutic applications of siRNA.....	24
2.4 Instrumentation	25
2.4.1 Nano ZS 3600	25
2.4.2 Zeta potential: theoretical knowledge.....	25
2.4.3 UV-vis spectrophotometer	27
2.4.3.1 Beer-Lambert's law.....	27
2.4.3.2 UV-vis spectrophotometer components.....	28
2.4.4 Quartz Crystal Microbalance	29
2.4.4.1 Sauerbrey equation: validity for the theory in thin films.....	30
Materials and methods	31
3.1 Gold nanoparticles.....	31
3.1.1 Materials.....	31
3.1.2 Ascorbic acid reduction	31
3.1.3 Sodium borohydride reduction	31
3.2 Chitosan.....	32
3.2.1 Material.....	32
3.2.2 Chitosan solutions preparation	32

3.3 siRNA	32
3.3.1 Materials.....	32
3.3.2 siRNA solutions	32
3.4 Coatings	33
3.4.1 AuNP/Chitosan.....	33
3.4.2 AuNP/Chitosan/siRNA.....	33
3.5 Zetasizer	33
3.6 UV-vis spectrophotometer	33
3.7 Quartz Crystal Microbalance	34
Results and discussion	35
4.1 Synthesis of AuNP/Chitosan/siRNA nanoparticles	35
4.1.1 Gold nanoparticles synthesis.....	35
4.1.1.1 Gold nanoparticles obtained by ascorbic acid reduction	35
4.1.1.2 Gold nanoparticles obtained by sodium borohydride reduction and MUA stabilizing.....	39
4.1.2 Coating of gold nanoparticles with chitosan (AuNP/Chitosan nanoparticles) 41	
4.1.2.1 QCM analysis simulating chitosan coating in a gold surface covered with MUA. 42	
4.1.2.2 Synthesis of new gold nanoparticles by ascorbic acid reduction	44
4.1.2.3 QCM analysis simulating chitosan coating in a gold surface covered with ascorbic acid	47
4.1.2.4 AuNP/chitosan nanoparticles obtaining and characterization	52
4.1.2.5 Coating of AuNP/chitosan nanoparticles with siRNA (AuNP/Chitosan/siRNA nanoparticles).....	55
4.1.2.6 QCM analysis simulating the siRNA deposition into a gold surface covered with ascorbic acid and chitosan.....	55
4.1.2.7 Characterization of AuNP/chitosan /siRNA nanoparticles.....	57
4.2 Synthesis of AuNP/C₁₆TAB/siRNA nanoparticles	60
4.2.1 Theory	60
4.2.2 Material and methods.....	60
4.2.3 QCM analysis simulating the siRNA deposition into a gold surface covered with C16TAB and a final layer of chitosan	61
4.3 Synthesis of AuNP/Chitosan nanoparticles crosslinked with EDAC	62
4.3.1 Material and methods.....	63
4.3.2 QCM analysis simulating the chitosan coating crosslinked with EDAC into a gold surface covered with MUA.....	63
4.3.3 Obtaining and characterization of AuNP/chitosan crosslinked with EDAC .68	
4.3.3.1 Magnetic gold nanoparticles 7.3nm.....	68
4.3.3.2 Gold nanoparticles 40 nm	72
Conclusion	77
Future work	79
References	81

List of figures

FIGURE 1-1. SCHEME OF LAYER-BY-LAYER ASSEMBLY FOR AuNP/CHITOSAN/SIRNA NANOPARTICLES.	1
FIGURE 2-1. PHOTOGRAPHS OF AQUEOUS SOLUTIONS OF GOLD NANOSPHERES (UPPER PANELS) AND GOLD NANORODS (LOWER PANELS) AS A FUNCTION OF INCREASING DIMENSIONS. CORRESPONDING TRANSMISSION ELECTRON MICROSCOPY IMAGES OF THE NANOPARTICLES ARE SHOWN; ALL SCALE BARS = 100 NM. THE DIFFERENCE IN COLOR OF THE PARTICLE SOLUTIONS IS MORE DRAMATIC FOR RODS THAN FOR SPHERES. THIS IS DUE TO THE NATURE OF PLASMON BANDS (ONE FOR SPHERES AND TWO FOR RODS) THAT ARE MORE SENSITIVE TO SIZE FOR RODS COMPARED WITH SPHERES. FOR SPHERES, THE SIZE VARIES FROM 4 TO 40 NM (TEMs A–E), WHEREAS FOR RODS, THE ASPECT RATIO VARIES FROM 1.3 TO 5 FOR SHORT RODS (TEMs F–J) AND 20 (TEM K) FOR LONG RODS.	4
FIGURE 2-2. ORIGIN OF SURFACE PLASMON RESONANCE DUE TO COHERENT INTERACTION BETWEEN OF THE ELECTRONS IN THE CONDUCTION BAND WITH LIGHT [15].....	5
FIGURE 2-3. SURFACE PLASMON RESONANCE OF METAL NANOPARTICLES IS DEPENDENT ON THE SIZE, SHAPE AND MATERIAL. SPHERICAL AuNPs HAVE THE PLASMON RESONANCE AT 520 NM WHEREAS THE SPECIAL SHAPED AuNPs EXHIBIT PLASMON RESONANCE AT LONGER WAVELENGTH [17].	6
FIGURE 2-4. SCHEMATIC REPRESENTATION OF ZETA POTENTIAL [22].	8
FIGURE 2-5. SCHEMATIC ILLUSTRATING HUCKEL AND SMOLUCHOWSKI'S APPROXIMATIONS USED FOR THE CONVERSION OF ELECTROPHORETIC MOBILITY INTO ZETA POTENTIAL.	9
FIGURE 2-6. SCHEME OF GOLD REDUCTION BY SODIUM CITRATE [26].	10
FIGURE 2-7. SCHEME OF BRUST REACTION [30].	11
FIGURE 2-8. CHEMICAL REACTION PRODUCED IN TETRACHLOROAUIC ACID REDUCTION WITH ASCORBIC ACID. .	11
FIGURE 2-9. VARIATION OF (1) THE PARTICLE SIZE OF GOLD NANOPARTICLES MEASURED BY DYNAMIC LIGHT SCATTERING AND (B) THE POSITION OF THE PLASMON BAND RESONANCE FOR THE GOLD SOLUTIONS PREPARED BY MIXING 4×10^{-4} MOL·DM ⁻³ TETRACHLOROAUIC (III) ACID SOLUTIONS WITH 6.6×10^{-4} MOL·DM ⁻³ ISO-ASCORBIC ACID AT 25°C AND AN [I-ASC]/[Au ⁺³] RATIO OF 1.65:1 [31].	12
FIGURE 2-10. SCHEME OF PERRAULT METHOD REACTIONS FOR OBTAINING GOLD NANOPARTICLES [35].	13
FIGURE 2-11. SCHEME OF THE TWO AuNP SURFACE STRUCTURES MOST COMMONLY USED IN DELIVERY APPLICATIONS [38].	16
FIGURE 2-12. STRUCTURES OF CELLULOSE, CHITIN AND CHITOSAN [48].	19
FIGURE 2-13. SIRNA STRUCTURE [50].	22
FIGURE 2-14. CLASSICAL MECHANISM RNA INTERFERENCE (RNAi) PATHWAY [49] [52].	23
FIGURE 2-15. ELECTROPHORETIC MOBILITY MEASUREMENT SCHEME.	26
FIGURE 2-16. CONFIGURATION OF THE ZETASIZER NANO SERIES FOR ZETA POTENTIAL MEASUREMENTS	26
FIGURE 2-18. GRAPHIC PROCEDURE IN QCM MEASUREMENTS [57].	29
FIGURE 3-1. CALIBRATION CURVE FOR GOLD SAMPLES.	34
FIGURE 4-1. A) TETRACHLOROAUIC ACID 10 mM ON THE LEFT AND 1 mM ON THE RIGHT, GOLD PRECURSOR BEFORE THE REDUCTION REACTION. B) GOLD NANOPARTICLES OBTAINED WITH THE REDUCTION OF TETRACHLOROAUIC ACID WITH ASCORBIC ACID WITH RELATION 1:10.	36
FIGURE 4-2. DIAMETERS OF GOLD NANOPARTICLES ACQUIRED WITH NANOSIZER WITH THE UNCERTAINTY ASSOCIATED FOR THE EXPERIMENT CARRIED OUT WITH DIFFERENT CONCENTRATION RATIO TETRACHLOROAUIC ACID (mM): ASCORBIC ACID (mM) A) 0.1:10, B) 1:10, C) 1:25, D) 1:30, E) 1:50, F) 1:100.	37
FIGURE 4-3. ZETA POTENTIAL OBTAINED WITH NANOSIZER MEASUREMENTS WITH THE UNCERTAINTY ASSOCIATED FOR THE GOLD NANOPARTICLES SYNTHETISED BY ASCORBIC ACID REDUCTION WITH RATIO TETRACHLOROAUIC ACID (mM): ASCORBIC ACID (mM) A) 0.1:10, B) 1:10, C) 1:25, D) 1:30, E) 1:50, F) 1:100.	37
FIGURE 4-4. UV-VIS SPECTRA OF GOLD NANOPARTICLES SYNTHESIZED BY ASCORBIC ACID REDUCTION IN A DIFFERENT RATIO TETRACHLOROAUIC ACID (mM): ASCORBIC ACID (mM). A) 0.1:10, B) 1:10, C) 1:25, D) 1:30, E) 1:50, F) 1:100.	38
FIGURE 4-5. GOLD NANOPARTICLES PRECIPITATED OUT 5 MONTHS AFTER THE SYNTHESIS REALIZED WITH THE RELATIONS SHOWED FOR A) EXPERIMENTS G AND H B) EXPERIMENTS I AND J.	39
FIGURE 4-6. DIFFERENT DIAMETERS (NM) WITH THE ASSOCIATED UNCERTAINTIES ASSOCIATED FOR GOLD NANOPARTICLES OBTAINED BY SYNTHESIS WITH SODIUM BOROHYDRIDE AS REDUCER AGENT. THE RELATION TCAA (mM): NABH ₄ (mM) IN THE EXPERIMENT WAS G) 1:10, H) 1:1, I) 5:10, J) 5:1.	40

FIGURE 4-7. ZETA POTENTIAL (mV) WITH ASSOCIATED UNCERTAINTY MEASURED IN GOLD NANOPARTICLES SYNTHESIZED WITH THE RELATION TCAA (mM): NABH ₄ (mM) g)1:10, h) 1:1, i) 5:10, j)5:1.....	40
FIGURE 4-8. UV-VIS SPECTRA OF GOLD NANOPARTICLES SYNTHESIZED WITH THE RELATION TCAA (mM): NABH ₄ (mM) g)1:10, h) 1:1, i) 5:10, j)5:1.....	41
FIGURE 4-9. DATA OBTAINED FROM SIMULATING WITH QCM: AU-COATED CRYSTAL COVERED WITH MUA/CHITOSAN K1/BUFFER.....	43
FIGURE 4-10. DATA ACQUIRED WITH QCM FOR AU-COATED CRYSTAL COVERED WITH MUA/CHITOSAN K2/BUFFER.....	43
FIGURE 4-11. GOLD NANOPARTICLES OBTAINED REDUCING THE TETRACHLOROAUIC ACID WITH ASCORBIC ACID WITH THE CONCENTRATION RATIO (mM) A) 0.1:10, B) 1:10, C) 1:50 AFTER 5 MONTHS.....	45
FIGURE 4-12. DIAMETER (NM) WITH UNCERTAINTIES OF NEW GOLD NANOPARTICLES OBTAINED BY ASCORBIC ACID REDUCTION WITH DIFFERENT RATIO TCAA (mM) : ASCORBIC ACID (mM) A) 0.1:10, B) 1:10, C) 1:25, D) 1:30, E) 1:50, F) 1:100.....	45
FIGURE 4-13. ZETA POTENTIAL (mV) WITH UNCERTAINTIES OF NEW GOLD NANOPARTICLES OBTAINED BY ASCORBIC ACID REDUCTION WITH DIFFERENT RATIO TCAA(mM):ASCORBIC ACID (mM) A) 0.1:10, B) 1:10, C) 1:25, D) 1:30, E) 1:50, F) 1:100.....	46
FIGURE 4-14. UV-VIS SPECTRA OF GOLD NANOPARTICLES OBTAINED WITH ASCORBIC ACID REDUCTION. DIFFERENT RATIO EXPERIMENTS TCAA (mM): ASCORBIC ACID (mM) A) 0.1:10, B) 1:10, C) 1:25, D) 1:30, E) 1:50, F) 1:100.....	47
FIGURE 4-15. OSCILLATING FREQUENCY VARIATION OBTAINED FOR THE SIMULATION AU-COATED CRYSTAL/ASCORBIC ACID/CHITOSAN K1/BUFFER.....	48
FIGURE 4-16. QCM ANALYSIS OF OSCILLATING FREQUENCY ACQUIRED FOR THE SIMULATION AU-COATED CRYSTAL/ASCORBIC ACID/CHITOSAN K2/BUFFER.....	48
FIGURE 4-17. OSCILLATING FREQUENCY EVOLUTION OBTAINED WITH QCM FOR THE SYSTEM AU-COATED CRYSTAL/ASCORBIC ACID/CHITOSAN K3/BUFFER.....	49
FIGURE 4-18. QCM ANALYSIS OF OSCILLATING FREQUENCY IN SYSTEM SIMULATION COMPOSED BY AU-COATED CRYSTAL/ASCORBIC ACID/CHITOSAN K4/BUFFER.....	50
FIGURE 4-19. OSCILLATING FREQUENCY EVOLUTION OBTAINED BY MEANS OF THE QCM FOR THE SYSTEM AU-COATED CRYSTAL/ASCORBIC ACID/CHITOSAN K5/BUFFER.....	50
FIGURE 4-20. COMPARISON OF GOLD NANOPARTICLES DIAMETER (NM) WITH UNCERTAINTIES ASSOCIATED BEFORE AND AFTER THE COATING WITH THE CHITOSAN SAMPLES K1 AND K2. THE DATA IS COMPARED AFTER FILTERING THE COVERED PARTICLES AuNP/CHITOSAN.....	53
FIGURE 4-21. ZETA POTENTIAL (mV) WITH ASSOCIATED UNCERTAINTIES OBTAINED FROM GOLD NANOPARTICLES BEFORE AND AFTER THE ADSORPTION OF CHITOSAN SAMPLE K1 AND K2.....	54
FIGURE 4-22. UV-VIS SPECTRA OF GOLD NANOPARTICLES COVERED WITH CHITOSAN SAMPLES K1 AND K2 AND UNCOATED AuNP. THE MEASUREMENTS WERE REALIZED BEFORE AND AFTER THE NANOPARTICLES FILTERING (FILTER 0.2 μm).....	55
FIGURE 4-23. OSCILLATING FREQUENCY ACQUIRED WITH QCM FOR THE SYSTEM AU- COATED CRYSTAL/ASCORBIC ACID/CHITOSANK1/BUFFER/SiRNA/BUFFER/CHITOSANK1/BUFFER.....	56
FIGURE 4-24. QCM ANALYSIS OF FREQUENCY CHANGES OBTAINED FOR THE SIMULATION AU-COATED CRYSTAL/ASCORBIC ACID/CHITOSANK2/BUFFER/SiRNA/BUFFER/CHITOSAN K2/BUFFER.....	56
FIGURE 4-25. COMPARISON OF GOLD NANOPARTICLES DIAMETER (NM) WITH ASSOCIATED UNCERTAINTIES BEFORE THE COATING, AuNP/CHITOSAN AND AuNP/CHITOSAN/SiRNA. THE EXPERIMENTS WERE CARRIED OUT WITH K1 AND K2 CHITOSAN SAMPLES.....	58
FIGURE 4-26. COMPARISON OF GOLD NANOPARTICLES ZETA POTENTIAL (mV) VALUES WITH ASSOCIATED UNCERTAINTIES BEFORE THE COATING, AuNP/CHITOSAN AND AuNP/CHITOSAN/SiRNA. THE EXPERIMENTS WERE CARRIED OUT WITH K1 AND K2 CHITOSAN SAMPLES.....	59
FIGURE 4-27. UV-VIS SPECTRA OF GOLD NANOPARTICLES COVERED WITH CHITOSAN SAMPLES K1 AND K2 AND SiRNA.....	60
FIGURE 4-28. EVOLUTION OF OSCILLATING FREQUENCY OBTAINED IN THE AU-COATED/CITRATE/C ₁₆ TAB/BUFFER/SiRNA/BUFFER/CHITOSANK1/BUFFER/C ₁₆ TAB SYSTEM SIMULATION.....	62
FIGURE 4-29. OSCILLATING FREQUENCY DATA ACQUIRED WITH QCM FOR THE SIMULATION OF AU-COATED CRYSTAL COVERED WITH MUA/CHITOSAN K1/EDAC/BUFFER.....	64
FIGURE 4-30. DATA OBTAINED FROM QCM ABOUT OSCILLATING FREQUENCY FOR THE SYSTEM AU-COATED CRYSTAL COVERED WITH MUA/CHITOSANK2/EDAC/BUFFER.....	64
FIGURE 4-31. OSCILLATING FREQUENCY OBTAINED IN QCM FOR THE SIMULATION AU-COATED CRYSTAL COVERED WITH MUA/EDAC/CHITOSAN/BUFFER. A SECOND STEP OF EDAC IS ADDED AFTER CHITOSAN TO CHECK IF IT WOULD BE ADSORBED AGAIN.....	66

FIGURE 4-32. DATA OBTAINED WITH QCM ABOUT OSCILLATING FREQUENCY IN THE SIMULATION Au-COATED COVERED WITH MUA/EDAC/BUFFER/CHITOSANK1/BUFFER..... 67

FIGURE 4-33. DIAMETER (NM) FOR DIFFERENT NANOPARTICLES SYNTHESIZED WITH THE ASSOCIATED UNCERTAINTIES. AuNP/EDAC+CHITOSAN IS REFERRED TO SYNTHESIS PRODUCED ADDING FIRST THE EDAC TO AuNP AND AFTER THE CHITOSAN, BEFORE AND AFTER FILTERING. AuNP/CHITOSAN+EDAC ARE THE NANOPARTICLES CONJUGATED WITH A PREADSORPTION OF CHITOSAN AND THE ADDITION OF EDAC TO CROSSLINK IT AFTER, BEFORE AND AFTER FILTERING. AuNP/EDAC + FILTERED CHITOSAN IS THE LABEL FOR NANOPARTICLES WITH THE ADDITION OF CHITOSAN PREVIOUSLY FILTERED..... 69

FIGURE 4-34. ZETA POTENTIAL (mV) FOR DIFFERENT NANOPARTICLES SYNTHESIZED WITH THE ASSOCIATED UNCERTAINTIES. AuNP/EDAC+CHITOSAN IS REFERRED TO SYNTHESIS PRODUCED ADDING FIRST THE EDAC TO AuNP AND AFTER THE CHITOSAN, BEFORE AND AFTER FILTERING. AuNP/CHITOSAN+EDAC ARE THE NANOPARTICLES CONJUGATED WITH A PREADSORPTION OF CHITOSAN AND THE ADDITION OF EDAC TO CROSSLINK IT AFTER, BEFORE AND AFTER FILTERING. AuNP/EDAC + FILTERED CHITOSAN IS THE LABEL FOR NANOPARTICLES WITH THE ADDITION OF CHITOSAN PREVIOUSLY FILTERED..... 70

FIGURE 4-35. UV-VIS SPECTRA FOR DIFFERENT AuNP/CHITOSAN NANOPARTICLES CROSSLINKED WITH EDAC. AuNP/EDAC+CHITOSAN BEFORE AND AFTER FILTERING, IN AuNP/CHITOSAN+EDAC, A PREADSORPTION OF CHITOSAN WAS MADE, MEASURED BEFORE AND AFTER FILTERING. IN AuNP/EDAC+CHITOSAN FILTERED, THE CHITOSAN WAS FILTERED BEFORE USE. 71

FIGURE 4-36. DIAMETER (NM) MEASURED WITH ZETASIZER WITH THE ASSOCIATED UNCERTAINTIES FOR THE GOLD NANOPARTICLE COVERED WITH MUA AND THE SYNTHESIS AuNP COVERED WITH MUA/CHITOSANK1 CROSSLINKED WITH EDAC IN DIFFERENT CONCENTRATIONS: 0.5, 0.1, 0.05, AND 0.01 MG/ML..... 73

FIGURE 4-37. COMPARISON OF ZETA POTENTIAL (mV) MEASURED WITH ZETASIZER WITH THE ASSOCIATED UNCERTAINTIES FOR AuNP COVERED WITH MUA AND FOR THE AuNP COVERED WITH MUA/CHITOSANK1 CROSSLINKED WITH EDAC IN DIFFERENT CONCENTRATIONS; 0.5, 0.1, 0.05, AND 0.01 MG/ML. 74

FIGURE 4-38. UV-VIS SPECTRA FOR AuNP/CHITOSAN NANOPARTICLES PREPARED BY CROSSLINKING WITH EDAC IN DIFFERENT CONCENTRATIONS: 0.5, 0.1, 0.05, AND 0.01 MG/ML 75

List of tables

TABLE 2-1. RELATIONSHIP BETWEEN STRUCTURAL PARAMETERS AND PROPERTIES [46].	20
TABLE 2-2. IMPORTANT EXAMPLES OF MODIFIED CHITOSAN	21
TABLE 3-1. CHITOSAN SAMPLES PROPERTIES. FA: DEGREE OF ACETYLATION. DPN: POLYMERIZATION DEGREE. AAM IS A TRISACHARIDE FORMED BY GLCNAC AND ANHYDROMANNOSE. SB IS A BRANCHED STRUCTURE VIA SCHIFF BASES.	32
TABLE 3-2. ABSORBANCE OBTAINED FOR DETERMINATED GOLD SAMPLES CONCENTRATION.	34
TABLE 4-1. RELATION OF TETRACHLOROAUIC ACID AND ASCORBIC ACID FOR DIFFERENT EXPERIMENTS IN GOLD NANOPARTICLES SYNTHESIS WITH ASCORBIC ACID REDUCTION.	36
TABLE 4-2. CHARACTERISATION WITH UV-VIS SPECTROPHOTOMETER. CONCENTRATION CALCULATED WITH ABSORBANCE AND WAVELENGTH OF THE PEAK OF PLASMON RESONANCE.	38
TABLE 4-3. CONCENTRATION OF CHEMICAL REACTANTS FOR DIFFERENT EXPERIMENTS IN GOLD NANOPARTICLES SYNTHESIS WITH SODIUM BOROHYDRIDE REDUCTION AND MUA STABILIZATION.	39
TABLE 4-4. CONCENTRATION CALCULATED FOR THE GOLD NANOPARTICLES SYNTHESIZED IN TCAA(MM): NABH ₄ (MM) G)1:10, H) 1:1, I) 5:10, J)5:1.	41
TABLE 4-5. QUART CRYSTAL MICROBALANCE DATA FOR K1, K2 CHITOSAN SAMPLES ACQUIRED THE THIRD HARMONIC, N=3. THE ΔT (MIN) IS THE TIME FROM THE BEGINNING OF FREQUENCY CHANGES TO THE STABILISATION OF THE FREQUENCY AFTER THE CHANGE, ΔF (Hz) IS THE CHANGE IN CRYSTAL OSCILLATING FREQUENCY AND ΔM (NG/CM ²) IS THE MASS ADSORBED CALCULATE.	43
TABLE 4-6. RELATION OF TETRACHLOROAUIC ACID AND ASCORBIC ACID IN DIFFERENT EXPERIMENTS FOR THE SYNTHESIS OF GOLD NANOPARTICLES.	44
TABLE 4-7. CHARACTERISATION WITH UV-VIS SPECTROPHOTOMETER. CONCENTRATION CALCULATED WITH ABSORBANCE AND WAVELENGTH OF THE PEAK PLASMON RESONANCE. EXPERIMENTS IN RATIO TCAA(MM):ASCORBIC ACID (MM) A) 0.1:10, B) 1:10, C) 1:25, D) 1:30, E) 1:50, F) 1:100.	46
TABLE 4-8. QUART CRYSTAL MICROBALANCE DATA FOR K1, K2, K3, K4 AND K5 CHITOSAN SAMPLES. THE ΔT (MIN) IS THE TIME FROM THE BEGINNING OF FREQUENCY CHANGES TO THE STABILISATION OF THE FREQUENCY AFTER THE CHANGE, ΔF (Hz) IS THE CHANGE IN CRYSTAL OSCILLATING FREQUENCY AND ΔM (NG/CM ²) IS THE MASS ADSORBED CALCULATE.	51
TABLE 4-9. COMPARISON WITH RESULTS OBTAINED WITH QCM INSTRUMENT FOR MUA OR ASCORBIC ACID WITH K1 AND K2 CHITOSAN SAMPLES.	51
TABLE 4-10. SURFACE AVAILABLE FOR COVERING IN GOLD NANOPARTICLES. MINIMUM CHITOSAN K1 AND K2 CONCENTRATION NECESSARY FOR NANOPARTICLES COVERING. K1 AND K2 CHITOSAN CONCENTRATION CHOSEN CONSIDERING THE SPHERICAL SHAPE.	52
TABLE 4-11. RESULTS OBTAINED FOR THE THICKNESS OF THE LAYER (NM) WITH THE UNCERTAINTIES ASSOCIATED TO CHITOSAN SAMPLES K1 AND K2.	53
TABLE 4-12. CHARACTERISATION WITH UV-VIS SPECTROPHOTOMETER. CONCENTRATION CALCULATED WITH ABSORBANCE AND WAVELENGTH OF THE PEAK PLASMON RESONANCE. THE DATA WAS OBTAINED FOR AUNP/CHITOSAN BEFORE AND AFTER THE FILTERING WITH 0.2μm FILTER AND FOR BOTH CHITOSAN SAMPLES, K1 AND K2.	54
TABLE 4-13. QUART CRYSTAL MICROBALANCE DATA FOR K1 AND K2 CHITOSAN SAMPLES IN THE REPRODUCE OF THE COATING AUNP/CHITOSAN/SIRNA. THE ΔT (MIN) IS THE TIME FROM THE BEGINNING OF FREQUENCY CHANGES TO THE STABILISATION OF THE FREQUENCY AFTER THE CHANGE, ΔF (Hz) IS THE CHANGE IN CRYSTAL OSCILLATING FREQUENCY AND ΔM (NG/CM ²) IS THE MASS ADSORBED CALCULATE.	57
TABLE 4-14. RESULTS OBTAINED FOR THE THICKNESS OF THE LAYER (NM) WITH THE UNCERTAINTIES ASSOCIATED TO AUNP/CHITOSAN SAMPLES K1 AND K2 AND AUNP/CHITOSAN/SIRNA.	58
TABLE 4-15. CHARACTERISATION OF AUNP/CHITOSAN/SIRNA NANOPARTICLES WITH UV-VIS SPECTROPHOTOMETER. CONCENTRATION CALCULATED WITH ABSORBANCE AND WAVELENGTH OF THE PEAK PLASMON RESONANCE. DATA OBTAINED FOR BOTH CHITOSAN SAMPLES, K1 AND K2.	59
TABLE 4-16. QUART CRYSTAL MICROBALANCE DATA FOR K1 CHITOSAN SAMPLES IN THE REPRODUCE OF THE COATING AUNP/C ₁₆ TAB/SIRNA/CHITOSAN. THE ΔT (MIN) IS THE TIME FROM THE BEGINNING OF FREQUENCY CHANGES TO THE STABILISATION OF THE FREQUENCY AFTER THE CHANGE, ΔF (Hz) IS THE CHANGE IN CRYSTAL OSCILLATING FREQUENCY AND ΔM (NG/CM ²) IS THE MASS ADSORBED CALCULATE. ...	62
TABLE 4-17. QUART CRYSTAL MICROBALANCE DATA FOR K1 AND K2 CHITOSAN SAMPLES IN THE REPRODUCE OF THE COATING AUNP/CHITOSAN CROSSLINKED WITH EDAC. THE ΔT (MIN) IS THE TIME FROM THE	

BEGINNING OF FREQUENCY CHANGES TO THE STABILISATION OF THE FREQUENCY AFTER THE CHANGE, ΔF (Hz) IS THE CHANGE IN CRYSTAL OSCILLATING FREQUENCY AND ΔM (NG/CM ²) IS THE MASS ADSORBED CALCULATE.	65
TABLE 4-18. QUART CRYSTAL MICROBALANCE DATA FOR K1 CHITOSAN SAMPLE IN THE REPRODUCE OF THE COATING AuNP/CHITOSAN CROSSLINKED WITH EDAC CONSIDERING THE PROCEDURE ADDING FIRST EDAC. THE ΔT (MIN) IS THE TIME FROM THE BEGINNING OF FREQUENCY CHANGES TO THE STABILISATION OF THE FREQUENCY AFTER THE CHANGE, ΔF (Hz) IS THE CHANGE IN CRYSTAL OSCILLATING FREQUENCY AND ΔM (NG/CM ²) IS THE MASS ADSORBED CALCULATE.	66
TABLE 4-19. QUART CRYSTAL MICROBALANCE DATA FOR K1 CHITOSAN SAMPLE IN THE REPRODUCE OF THE COATING AuNP/CHITOSAN CROSSLINKED WITH EDAC CONSIDERING THE PROCEDURE ADDING FIRST EDAC AND BUFFER BETWEEN COMPOUNDS. THE ΔT (MIN) IS THE TIME FROM THE BEGINNING OF FREQUENCY CHANGES TO THE STABILISATION OF THE FREQUENCY AFTER THE CHANGE, ΔF (Hz) IS THE CHANGE IN CRYSTAL OSCILLATING FREQUENCY AND ΔM (NG/CM ²) IS THE MASS ADSORBED CALCULATE.	67
TABLE 4-20. CHARACTERISATION WITH UV-VIS SPECTROPHOTOMETER FOR AuNP/CHITOSAN CROSSLINKED WITH EDAC. CONCENTRATION CALCULATED WITH ABSORBANCE AND WAVELENGTH OF THE PEAK PLASMON RESONANCE. AuNP/EDAC+CHITOSAN BEFORE AND AFTER THE FILTERING WITH 0.2 μ M FILTER. AuNP/CHITOSAN+EDAC, THE ADDITION OF CHITOSAN WAS MADE FIRST FOR PREADSORBING, MEASURED BEFORE AND AFTER THE FILTERING WITH 0.2 μ M FILTER. AuNP/EDAC+FILTERED CHITOSAN, THE CHITOSAN WAS FILTERED BEFORE THE REACTION.	71
TABLE 4-21. EXPERIMENTS CARRIED OUT FOR THE DISPLACEMENT OF ASCORBIC ACID OR CITRATE WITH MUA. THE VOLUME RATIO IS REFERRED IN ML.	72
TABLE 4-22. DATA OF ABSORBANCE OBTAINED WITH UV-VIS SPECTROPHOTOMETER, CALCULATIONS OF CONCENTRATION AND PLASMON RESONANCE PEAK WAVELENGTH (NM).	74

List of abbreviations

<i>AuNP</i>	Gold nanoparticles
<i>C₁₆TAB</i>	Hexadecyltrimethylammonium bromide
<i>DD</i>	Deacetylation degree
<i>DNA</i>	Deoxyribonucleic acid
<i>DP_n</i>	Polymerization degree
<i>dsRNA</i>	double-stranded ribonucleic acid
<i>EDAC</i>	N-(3-Dimethylaminopropyl)-N-ethylcarbodiimide hydrochloride
<i>FA</i>	Acetylation degree
<i>LDV</i>	Laser Doppler Velocimetry
<i>LSPR</i>	Localized surface plasmon resonance
<i>miRNA</i>	micro ribonucleic acid
<i>mRNA</i>	messenger ribonucleic acid
<i>MUA</i>	11-mercaptoundecanoic acid
<i>PEI</i>	Polyethyleneimine
<i>PEG</i>	Polyethylene glycol
<i>PNIPAAm</i>	Poly(N-isopropylacrylamide)
<i>QCM</i>	Quartz Crystal Microbalance
<i>RNA</i>	Ribonucleic acid
<i>siRNA</i>	small interfering ribonucleic acid
<i>TCAA</i>	Tetrachloroauric acid
<i>TEM</i>	Transmission electron microscopy
<i>TOABr</i>	Tetraoctylammonium
<i>UV-vis</i>	Ultraviolet-visible

Chapter 1

Introduction

Gold nanoparticles are constituted for only several atoms or molecules due to their nanometric size. According to this, their optical, magnetic, electronic, physical, and chemical properties are different from the properties natural in bulk [1]. Recently, these characteristics have been investigated and gold nanoparticles have become in an excellent material for different applications in several fields, from environmental to biomedical [2].

Small interfering RNA (siRNA) is a short (21-25 nt long) dsRNA strands with 2 nt overhangs at the 3'-end [3]. This type of RNA is responsible to trigger the RNA interference, a potent highly specific gene-silencing mechanism [4]. The technique of siRNA delivery is possible to knockdown the expression of target gene involved in various human diseases, such as cancer or viral infections. Delivery by means of vectors has been developed last years because of the several advantages over the delivery of individual nucleic acids such as the continuous expression of siRNA [5]. Gold nanoparticles have emerged as a possible nanocarriers due to the fact that present suitable characteristics; is an inert non-toxic material, ease synthesis, and the possibility of size, shape and surface tuning. Nevertheless, some investigations reported the possibility of aggregations after the siRNA assembly to gold nanoparticles. New investigations are focused in the layer-by-layer assembly of this RNA through the deposition of oppositely charged polyelectrolytes, for example polyethyleneimine or chitosan (Figure 1-1) [6].

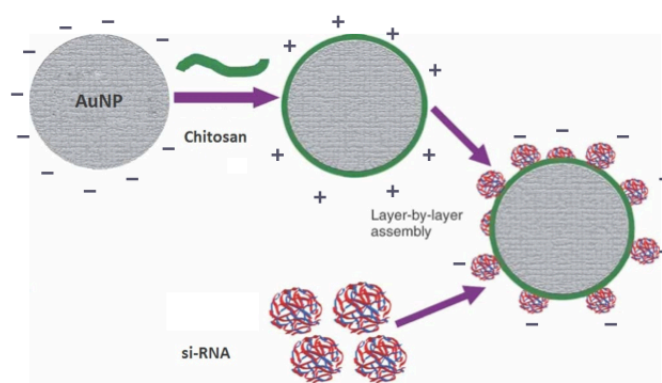


Figure 1-1. Scheme of layer-by-layer assembly for AuNP/Chitosan/siRNA nanoparticles.

Chitosan is a cationic biopolymer derived from the deacetylation of chitin, a polysaccharide constituent of exoskeleton in animals. This material presents unique properties for several applications; such as biocompatibility, biodegradability and its products are non-toxic, non-immunogenic, and non-carcinogenic [7]. The presence of reactive functional groups offers the opportunity for chemical modification and adaptation of this material for the different purposes [8]. Drug delivery, tissue

engineering, wound-healing, gene therapy, bioimaging, and green chemistry are some of the fields where the chitosan use has been exploited.

The main goal of this work was to investigate the new possibility of designing a new delivery vector for siRNA using gold nanoparticles. This vector is based on layer-by-layer strategy to assemble the siRNA to gold nanoparticles by means of the charge reversal coating with chitosan. The successful assembly gold nanoparticle/Chitosan/siRNA vector would mean an excellent change in drug delivery because of the biocompatibility of the components and the exceptional ability of siRNA to initiate the phenomenon of gene-silencing.

Chapter 2

Theory

2.1 Gold nanoparticles

The study of atoms and molecules is the conventional field of chemistry as was studied in the late 19th and 20th centuries. An atom measures around 1 ångstrom and a nanometer (nm), 10^{-9} meters; represent a group of a few atoms or molecules. Properties of bulk substances of micrometer sizes or larger have been widely studied for years by solid-state physic. Materials with 1-100 nm scale were not studies before but recently they have gained interest because of the properties of the material become dependent of the size and shape in this size scale [9].

Noble metal nanoparticles, and more specifically gold nanoparticles (AuNPs), exploit their exceptional chemical and physical properties and present several advantages. Nanoparticles are obtained by a straightforward synthesis and they can be formed in different size ranges with narrow size distribution from 1nm to 150nm. Hence, these nanoparticles can be functionalized with various linkages (antibodies, polymers, genetic material, diagnostic probes, drugs, etc.) and the surface is easily modifiable. High biocompatibility with cells or tissues made them a suitable material [10] [2].

The overall nature of a colloidal system depends of a number of factors: particle size and shape, surface properties, particle-solvent interactions, particle-particle interactions, and the optical properties of the particle-solvent system [11]. Gold solutions are characterized by an attractive color, which can vary from ruby red through purple to blue. This colour is caused by uniformly dispersed colloid gold and it is strongly dependent of size and shape [12] due to the optical properties (Figure 2-1).

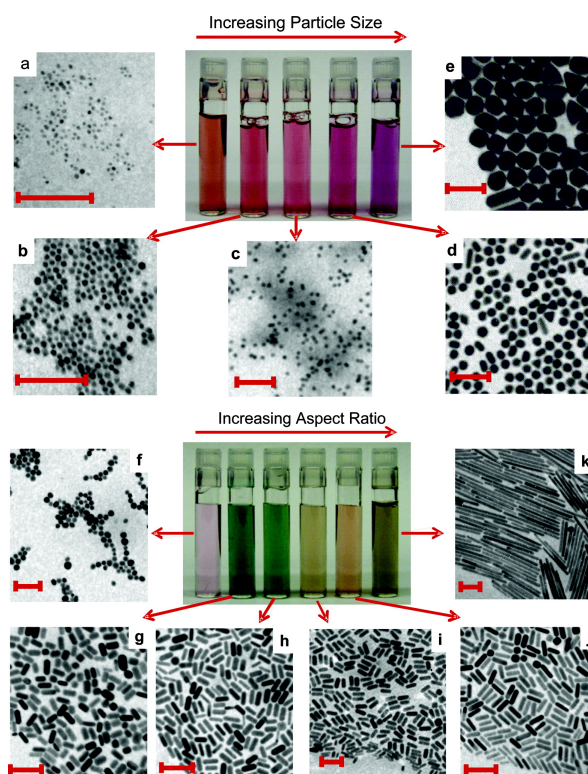


Figure 2-1. Photographs of aqueous solutions of gold nanospheres (upper panels) and gold nanorods (lower panels) as a function of increasing dimensions. Corresponding transmission electron microscopy images of the nanoparticles are shown; all scale bars = 100 nm. The difference in color of the particle solutions is more dramatic for rods than for spheres. This is due to the nature of plasmon bands (one for spheres and two for rods) that are more sensitive to size for rods compared with spheres. For spheres, the size varies from 4 to 40 nm (TEMs a–e), whereas for rods, the aspect ratio varies from 1.3 to 5 for short rods (TEMs f–j) and 20 (TEM k) for long rods.

2.1.1 Properties

2.1.1.1 Optical properties

Nanoparticles with dimensions significantly smaller than the wavelength of the incident light are characterized with intense, broad absorption band in the visible range of the spectrum. The intense red color of aqueous dispersion of colloidal gold nanoparticles is a manifestation of localized plasmon resonance. The incidence of white light on the gold nanoparticles shows this color because they absorb blue and yellow color preferably.

Nowadays, the development of colloidal gold for biological labels, markers and stains for various microscopies have increased. Recently, metallic nanoparticles have been used as a molecular-recognition elements and amplifiers sensors and biosensors.

The concept of a molecular LSP-based sensor is simply. The surface plasmon resonance is very sensitive to the presence of adsorbed molecules in the surface due to the strong confinement of charge density oscillations in this part. According to this property, these sensors have gained a high interest in chemistry and biology because of the information they can give about what is happening near of them (e.g., the evolution of

various chemical reactions in the surface). These plasmons are the one localized in metallic particles.

Every metallic surface (flat, spherical, cylindrical or another shape) has a localized surface plasmon and it appears at certain wavelength depending on the metal type, particle size distribution and shape, as well as to the environment which surround it. At this wavelength, the electromagnetic field is localized around the metal surface. When incident light has the same wavelength that localized plasmons, the electron density in the particle is polarized to one surface and oscillates in resonance with the frequency of the light causing a standing oscillation (Figure 2-2) [13] [14] [9].

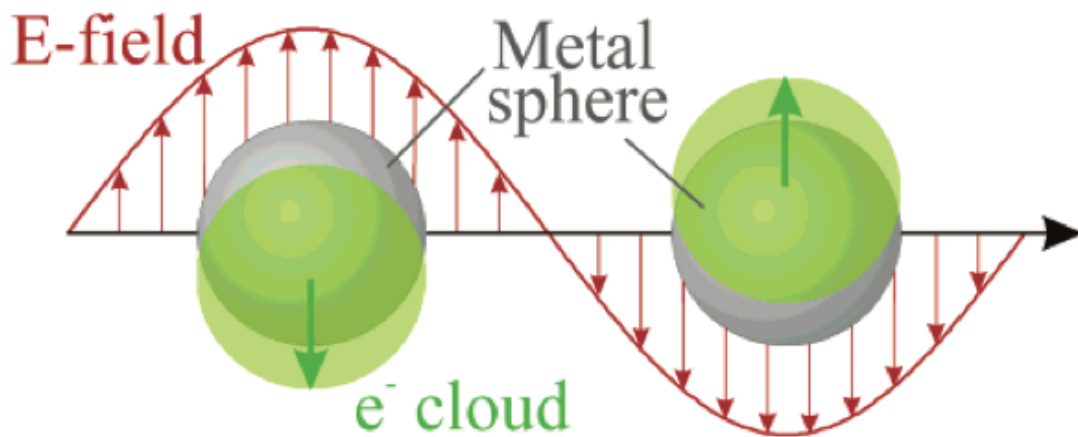


Figure 2-2. Origin of surface plasmon resonance due to coherent interaction between of the electrons in the conduction band with light [15].

Mie originally solved the Maxwell's equations for small spheres interacting with an electromagnetic field for calculating the surface plasmon resonance. The classical Mie theory is versatile, simple, and assumes that the particle and the surrounding medium are homogeneous and can be described by bulk optical dielectric functions. For nanoparticles which are significantly smaller than the wavelength of the exciting light ($\lambda \gg 2R$), Mie's theory is reduced to:

$$\sigma_{ext}(\omega) = 9 \frac{\omega}{c} \varepsilon_{3/2} V_0 \frac{\varepsilon_2(\omega)}{[\varepsilon_1(\omega) + 2\varepsilon_m]^2 + \varepsilon_2(\omega)^2}$$

where $V_0 = (4\pi/3)R^3$, ω is the angular frequency, ε_m is the dielectric function of the medium surrounding (or embedding), and ε_1 and ε_2 are the real and imaginary part of the dielectric function of the metallic nanoparticles, respectively. The surface plasmon appears when $\varepsilon_1(\omega) \approx -2\varepsilon_m$ if $\varepsilon_2(\omega)$ is small or only weakly dependent on ω [14].

UV-vis spectroscopy is a very useful technique to analyse the surface plasmon resonance due to the fact that the extinction spectrum generated allows estimating some parameters. This spectrum depends on the size, shape, and aggregation level of gold nanoparticles (Figure 2-3) and can be analysed by Mie theory with the appropriate corrections of the metal dielectric constant for the medium. The higher LSPR value, the larger the particle diameter. However, this is only an approximation because of the

position of the plasmon resonance is affected by different factors like environment dielectric properties, physical or chemical interactions on the surface, charge, interparticles distance and aggregations [16].

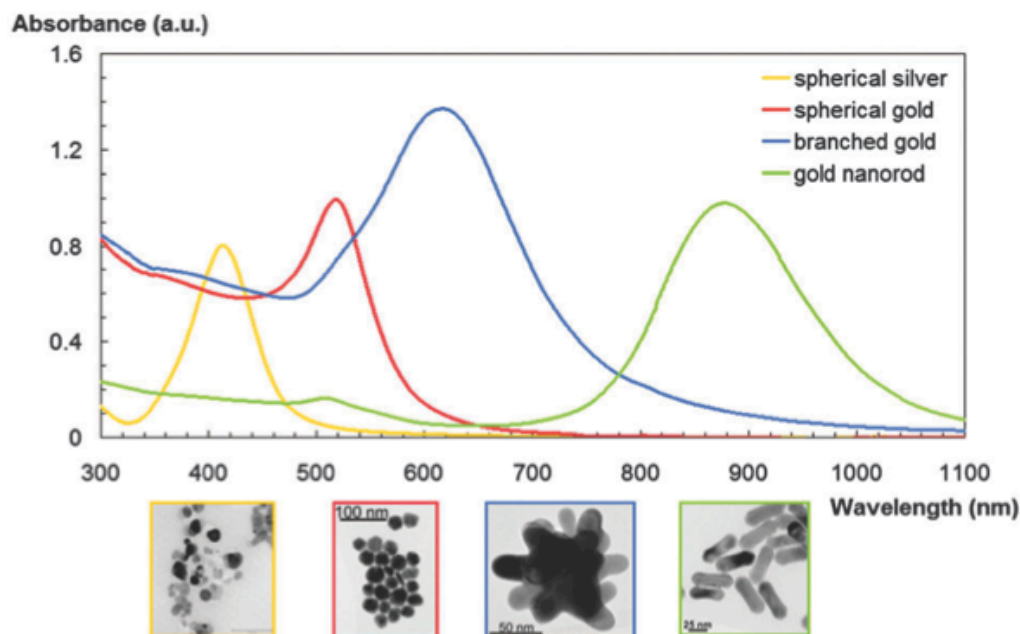


Figure 2-3. Surface plasmon resonance of metal nanoparticles is dependent on the size, shape and material. Spherical AuNPs have the plasmon resonance at 520 nm whereas the special shaped AuNPs exhibit plasmon resonance at longer wavelength [17].

2.1.1.2 Biological properties

Gold nanoparticles have several applications but recently is emerging a special interest in biomedical applications. Hence, biological properties are considered very significant due to the possible final destination of all these studies, the *in vivo* application.

The earliest application of gold as a beneficial agent was traced back in 2500 BC in China, where a mixture with gold was used to treat diseases. Nowadays, red colloidal gold is still used in India in the form of Ayurvedic medicine for rejuvenation and revitalization during old age under the name of Swarna Bhasma. Gold also has a long history of use in the western world as nervine, a substance that could revitalize people suffering from nervous conditions. In the beginning of 16th century, gold was recommended in the treatment of epilepsy, and in the beginning of 19th it was used for the treatment of syphilis. Nevertheless, the beginning of modern medicinal gold as a therapy was introduced in 1920s with the discovery of the bacteriostatic effect of gold cyanide towards the tubercle bacillus. Biocompatibility of gold nanoparticles has been verified by several tests *in vitro* and *in vivo* and use throughout the history of the civilization [18].

2.1.1.3 Adsorption

Adsorption process can be promoted by several causes, chemical (chemisorption) or physical (physisorption) or a combination of both. Physical adsorption is fragile and reversible in the most of the cases and Van der Waal and electrostatic forces cause it principally. This type of adsorption decreases with the increasing of temperature. On the other hand, chemical adsorption is strong and irreversible and limited to the monolayer formation, and increases with the increase of the temperature. The adsorption density can be calculated mathematically:

$$\Gamma_i = 2rC \cdot \exp\left(\frac{-\Delta G_{ads}^0}{RT}\right)$$

where Γ_i is the adsorption density, r is the effective radius of the adsorbed ions, C the concentration of adsorbate, R gases constant, T the temperature and $-\Delta G_{ads}^0$ is the standard free energy of adsorption. Nevertheless, the adsorption in practice is calculated as the depletion of adsorbate from the solution:

$$\Gamma_i = (C_f - C_i) \frac{V}{W}$$

where C_f, C_i are referred to final and initial concentration respectively, V is the volume of the solution and W the mass of adsorbent.

Adsorption is affected by various factors; nature of the surface and the solvent considering the are available and the possible interactions between solvent with solute/surface, chemical structure of the solute and its interactions with the solvent, nature of the interactions between the surface and the adsorbed solute, and temperature, capable of altering the properties of solute, surface, and solvent [19].

2.1.1.4 Stability: zeta potential

Any particle in suspension exhibits a physical property called zeta potential. The knowledge of this property can optimize the production of trial formulations reducing the time needed and it is a predictor of long-term stability.

Matter has three fundamental states: solid, liquid and gas. If one of these three states is finely dispersed in another then we have a colloidal system [20]. This system will be stable when the particles resist flocculation or aggregation and exhibits a long shelf-life [21]

In certain circumstances, the particles in suspension can adhere to one another and form aggregates of successively increasing size. The initial aggregate is called floc and the process of its formation flocculation. An aggregate usually can be separated by sedimentation if it is more dense than the medium or by creaming if it less dense than the medium.

If the aggregate changes to a much denser form, it is said to undergo coagulation. This term and flocculation have been often been used interchangeably. Usually coagulation is irreversible whereas the process of deflocculation can reverse flocculation.

Zeta potential and Electrical double layer

The development of a net charge at the particle surface affects the distribution of ions in the surrounding interfacial region, resulting an increased concentration of counter ions (ions opposite charged to that of the particle) closet to the surface. Thus an electrical double layer exists around each particle.

Surrounding the particle there is a liquid layer that exists as two parts; an inner region called Stern layer and an outer region known as diffuse. In the stern layer the ions are strongly bounded and in the diffuse the particles are less firmly associated. Within the diffuse layer there is a notional boundary inside which the ions and particles form a stable entity. When a particle moves, under Brownian motion for example, ions within the boundary move it, but any ions beyond the boundary do not travel with the particle. This boundary is called the surface of hydrodynamic shear or slipping plane (Figure 2-4).

The potential that exists at this boundary is known as the Zeta potential [22].

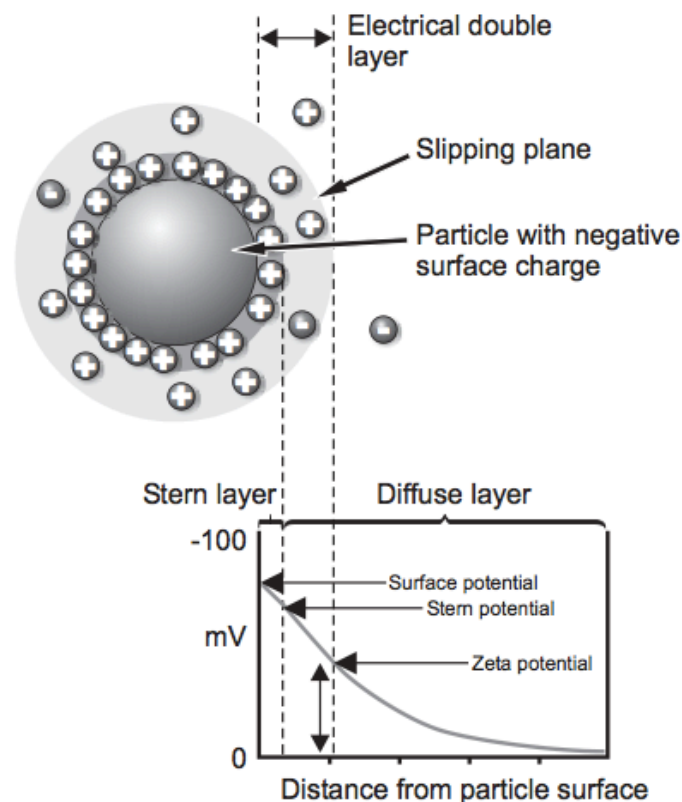


Figure 2-4. Schemating representation of zeta potential [22].

Zeta potential gives an approximation about the stability of the potential stability of the colloidal system. If all the particles have a large negative or positive zeta potential then they will tend to repeal each other and there will be no tendency for the particles to come together. However, if the particles have a low value of zeta potential they tend to come together and precipitate because there are not forces to prevent it. Conventionally, particles with zeta potentials more positive than +30mV or more negative -30mV are normally considered stable.

A zeta potential value on its own without defining the solution conditions is a virtually meaningless number. The most important properties affecting the zeta potential are: pH, conductivity and concentration

The Zeta potential can be obtained with the Henry equation:

$$U_E = \frac{2\varepsilon z f(\kappa a)}{3\eta}$$

where z is the Zeta potential, U_E the electrophoretic mobility, ε the dielectric constant, η the viscosity, and $f(\kappa a)$ the Henry's function. κ is termed Debye length and the units are reciprocal length and κ^{-1} is often taken as a measure of thickness of the electrical double layer. The parameter a refers to the radius of the particle; consequently κa measures the ratio of the particle radius to electrical double layer.

In the approximation of function, two values are commonly used for $f(\kappa a)$: 1.5 or 1.0. The most common electrophoretic determination of zeta potential is made in aqueous media. In this case, the value of $f(\kappa a)$ is 1.5 and is referred to as the Smoluchowski approximation. In the case of small particles in low dielectric constant media the value of $f(\kappa a)$ is 1.0 and this is related with the Huckel approximation (Figure 2-5).

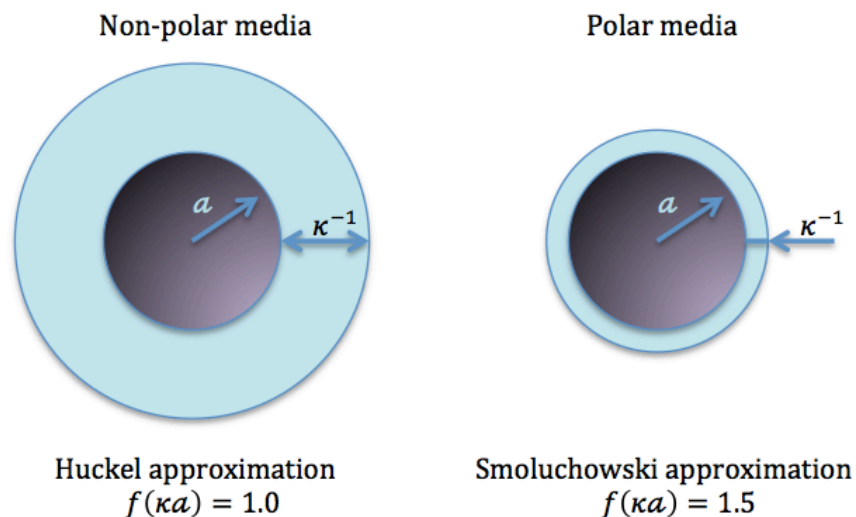


Figure 2-5. Schematic illustrating Huckel and Smoluchowski's approximations used for the conversion of electrophoretic mobility into zeta potential.

2.1.2 Synthesis

Metal colloid solutions can be produced in two general ways: top-down and bottom-up method. Top-down approach consists in the dispersion of larger particles to direct their assembly whereas the bottom up method builds larger particles starting at the molecular level and maintaining control on the structure [23] [24]. Common techniques top-down are lithographic techniques (e.g., UV, electron or ion-beam, scanning probe, optical near field), film deposition and growth, laser-beam processing, and mechanical techniques (e.g., machining, grinding and polishing). On the other hand, examples of bottom-up approaches are chemical synthesis, laser-induced assembly (i.e., laser-

trapping), self-assembly, colloidal aggregation, and 2-photon confocal processing. The main difference is top-down method has been developed widely on the industrial scale but exists a size limitation; it cannot achieve the size possible with the bottom-up approach [25].

The bottom-up technique has become favoured according to the improvement in synthetic protocols resulted in gold nanoparticles with monodispersity and controlled size. The most common synthetic route to prepare several sizes nanoparticles is by reduction of gold salts of the presence of stabilizing agents to avoid particle agglomeration. Some techniques usually use capping materials, such as a surfactant or polymer to prevent aggregation between nanoparticles and precipitation [25] [9].

The usual methods for reducing the gold precursor are detailed below.

2.1.2.1 Turkevich method

Turkevich method, further optimized by Frens, became in the classical method for Gold Nanoparticles synthesis. It dates from 1951 and is the most common because of its simplicity. This reaction is carried on by the reduction with sodium citrate of a chloride precursor (Figure 2-6). The result is colloidal gold particles approximately spherical with a negative surface charge due to the citrate coverage.

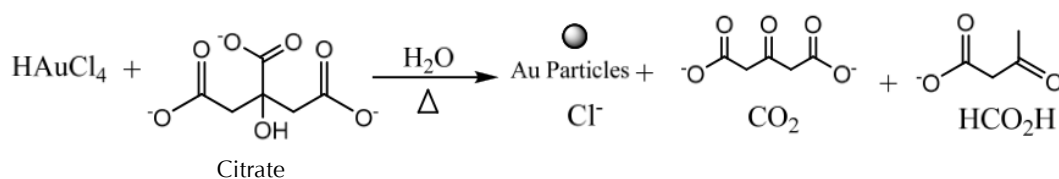


Figure 2-6. Scheme of gold reduction by sodium citrate [26].

In the procedure denominated “standard”, 100 mL of 1 mM HAuCl₄ aqueous solution is brought to 100°C with vigorous stirring under refluxing conditions. Quick addition of 10 mL of 38.8 mM sodium citrate resulted in about 25 seconds in a colour change from pale yellow to faintly blue (nucleation). After 2 minutes approximately, the blue colour suddenly changes into a burgundy red, indicating the formation of monodisperse spherical particles. The mixture is kept at 100°C for 15 minutes and cooled to room temperature while stirring [27] [28] [19].

2.1.2.2 Brust method

This method consists on a biphasic reduction of HAuCl₄ by sodium borohydride in the presence of an alkanethiol acting as a capping agent. Can be used to produce gold nanoparticles in organic liquids that are normally not miscible in water.

Faraday introduced the preparation of colloidal metals in two-phase system, who reduced an aqueous gold salt with phosphorus in carbon disulfide and obtained a coloured aqueous solution of dispersed gold particles. This technique has been combined with ion extraction methods and monolayer self-assembly with alkane thiols and the result was a one-step method for preparing nanometre-sized gold nanoparticles.

In the Brust synthesis, tetrachloroauric acid (HAuCl_4) is in aqueous solution with a phase transfer agent, tetraoctylammonium bromide (TOABr). Dodecanethiol ($\text{C}_{12}\text{H}_{25}\text{SH}$) in toluene is added and the AuCl_4^- is transferred by TOA^+ counterion from aqueous to organic phase. Au^{3+} to Au^{1+} is reduced by thiols, yielding a $(\text{Au}^{\text{I}}\text{C}_{12}\text{H}_{25}\text{S})_n$ polymer. Finally, aqueous NaBH_4 is added to reduce the gold and the $\text{Au}_x(\text{C}_{12}\text{H}_{25}\text{S})_y$ nanoparticles are formed changing the colour of the solution from orange to deep brown in a few seconds (Figure 2-7) [29] [30].

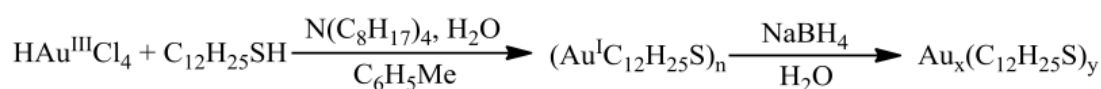


Figure 2-7. Scheme of Brust reaction [30].

The conditions of the procedure determine the ratio of thiol to gold. In the standard preparation technique an aqueous solution of hydrogen tetrachloroaurate (30 mL, 30 mmol dm^{-3}) is mixed with a solution of tetraoctylammonium bromide in toluene (80 mL, 50 mmol dm^{-3}). The two-phase mixture is stirred until the tetrachloroaurate is transferred into the organic layer and dodecanethiol (170mg) is then added to the organic phase. An aqueous solution of sodium borohydride (25 mL, 0.4 mol dm^{-3}) is slowly added with stirring. After 3 hours the organic phase is separated, evaporated to 10 mL in a rotary evaporator and mixed with 400 mL ethanol to remove the excess of thiol. This mixture is kept for 4 hours at -18°C and the dark Brown precipitate is filtered and washed with ethanol [29].

2.1.2.3 Ascorbic acid reduction in a single reduction/stabilizing step

The typical synthesis of gold nanoparticles requires the addition of protective specie is necessary to obtain a stable gold solution. This addition is essential but the presence of these compounds in many cases affects the physical and chemical properties of the solid surface. Hence, this type of synthesis was investigated with the aim of avoid the use of stabilizers. This synthesis is simply and rapid process that uses iso-ascorbic acid (i-Asc) as reductant and yields in several seconds at room temperature electrostatically stabilized gold nanoparticles in a single reduction/stabilization step without the presence of dispersing agents. The absence of this allows modifications in the surface for applications in medicine, biology, and catalysis.

The simultaneous mixing of the tetrachloroauric acid and iso-ascorbic acid solutions rapidly produces a stable gold solution indicated with the typical red color of the final dispersion. The reduction that takes place in this process is showed in (Figure 2-8).

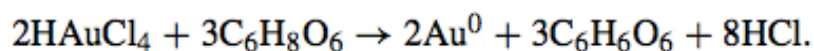


Figure 2-8. Chemical reaction produced in tetrachloroauric acid reduction with ascorbic acid.

The size resulting of the metal particles increases only slightly with the concentration of the reacting gold solutions. Regarding the pH, the resulting gold nanoparticles decreases with the decrease in the pH of the solution reaching a minimum in pH 4 and then increases again. The same behaviour is observed in the plasmon resonance due to

size and this parameter are directly related; the higher is the size, the higher is the plasmon peak wavelength (Figure 2-9).

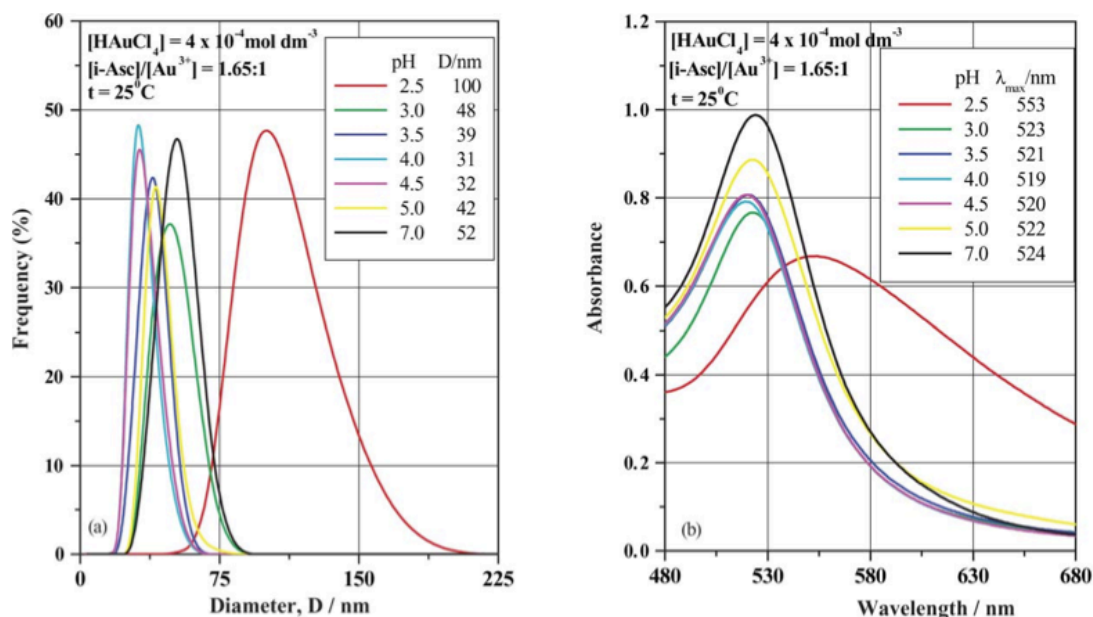


Figure 2-9. Variation of (1) the particle size of gold nanoparticles measured by dynamic light scattering and (b) the position of the plasmon band resonance for the gold solutions prepared by mixing $4 \times 10^{-4} \text{ mol} \cdot \text{dm}^{-3}$ tetrachloroauric (III) acid solutions with $6.6 \times 10^{-4} \text{ mol} \cdot \text{dm}^{-3}$ iso-ascorbic acid at 25°C and an $[i\text{-Asc}]/[Au^{3+}]$ ratio of 1.65:1 [31].

The synthesis is carried out mixing in a beaker tetrachloroauric acid and iso-ascorbic acid simultaneously added. The conditions for this experiment are room temperature and mechanical stirring [31].

2.1.2.4 Sodium borohydride reduction with MUA as stabilizer

In this synthesis, the capping agent 11-mercaptoundecanoic acid (MUA) is dissolved in ethanol, for preparing the solution, and added to a tetrachloroauric acid solution under stirring. After wait some minutes the reducer agent is introduced, the sodium borohydride [32]. At low pH, carboxylic acid-stabilized nanoparticles agglomerate due to the protonation and hydrogen bonding, rendering them soluble only in basic conditions. On the contrary, at high pH, the carboxylic acid groups deprotonate and stabilize the particle dispersion through electrostatic repulsion. Regarding this pH considerations, it is recommended to achieve a high pH value with the help of the addition of a basic compound such as sodium hydroxide. This method produces thiol-stabilized particles with carboxylic acid functionality [33].

2.1.2.5 Perrault method

This method was discovered by Perrault and Chan in 2009 trying to provide a greater size range and better size distribution. With this strategy, a size range of at least 2-200 nm can be obtained.

This method uses hydroquinone to reduce tetrachloroauric acid in aqueous solution that contains gold nanoparticle seeds. These preformed seeds are typically produced

using the citrate method. They can act as surface-catalyzed centers and gold atoms in exterior can be reduced on the surface avoiding a secondary nucleation. The reduction from Au^{3+} to Au^0 has a middle state considered the direct source for nanoparticles growth. Au^{3+} is reduced to Au^{1+} by citrate and from Au^{1+} to Au^0 by hydroquinone (Figure 2-10) Hydroquinone has a high selectivity and reduces from Au^{1+} to Au^0 on the gold seed surface [34] [35].

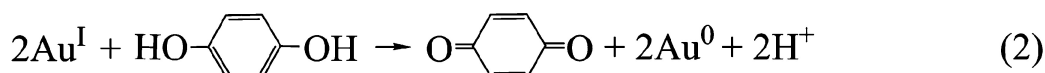
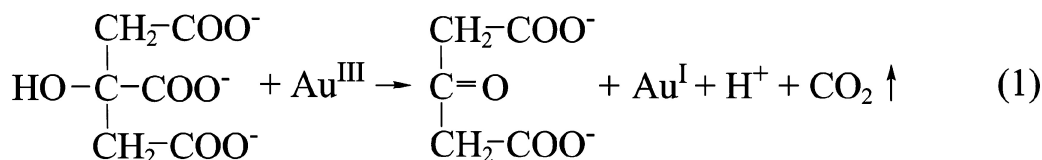


Figure 2-10. Scheme of Perrault method reactions for obtaining gold nanoparticles [35].

2.1.2.6 Martin method

This method was performed in 2010 by Eah Group and synthesizes “naked” gold nanoparticles in water by reducing tetrachloroauric acid with sodium borohydride. The nanoparticles are called “naked” because they are stably dispersed without the presence of a stabilizer like citrate. This new strategy combines the ease of the Turkevich method and the monolayer-protection of Brust method.

The foundation of this procedure is to stabilize the solution of tetrachloroauric acid with hydrochloric acid for more than 3 months and the sodium borohydride with sodium hydroxide more than 3 hours. Moreover, the ratio of NaBH_4 - NaOH ions to HAuCl_4 - HCl ions has to be controlled in the denominated “sweet zone”.

The gold nanoparticles are coated with a monolayer of 1-dodecanethiol (10% of gold atoms number) and after phase-transferred to hexane by shaking a simply solution of water, acetone and hexane for 30 seconds. Every reaction occurs in the water-acetone phase and a posterior cleaning of the hexane phase is not needed.

The precise size control in the diameter range of 3.2-5.2 nm is critically important for both the phase-transfer of gold nanoparticles from water to hexane and their 2D self-assembly on a toluene droplet.

This new method is simple, cheap and easy to adopt and is remarkable the fact that TOABr, used in Brust method, is not necessary. This is an advantage due to the difficulty for removing this phase-transfer agent [36].

2.1.3 Surface modifications and coatings

Stabilizing molecules encloses colloidal gold nanoparticles synthesized with the methods proposed. These molecules have two different parts; one of them is adsorbed or chemical crosslinked to the gold and the other is in the solution providing stability. Once the colloid gold is obtained, the stabilizer agent molecules can be displaced by other stabilizer. For example, thiol groups present a high affinity to gold surfaces and

thiol-modified ligands are commonly used in binding gold nanoparticles by formation of Au-sulfur bonds. Ligand exchange is motivated by different reasons, for example transfer the gold particles from an aqueous to an organic phase by exchanging hydrophilic with hydrophobic surfactants.

In aqueous solution applications, the most common used are thiol-based surfactants with carboxylic groups at the other end pointing towards the solution. These types of molecules provide colloidal stability because of the negative charges and linking points for the attachment of biological molecules.

The method to attach the biological molecules to the particles can be carried out in a different ways. If these molecules have a functional group with the possibility to bind directly to the gold surface (e.g., thiols or peptide sequences), the biological molecules have the capacity for displacing the original stabilizer directly to the particle solution. In this way, molecules like oligonucleotides, peptides or PEG can be readily linked to gold nanoparticles allowing the production of gold nanoparticles with a fixed number of attached molecules per particles. On the other hand, biological molecules can be attached by means of bioconjugate chemistry to the shell of stabilizer molecules. The most typical method is the linkage of amino-groups on the biological molecules with carboxy groups at the free ends of stabilizer molecules by using EDC (1-ethyl-3-(3-dimethylaminopropyl)-carbodiimide-HCl).

The two strategies commented are useful for attaching almost all kinds of biological molecules to the nanoparticle surface. Despite of the fact that the two protocols are well defined, the characterization of synthesized conjugates is necessary, in particular to reject aggregation effects or unspecific coating during the conjugation reaction. Particularly, in many bioconjugations protocols, the number of molecules attached per gold nanoparticle is only estimated, as no standard method for obtaining the surface coverage of particles modified with molecules has yet been established [37].

2.1.4 Applications

2.1.4.1 Gold nanoparticles as vector for drug delivery

Several nanocarriers including liposomes, polymer micelles and vesicles, dendrimers, nanocapsules, and metal nanoparticles have been used as promising delivery vectors [38]. Recently, gold nanoparticles have emerged as a smart candidate for delivery several payloads, such a small drug molecule or large biomolecules such as RNA [6]. Gold nanoparticles can be designed to carry out the release of drug with internal stimuli; such as pH change or glutathione liberation, or external stimuli; such as release started with a laser light [2] [6]. One of the most recent discovers are focused in gold nanoparticles with magnetic properties that allow the drug leading in the desirable zone applying an external magnetic field [39].

When a pharmaceutical agent, practically independently of the route of administration, is distributed within the body has to cross many biological barriers, such as other organs, cells and intracellular compartments. As a result, the agent can be inactivated or express undesirable effect on organs and tissues, hence the use of big quantities of drug supplied to achieve the objective. The targeting drug delivery emerges such a solution for these problems; the drug quantity and cost of therapy are reduced; and the

concentration of drug can be sharply increased without negative effects on nontarget compartments.

The most natural and universal way to impart a nonspecific drug affinity towards its target is the binding to a target site. The substances that can be used as a targeting vehicle are: antibodies, lectins, other proteins, lipoproteins, hormones, charged molecules, mono-, oligo- and polysaccharides, and some low-molecular-weight ligands, such as folate. The coupling of a drug directly into the targeting moiety is the simplest way to prepare the vector [39].

These vectors can be classified into viral and non-viral. Non-viral vector application is limited in some cases due to the parameters affecting such as colloidal stability, covering efficiency, target internalization, and endosomal escape. Above all, this vector efficiency is lower than in the case of viral vectors. Viral carriers take benefit of the mechanisms developed by viruses to allow their genomes to entry into the cell's cytoplasm [40] but they are not suitable for the delivery of drugs and short oligonucleotides [19]. The advantages of these carriers are: high transduction efficiency for different quiescent and dividing cell type, and high level of short-term expression. Nevertheless, there is a possibility of immune and toxic reactions besides to the potential for viral recombination.

The properties of these nanocarriers can affect to the resulting biodistribution through passive and/or active targeting. Hence, it is important to define the physicochemical properties required in the delivery vehicle. Two important factors that control the biodistribution and transfection are charge and size of the delivery vector. Regarding the charge, it affects significantly; highly charged particles can lead to complement activation, whereas neutral particles show reduced phagocytic uptake. Particularly, cationic polymers such as polyethyleneimine (PEI) has been shown to activate the complement system, whereas increased polycation length and surface charge density leads to higher complement activation and/or cytotoxic effects due to electrostatic interactions with negatively charged cell membranes. Fast binding of charged molecules by complement proteins or other opsonins can lead to immune stimulation and rapid clearance of the delivery vehicles from the bloodstream. The other important parameter to consider in the design of a drug delivery vehicle is the size. Generally, particles with a size between 200 and 500 nm can entry into target cells via endocytosis and permeate the nuclear membranes through the nuclear pores. The suitable size depends on the application of the vector; to target tumors, for example, the vector has to be as small as possible being the best option less than 100 nm [40].

Gold nanoparticles have several suitable properties that make them exceptional option for use in delivery applications. The gold core is principally inert, non-toxic, and biocompatible, it can be simply synthesized in a broad size range (1-200 nm) with controlled dispersity. The high surface area-to-volume ratio offers dense loading of functionalities incorporating targeting and therapeutic materials. Finally, there is a high diversity of drugs and biomacromolecules that can be covalent or non-covalent conjugated to the surface because of the high multivalent structures [38].

There are two surface structures for the delivery applications in gold nanoparticles; the monolayer coated and the biomolecule coated (Figure 2-11). The delivery of DNA/RNA required a high surface-to-volume ratio to maximize the compaction and the payload. The monolayer coverage of gold nanoparticles allows the modification of

parameters such as charge and hydrophobicity to maximize transfection efficiency whereas the toxicity is reduced. The proteins delivery is achieved with engineered monolayer gold nanoparticles rejecting the problems due to the poor permeability through the cell membrane. Drug delivery is accomplished due to the suitable properties commented and the possibility of modify them. Several approaches have been studied; covalent attachment provides stability but required intracellular processing of the drug, non-covalent loading allows the direct discharge of the drug but this can be produced prematurely. The targeted delivery to disease sites is the major challenge achieved in biomedicine. There are two strategies to carry it out; “passive” targeting, depending on the leaky vasculature of the diseased tissue whereas “active” targeting includes the attachment of functionality to the delivery vehicle for interaction with specific cell receptors.

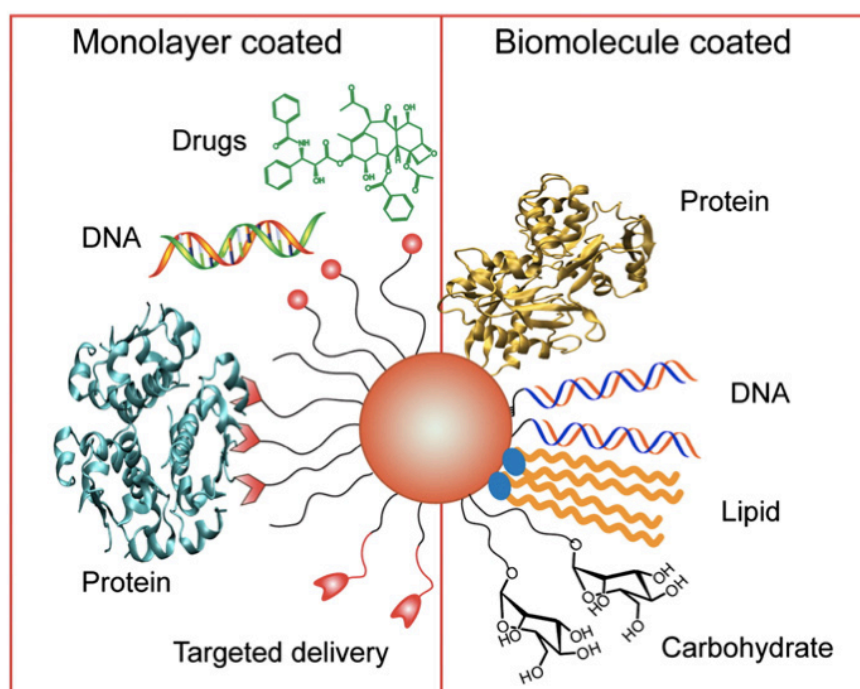


Figure 2-11. Scheme of the two AuNP surface structures most commonly used in delivery applications [38].

The second one are the biomolecules coated gold nanoparticles emerged because of the efficient transport of biomacromolecules with minimal cytotoxicity. Monolayers created by biomolecules can solve many problems in delivery such as endosomal escape and specific targeting without conjugation. Cellular internalization of negatively charged oligonucleotide-functionalized gold nanoparticles has emerged as a new approach. Gold nanoparticles attached with peptides or proteins present another paradigm for delivering cargo into cells. Delivery studies using peptide/protein coated gold nanoparticles focus on attaching targeting peptide sequences or receptor specific antibodies. Lipids have been used extensively to modify AuNPs for cellular delivery [38].

2.1.4.2 Gold nanoparticles for labelling in biological imaging

Optical properties exposed before in addition to the advantages in synthesis, conjugation and assembly have motivated the studies due to their properties such as an enhanced absorption and scattering, biocompatibility, ease synthesis and conjugation to several ligands. A significant use has been reports as contrast agents in cellular and biological imaging.

Contrast agents have the role of sensitivity improvement and diagnostic ability by site-specifically labelling tissues or cells of interest. Anatomic details of cells and tissues can be provided using different techniques such as microscopy techniques and immunotargeted optical contrast agent; allowing the knowledge of tissue architecture for diagnosis of cancer, for example. Traditional contrast agents have been based on photoabsorbing and fluorescent dyes such as malachite green and rhodamine-6G. Recently, quantum dots have been studied for biological and cell imaging taking advantage of their unique size-dependent fluorescence properties. Nonetheless, semiconductor material has a potential human toxicity and cytotoxicity, problems not allowed for its in vitro and in vivo application. Gold nanoparticles have become in an alternative due to their potential noncytotoxic, facile immunotargeting and their nonsusceptibility to photobleaching or chemical/thermal denaturation. They can be considered promising on the use of techniques such as multiphoton plasmon resonance microscopy and photoacoustic tomography. The gold nanoparticles strong light scattering has been exploited for real-time optical imaging of precancer by the use of confocal reflectance microscopy [41].

2.1.4.3 Gold nanoparticles as a heat source

Gold nanoparticles have the property of absorb light and transform it in heat. When the particles are stimulated with a determined frequency of laser light or another heat source (microwaves, radiofrequency, ultrasounds) they are able to emit an intense heat. This mechanism opens a new investigation field in another medical application; the thermal treatment. This type of treatment can be used in diseases with tumoral cells [2]. For the use of this method, the shift of the wavelength of maximum absorption into the near infrared it is suitable due to the body is more transparent at those wavelengths. This possibility can be accomplished with gold nanoshells by enhancing the dipole-dipole interaction between aggregated nanospheres or by decreasing the symmetry of the particles, for example forming nanorods. Gold nanorods have two plasmon absorption peaks, and the position of the second peak can be moved deep into the near infra-red (NIR) region by controlling the aspect ratio of the nanorod [42].

2.1.4.4 Gold nanoparticles in environmental applications

Gold nanoparticles have been studied as a potential agent to solve some environmental issues, such as greener production methods, water purification and pollution control.

Gold is traditionally considered catalytically inactive as a practical catalyst, but this property changes when gold is found in size inside the nanometric scale. The key of the catalytic process is the interaction between the gold nanoparticle surface and the chemical reactant. To maximize the interaction the use of nanoparticles offers; a large surface area-to-volume ratio, high surface concentration of corner and edge atoms, low coordination number of surface atoms, and unique electronic properties [25]. Gold can

be used in catalysis in different process; CO oxidation, hydrogenation of unsaturated substrates, electrochemical redox catalysis of CO and CH₃OH oxidation and O₂ reduction are some examples of this. This is possible due to the condition of stable metal of gold that make it resistant to oxidation. A remarkable property as catalyst is the promising use to control and oxidation of mercury, one of the most toxic materials existing, cause of diseases as Alzheimer or autism.

Regarding the purification of water and air, gold nanoparticles are able to oxidize the CO to CO₂, a far less toxic substance. Recent studies show the use of gold nanoparticles to remove significant levels of mercury from water [1].

2.2 Chitosan

Chitosan is a polysaccharide obtained from chitin, one of the most abundant natural biopolymers. Chitosan is a renewable resource that is being explored intensively for the applications in pharmaceutical, cosmetics, biomedical, biotechnological, agricultural, food and non-food industries as well (water treatment, paper and textile). During the past 40 years this polymer has been widely studied because of this unique polymer has emerged as a new type of physiological material of high sophisticated functions. It is considered an attractive material due to its versatile biological activity, biocompatibility, and complete biodegradability with a low toxicity. To achieve the exploitation of its unique properties trials are being made to derivatize them [43] [44].

2.2.1 Source and structure of chitosan

Chitin, poly (β -(1 \rightarrow 4)-*N*-acetyl-D-glucosamine) is a natural polysaccharide synthesized by certain type of living organisms and is one of the polymer widely produced annually in the world, being the second after the cellulose [45]. The chemical structure of chitin is very similar to cellulose except that the acetamino group replaces the hydroxyl group on the C2 position (Figure 2-12). It is a principal component of the exoskeleton in animals, specifically in crustaceans, molluscs and insects and chitin is the principal fibrillar polymer in the cell wall of several fungi [7]. Several millions tons of chitin are produced annually and hence this biopolymer represents a cheap and readily available source, being the main commercial sources the shell waste of shrimps, lobsters, krills and crabs [46].

Chitin is a copolymer of *N*-acetyl-glucosamine and *N*-glucosamine units randomly or block distributed in the polymer chain depending on the method used to derive the biopolymer. The content of glucosamine in chitin is called deacetylation degree (DD). The polymer is termed chitin when the number of *N*-acetyl-glucosamine units is higher than 50% whereas if the number of *N*-glucosamine units is higher, the term chitosan is used [7]. Probably one of the most interesting differences between chitin and chitosan is Chitosan lies in their solubilities. There are a few solvents for chitin, while nearly all aqueous acids dissolve chitosan, of which the most commonly used are formic acid and acetic acid [43].

Chitosan is a linear copolymer polysaccharide composed by β (1 \rightarrow 4)-linked 2-amino-2-deoxy-D-glucose (D-glucosamine) and 2-acetamido-2-deoxy-D-glucose (*N*-acetyl-D-glucosamine) units. The proportion of *N*-acetyl-D-glucosamine and D-glucosamine residues affects directly to the properties like biodegradability and biological [47].

This cationic polysaccharide has increased due to the applications in biomedical and pharmaceutical fields, abundant accessibility [8].

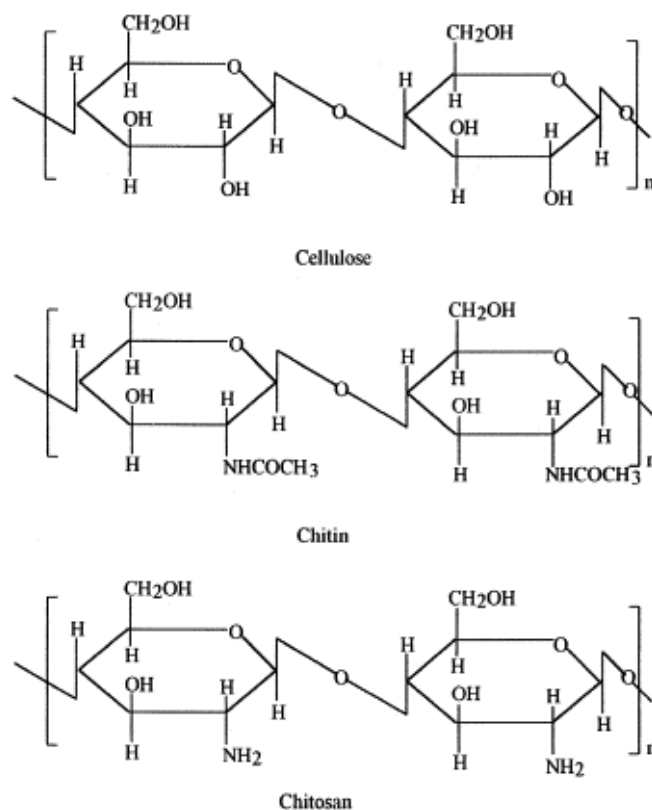


Figure 2-12. Structures of cellulose, chitin and chitosan [48].

2.2.2 Physicochemical and biological properties of chitosan

Chitosan is a semicrystalline polymer that exhibits polymorphism and the appearance is colourless, odourless flakes. This polymer has a low solubility at a physiological pH of 7.4 as it is a weak base (pK_a 6.2-7). However, chitosan is readily to use in aqueous acidic solution due to the conversion into a polycation by means of the protonation of amino groups on the C-2 position of D-glucosamine residues.

The two most important physicochemical properties of chitosan are the molecular weight (M_w) and the deacetylation degree (DD) due to the influence they have in another parameters (Table 2-1). Both can be altered introducing different changes in the reaction conditions during the manufacturing from chitin to chitosan. The DD of typical commercial chitosan is usually between 70 and 95%, and the M_w between 10 and 1,000kDa. Higher M_w chitosan, approximately 1,400kDa, has a higher level of viscosity and, for example, shows a stronger level of mucoadhesion than low M_w of 500-800 kDa. The viscosity increases with DD and concentration but decreases with temperature and pH.

Chitosan has the ability of good complexing with an oppositely charged polymer such as poly(acrylic acid), sodium salt of poly(acrylic acid), carboxymethyl cellulose, xanthan, etc. [47]

Regarding biological properties, chitosan is biocompatible and has excellent properties as an antioxidant and antimicrobial. It is mucoadhesive in its swollen state and a natural adhesive in hard and soft tissues. Other properties known are: antitumor effects, angiogenesis stimulation, macrophage activation, adsorption enhancer, analgesic, hypercholesterolemic and haemostatic agent [47].

Table 2-1. Relationship between structural parameters and properties [46].

PROPERTY	STRUCTURAL CHARACTERISTICS
Solubility	↑ DD
Crystallinity	↓ DD
Biodegradability	↓ DD, ↓ Molecular weight
Viscosity	↑ DD
Biocompatibility	↑ DD
Biological	
Mucoadhesion	↑ DD, ↑ Molecular weight
Analgesic	↑ DD
Antimicrobial	↑ DD, ↑ Molecular weight
Permeation enhancing effect	↑ DD
Antioxidant	↑ DD, ↓ Molecular weight
Hemostatic	↑ DD

↑ - Directly proportional to property; ↓ - inversely proportional to property.

2.2.3 Preparation of chitosan

Preparation of chitosan involves four steps: deproteinization, demineralization, decoloration and deacetylation. Firstly, for deproteinizing an alkaline treatment with 3-5% NaOH (w/v) aqueous solution is applied at room temperature overnight. After this, a treatment with 3-5% HCl (w/v) aqueous solution is carried out for 5 h at room temperature for removing other inorganic constituents remaining. This product is again reacted with 40-45% NaOH solution at 120°C for 4-5 h and the result is the crude sample of chitosan. The crude sample is purified by precipitating the chitosan from its aqueous acetic acid solution to NaOH and by washing with distilled water until neutralized [47].

2.2.4 Chitosan modifications

Chitosan is an amenable molecule due to the ability to be modified because of the functional groups as a primary amine and primary as well as secondary hydroxyl groups in its monomers. The most important and promising chitosans are shown in Table 2-2 [43].

Table 2-2. Important examples of modified chitosan .

Derivatives	Examples (uses)
Quaternized chitosan, alkyl chitosan	Trimethylchitosan chloride, <i>N</i> -propyl- <i>N,N</i> -dimethyl chitosan and <i>N</i> -furfuryl- <i>N,N</i> -dimethyl chitosan <i>N</i> -diethylmethylamino chitosan
Highly cationic chitosan	
<i>N</i> -Acylchitosans	Formyl, acetyl, propionyl, butyryl, hexanoyl, octanoyl, decanoyl, dodecanoyl, tetradecanoyl, lauroyl, myristoyl, palmitoyl, stearoyl, benzoyl, monochloroacetyl, dichloroacetyl, trifluoroacetyl, carbamoyl, succinyl, acetoxycarbonyl (aspirin) (textiles, membranes, and medical aids)
<i>N</i> -Carboxyalkyl/(aryl) chitosans	<i>N</i> -Carboxymethyl chitosan (glycine glucan), <i>N</i> -carboxypropyl chitosan, <i>N</i> -carboxybenzyl, alanine glucan, phenylalanine glucan, tyrosine glucan, serine glucan, glutamic acid glucan, methionine glucan, leucine glucan (chromatographic media and metal ion collection)
<i>O</i> -Carboxyalkyl	<i>O</i> -Carboxymethyl, cross-linked <i>O</i> -carboxymethyl chitosans (molecular sieves, viscosity builders, and metal ion collection)
<i>N</i> -Carboxyacyl-chitosan	From anhydrides such as maleic, succinic, itaconic, glutaric, trimellitic, pyromellitic, thiosuccinic, phthalic, <i>cis</i> -1,2,3,6-tetrahydrophthalic; 5-norbornyl- <i>endo</i> -2,3-dicarboxylic, acetylthiosuccinic, cyclohexane 1,2-dicarboxylic, diphenic, salicyl
Thiolated chitosan	Chitosan–cysteine conjugate, chitosan–thioglycolic acid, chitosan–4-thio-butylamine, chitosan–2-iminothiolane conjugate
Sugar derivatives	1-Deoxygalactose-1-yl-, 1-deoxyglucose-1-yl-, 1-deoxymelibiose-1-yl-, 1-deoxylactose-1-yl-, 1-deoxylactose-1-yl-4-(2,2,6,6-tetramethylpiperidine-1-oxyl)-, 1-deoxy-6'-aldehydolactose-1-yl-, 1-deoxy-6'-aldehydomelibiose-1-yl-, cellobiose-1-yl chitosans, products obtained from ascorbic acid
Metal ion chelates	Palladium, copper, silver, iodine (catalyst, photography, health products, and insecticides)
Semisynthetic resins of chitosan	Copolymer of chitosan with methyl methacrylate, resins of polyurea–urethane, poly(amide ester), chitosan acrylamide–maleic anhydride
Natural chitosan	Glucans from various organisms (flocculation and metal ion polysaccharide chelation complexes)
Miscellaneous	Cyanoethyl chitosan (desalting, filtration, dialysis, and insulating papers) Glycol chitosan (enzymology, dialysis, and special papers) Glutaraldehyde chitosan (enzyme immobilization) Linoic acid–chitosan complex (food additive and anticholesterolemic) Uracylchitosan, theophylline chitosan, adenine chitosan, chitosan salts of acid polysaccharides, chitosan–streptomycin, <i>N</i> -cyclohexane chitosan, 2-amido-2,6-diaminoheptanoic acid chitosan Hydroxyalkyl chitosans, cyanoethyl chitosan Chitosan ascorbate ketimine and its reduced form (used to treat parodontopathies) Imidazole chitosan (proposed for treatment of bone lesions) Chemically cross-linked glycine glucan (suitable for collection of carrier-free radioisotopes) Sulfated chitosan (hemostatic) Phosphorylated chitosan (metal chelation)

2.2.5 Chitosan applications

Chitosan has proved to be a safe excipient in drug formulations, it is an excellent mucoadhesive in its swollen state and a natural adhesive can be adhered to hard and soft tissues [46]. This polymer has biocompatibility properties such as a good blood compatibility and cell growth efficiency, grafted chitosan is used in cardio-vascular applications. Chitosan derivatives can exhibit enhanced bacteriostatic activity very interesting for woundhealing applications [7].

Chitosan and its derivatives can be covalently cross-linked to prepare nano-sized particles as the drug carriers. The cross-linking process involves the formation of the covalent bonds between the chitosan chains and the cross-linker, commonly include bifunctional agents such as PEG dicarboxylic acid, glutaraldehyde, or monofunctional agents such as epichlorohydrin. One advantage of this is that the crosslinking is easy to carry out without using organic solvents. The ionically cross-linked nanoparticles have often been prepared using the chitosan and its derivatives by exploiting their cationic nature, in which the amino group of the chitosan backbone can interact with salts such as sodium sulphate, tripolyphosphate, or other multiple-charged anion molecules.

Since chitosan is a hydrophilic and cationic polysaccharide, chitosan-based self-assembled nanoparticles can be prepared by chemically attaching the hydrophobic moiety to the backbone of chitosan and its derivatives. These nanoparticles can circulate

in the bloodstream for a relatively long time without recognition of phagocytes and can easily be accumulate at the leaky vasculature. It is possible to achieve the accumulation on the action site by conjugating the targeting moiety to the self-assembled nanoparticles. Owing to the insoluble nature of chitosan in water, the nanoparticles from chitosan amphiphiles are rapidly precipitated in biological solution. Therefore, water-soluble chitosan derivatives have been often used for developing the nanoparticles in drug delivery systems [8].

2.3 siRNA

Small interfering RNA (siRNA) were discovered as a defense mechanism of cells in plants and other organisms and has been studied to become in a potential therapeutic agent [49].

RNA interference (RNAi) is a post-transcriptional gene-silencing mechanism reported in plants, some invertebrates and mammalian cells. By means of this process, double-stranded RNA (dsRNA) can mediate the destruction of its homologous mRNA target. The design of RNA sequences that can stop the expression of selected genes responsible of several diseases, including viral infection, cancer and genetic disease. The simplicity and versatility of RNA engineering has increased the use on nucleic-acid and RNA-based approaches for therapy [3].

2.3.1 Small interfering RNA

siRNA stands for small interfering RNA, also known as silencing or short interfering RNA. In comparison with classical antisense oligonucleotides, siRNA is a class of double-stranded RNA molecules, 19-25 nucleotides in length with 2 nucleotides 3' overhangs on both end and a phosphate group at each 5' end (Figure 2-13).

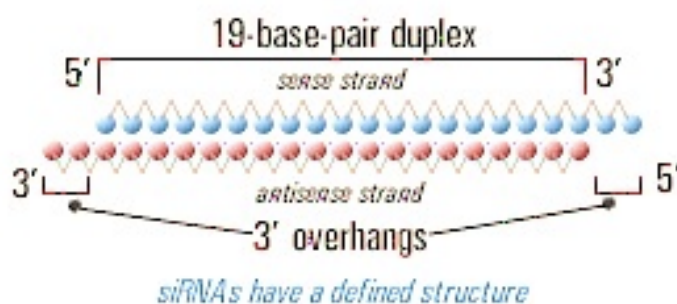


Figure 2-13. siRNA structure [50].

siRNA can knock down the expression of target genes through the RNA interference (RNAi) pathway, which was first described in the nematode worm *Caenorhabditis elegans* in 1998 by Andrew Z. Fire and Craig C. Mello. Any gene can be targeted by siRNA if the sequence is known. Moreover, siRNA may promote RNAi-related pathways, including activation of cellular antiviral mechanisms or interference with the chromatin structure of the genome [51].

2.3.2 RNAi gene-silencing mechanism

The RNAi phenomenon of gene-silencing can be triggered by various fonts of RNA molecules, including RNA viruses, exogenously introduced dsRNAs (siRNA) and endogenous small non-coding miRNAs. RNA viruses can start the RNAi with two methods: viral RNA can produce itself the cleavage and introduce the siRNA or miRNA, or the virus can encode miRNAs that use the host RNAi machinery for specific gene silencing [4].

In the second way to trigger the RNAi (Figure 2-14) exogenous double-stranded RNAs (dsRNA) appear in the cell and are recognized and cleaved into siRNAs with a size of 21-23 nt. The responsible of cleaving these RNAs is a protein known as DICER. This process is thought to be limited to the cytoplasm. The small dsRNA produced by DICER are incorporated into a multiprotein complex called RISC (RNA-Induced Silencing Complex) that guides its cleavage of targets RNAs. The complex RISC includes four different subunits including helicase, exonuclease, endonuclease, and homology searching domains. If siRNA binds to RISC, helicase unwound the siRNA resulting in two singles strands, one of them guides RISC to its complementary target mRNA. The complex RISC includes four different subunits including helicase, exonuclease, endonuclease, and homology searching domains. If siRNA binds to RISC, helicase unwound the siRNA resulting in two singles strands, one of them guides RISC to its complementary target mRNA.

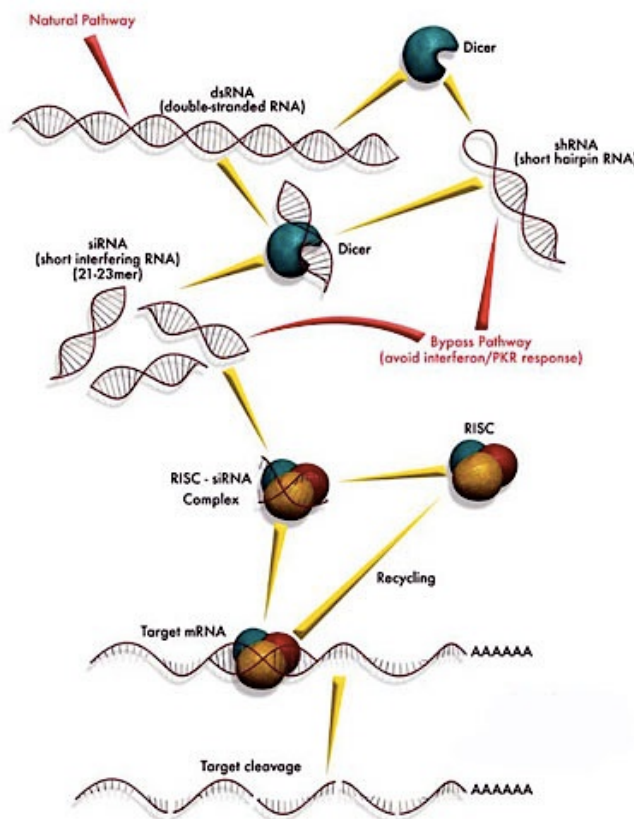


Figure 2-14. Classical mechanism RNA interference (RNAi) pathway [49] [52].

The RISC-siRNA complex recognizes and binds to the target mRNA. RISC-siRNA-mRNA complex causes a specific cut in the linked strand of mRNA and this produces the release and posterior degradation of mRNA cut. When the mRNA is liberated, RISC-siRNA free complex can be linked again to another molecule of mRNA and cut it. The repetition of this cycle linking-cut-release-degradation produces the degradation of all mRNA molecules transcribed and the gene silencing [49] [53].

2.3.3 siRNA delivery

There are two different ways of nucleic acid delivery: endogenous and exogenous delivery. The exogenous delivery implicates the *in vitro* preparation of the molecules and their delivery to the cells. Cells present obstacles to the entry of molecules with a high charge or molecular weight; hence the delivery into the cytoplasm is the principal challenge. Many transfection techniques have been used with the purpose to solve this problem, for example, electroporation, microinjection, and cationic liposome-mediated transfection. The exogenous delivery provides the possibility to develop compounds with a therapeutic potential.

The endogenous delivery of siRNA involves the cloning of these molecules into a vector, viral or non-viral. The most important advantage of the endogenous delivery is related with the continuous expression of siRNA and the possibility of switch it on and switch it off by means of the use of an inducible promoter (e.g., U6 and H1 promoters) [5].

2.3.4 siRNAs generation and chemical modification

Small interfering RNA (siRNA) can be generated in different ways. dsRNA is introduced into a cell by a virus, endogenous RNA expression or exogenously delivered and is cleaved by DICER complex in siRNAs. In other way, perfect matching hairpin RNA, which are also known as hairpin siRNA or small hairpin RNA (shRNA) is used. shRNA is delivered as an encoded sequence in a plasmid or viral vector, usually together with RNA polymerase III (pol-III) promoter elements. This shRNA folds into a structure similar to a siRNA duplex and is processed by DICER. Alternatively, chemically synthesized siRNAs mimicking the structure of DICER processed products can be introduced directly into the cytoplasm bypassing the DICER cleavage [53] [3].

RNA is not a stable molecule because its 2'-OH groups promote RNA hydrolysis under acidic and basic conditions. Moreover, nucleases can reduce the half-life of an RNA application *in vivo*. As a result, siRNA is chemically modified to increase the stability in extracellular and intracellular environments, essential to extend the application fields. The second reason for the chemical modification is the possibility of influence in specific steps of RISC function and reduction of off-target effects or RNAi that arise from partial complementarity between the guide and target mRNA-strands [4].

2.3.5 Therapeutic applications of siRNA

One of the most important advantages of siRNA is that the technology necessary for its development is very similar to the one to produce a chemical drug. The straightforward synthesis of siRNA is cheaper compared to other treatments based on proteins or antibodies and the pharmacokinetics properties are suitable considering the degradability and residence time on the body to be released in several organs. siRNA would be administered by the typical way for drugs (skin, intravenous, inhaled) [49].

siRNA has been proved as an effective treatment in infection by viruses, due to the fact that many viruses are RNA viruses, and both vault RNA and complementary RNA (vRNA and cRNA) in addition to mRNA, could be targets with specific siRNA. On the contrary to the vaccines, which require a normal working immunologic system, siRNA treatment is not directly related with the immunological function state. Hence,

siRNA can be delivered in the elderly whose immune system is considered weak. In vivo studies, liver was revealed as one of the organs capable of significant siRNA uptake, considering the possibility of hepatitis virus as a good target for the therapy. Promising studies in infection prevention of vulnerable cells against HIV and the influenza virus has been realized these last years obtaining optimistic results.

siRNA is not only effective silencing pathogenic viral genes but also knockdowning oncogenes such as K-RAS (founded in 20-30% human cancers), BCR-ABL (leukaemia cause), VEGF (tumor developer in diverse facets), FAK (brain tumor promoter) or BCL-2 (implicated in a number of cancers, including melanoma, breast, prostate, leukaemia, lung as well as schizophrenia and autoimmunity). In a study realized in mouse, the injection of siRNA potentiated the gemcitabine-induced (chemotherapy agent) antitumor effect, stimulating apoptosis and reducing tumor size proving that this anticancer therapy is achievable in vivo.

Neurologic diseases can be also treated with siRNA delivery therapy considering targets the genes related with the development of neurodegenerative disorders. Alzheimer, amyotrophic lateral sclerosis and prion-based diseases are some examples of the objective of this of siRNA treatment.

Recently, it is reported that chemical stabilization and cholesterol conjugation could improve the siRNA permeability. The expecting pharmacological effect was proved with the silencing of apolipoproteinB (apoB) with this chemically modified siRNA and reduced total cholesterol in a rat using conventional intravenous injection [53].

2.4 Instrumentation

2.4.1 Nano ZS 3600

The Zetasizer Nano series calculates the zeta potential by determining the electrophoretic mobility of the particles and applying the Henry equation. Performing an experiment on the sample and measuring the velocity of the particles, the electrophoretic mobility is calculated using Laser Doppler Velocimetry (LDV).

2.4.2 Zeta potential: theoretical knowledge

The essence of a classical microelectrophoresis system is a capillary cell with electrodes at either end to which a potential is applied. Particles move towards the electrode of opposite charge, their velocity is measured and expressed in unit field strength as their mobility (Figure 2-15).

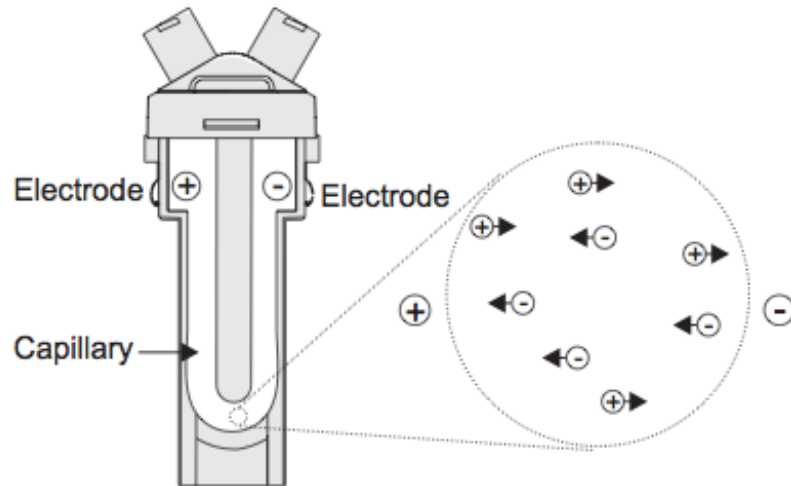


Figure 2-15. Electrophoretic mobility measurement scheme.

A zeta potential measurement system is composed by six components (Figure 2-16). Firstly, a laser (1) is used to supply a light source to illuminate the particles within the sample; for zeta potential measurements an incident and reference beam is provided with the split light. A modulation of the reference beam provides with the Doppler effect necessary.

The laser beam passes through the centre of the sample cell (2) and the scattering at an angle of about 13° is detected. When the dip cell is inserted into the cell holder the terminals on the cell allow the system to recognize the type of cell fitted and adjusts the applied voltage.

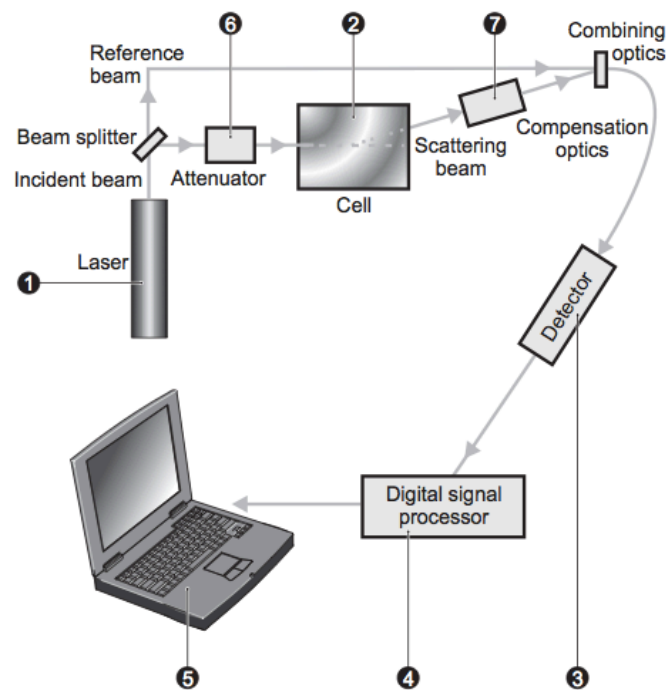


Figure 2-16. Configuration of the Zetasizer Nano series for zeta potential measurements

Particles moves when an electric field is applied to the cell and this movement will cause the intensity of light detected to fluctuate with a specific frequency.

The detector (3) sends the information obtained to a digital signal processor (4) and then is passed to a computer (5). In this moment, the software produces a spectrum from which the electrophoretic mobility and hence the zeta potential information is calculated.

The intensity of the scattered light through the sample must be within a specific range to achieve satisfactory results. If too much is detected, an attenuator (6) acts to reduce the intensity of the laser and the scattering. However, for samples that do not scatter much light, such as very small particles or samples of low concentration, the attenuator will automatically allow more light through the sample.

Within the scattering beam path, compensation optics (7) are installed to correct differences in the cell wall thickness and dispersant refraction [22].

2.4.3 UV-vis spectrophotometer

Spectrophotometry is any technique that uses light to measure chemical concentrations by the estimation of the absorption of ultraviolet and visible radiation (in the wavelength region of 160 to 780nm). This is one of the most widely methods of quantitative analysis used in any analytical laboratory [54] [55].

To calculate the absorbance of the sample is necessary to know the irradiance, P , the energy per second per unit area of the light beam. The monochromatic light, with irradiance P_0 , strikes a sample and the irradiance of the beam emerging is P . Then, absorbance is defined as:

$$A = \log\left(\frac{P_0}{P}\right)$$

This parameter is the spectrophotometer output and it is so important because it allows calculate the concentration of the sample with Beer-Lambert's law [56].

Not only it is possible the calculation of the concentration but also it is feasible to make a prediction about the shape, aggregations, and size with the surface plasmon resonance originated. The extinction spectra can be analysed using the Mie theory, once is considered the appropriate correction of the metal dielectric constant for the nanoparticle size and the physicochemical environment [16].

2.4.3.1 Beer-Lambert's law

Beer-Lambert's equation is the basic law applied in spectrophotometry because it allows calculate the concentration of a sample. Absorbance is directly proportional to the concentration, c , of the light-absorbing species in the sample by the following equation:

$$A = \varepsilon \cdot l \cdot C$$

which A is the absorbance, an optical parameter without units measured with a spectrophotometer; l is the thickness of solution through which incident light is assed; C is the molar concentration; and ϵ is the molar absorption coefficient ($\text{L}\cdot\text{mol}^{-1}\cdot\text{cm}^{-1}$) at a given wavelength. The value of molar absorptivity corresponds to the absorbance of a solution with a 1 M concentration and a thickness of 1 cm.

2.4.3.2 UV-vis spectrophotometer components

A UV-vis spectrophotometer is an instrument for chemical analysis and consists of three components: the light source, the dispersive system and a detector.

Visible light comes from a quartz-halogen lamp and the ultraviolet source is a deuterium arc lamp that emits in the range 200 to 400 nm. The monochromator disperses light into its components wavelengths and select a narrow band of wavelengths to pass on to the sample.

In a double-beam spectrophotometer, the light passes through the sample and the reference (blank) alternatively, directed by a rotating mirror (the chopper) into and out of the light path. When light passes through the sample, the detector measures the P and when the chopper diverts the beam to the blank, P_0 . The beam is chopped several times and it allows the comparison the two values of irradiance and the calculation of absorbance (**Error! Reference source not found.**) [56].

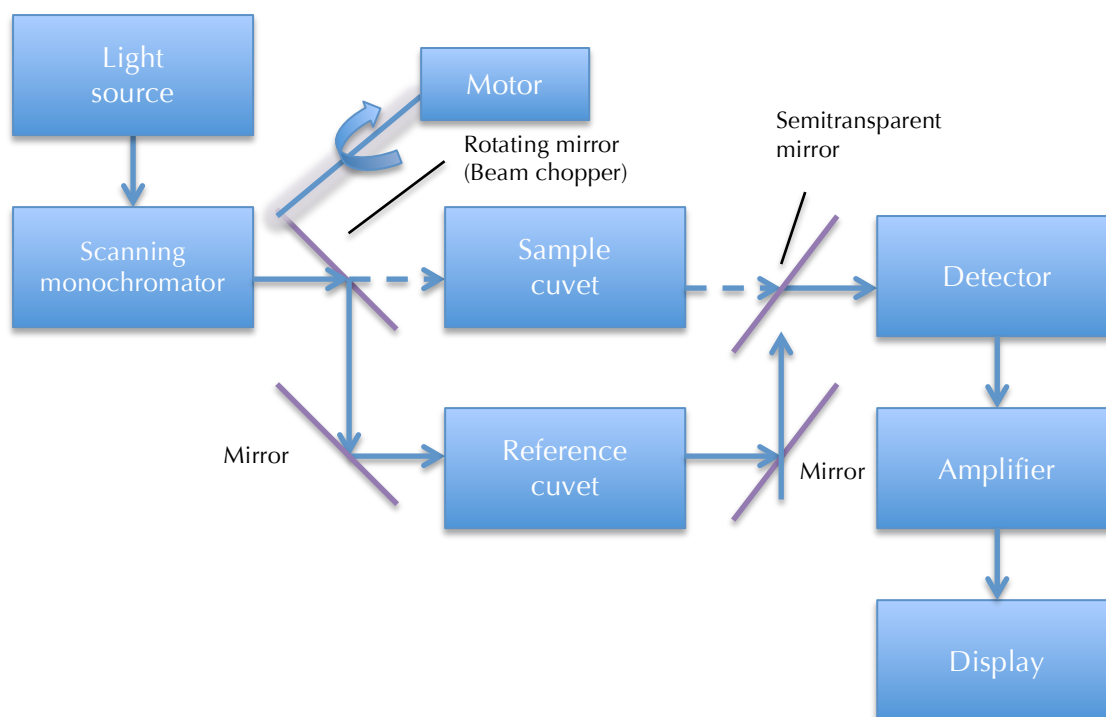


Figure 2-17. Scheme of spectrophotometer components [56].

2.4.4 Quartz Crystal Microbalance

Quartz crystal microbalance (QCM) is an ultrasensitive device that measures the mass of a certain material deposited on a quartz crystal surface. This is possible due to a change in the oscillating crystal's resonant frequency when is placed into alternating electric field and mass is deposited. There are different parameters affecting the frequency: the environment at crystal's surface, the mass and characteristics of the coating, and the properties of the solution near the electrode surface. In this factors, viscosity, density, concentration and charge density are included.

QCM allows the measurement of changes referred to mass and structural properties. The quartz crystal oscillates at its resonance frequency and mass changes in the surface are measured in frequency changes, as Δf . Moreover, changes in dissipation of the oscillating crystal give an idea of structural properties. Dissipation is determined from the time it takes for the oscillation to stop when the power is disconnected. A formation of a soft molecular layer increases the dissipation (Figure 2-18) [57].

The basic components of a QCM are: a source of alternating current (the oscillator), a quartz crystal, two metal electrodes on opposites sides of the thin crystal wafer, and a frequency counter.

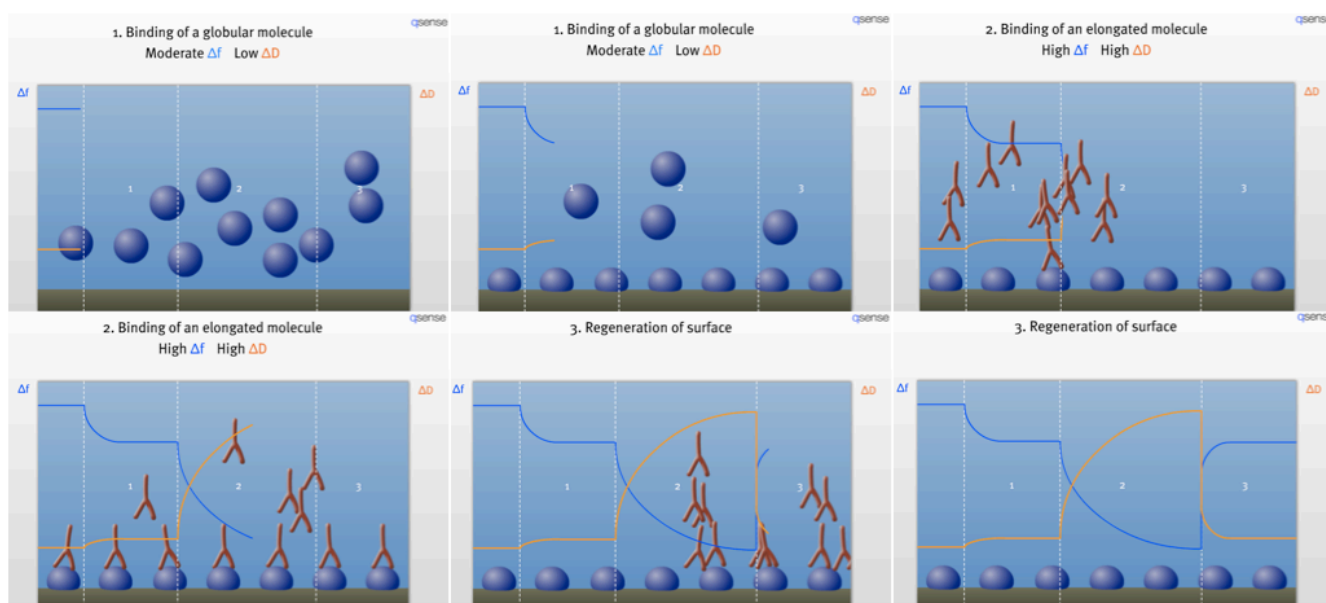


Figure 2-18. Graphic procedure in QCM measurements [57].

Masses range of measurements in QCM includes from micrograms to fractions of a nanogram, the mass of a layer or even a partial layer of atoms. This mass can be calculated with the Sauerbrey equation:

$$\Delta m = -\frac{C \cdot \Delta f}{n}$$

in which Δm is the change in mass, C is the sensitivity constant ($17.8 \text{ ng cm}^{-2} \text{ Hz}^{-1}$), Δf is the shift in frequency, and n is the number of the harmonic.

2.4.4.1 Sauerbrey equation: validity for the theory in thin films

Sauerbrey equation can be applied successfully as long as the film is thin enough. Demonstration of the validity of the Sauerbrey equation for thin thickness, the frequency and dissipation of quartz crystals coated with poly(4-ammonium styrenesulfonic acid) film was measured during expose to saturated water vapour. The film becomes less rigid as substance is absorbed, allowing for deviations from the Sauerbrey equation. Nevertheless, not all films presented a deviation from ideal behaviour despite equal water content in the films. There were three parameters affecting the deviation: the film viscosity, thickness and resonator frequency. A term $\beta_1 D$ can be used to determine the deviations from ideality. These deviations were observed for $\beta_1 D > 0.26 \pm 0.10$, in agreement with the theoretical limit of 0.28. According to this, Sauerbrey equation can be applied to thin films successfully [58].

Chapter 3

Materials and methods

3.1 Gold nanoparticles

3.1.1 Materials

Tetrachloroauric (III) acid ($\text{HAuCl}_4 \cdot 3\text{H}_2\text{O} \geq 99.99\%$), sodium borohydride ($\text{NaBH}_4 \geq 99.99\%$), were all purchased from Sigma-Aldrich. Ascorbic acid (D-(-)Isoascorbic acid $\geq 99\%$) was obtained from Fluka. 11-Mercaptoundecanoic acid was provided by Ugelstad Laboratory of NTNU (Trondheim, Norway).

3.1.2 Ascorbic acid reduction

Gold nanoparticles were synthesized by the reduction of the gold precursor HAuCl_4 with ascorbic acid. 10 mM tetrachloroauric acid (34 mg/10 mL) and 100 mM ascorbic acid (176.1 mg/100 mL) in aqueous (MilliQ water) solution were prepared. The stock solution of gold is stable for several months but the ascorbic acid solution was prepared fresh and only stored for some days to eliminate the risk of degradation by oxidation [31].

In a beaker under mechanical stirring at room temperature, gold precursor was added and mixed with the volume ratio 1:1 with ascorbic acid.

All dilutions of tetrachloroauric acid and ascorbic acid were made with MilliQ water.

3.1.3 Sodium borohydride reduction

The synthesis of gold nanoparticles was carried out by reduction of HAuCl_4 with NaBH_4 and MUA as stabilizer. 10 mM tetrachloroauric acid in aqueous (MilliQ water) solution, MUA 10 mM (10.9 mg/5 mL ethanol) and NaOH 0.25M were prepared.

At room temperature, MUA was added to the gold precursor to stabilize the gold nanoparticles were going to be synthesized. After this, an addition of NaOH is made to reach an alkaline pH due to the stability achieved by carboxylic group deprotonation [33]. The posterior addition was NaBH_4 , the reducer agent.

All dilutions made for preparing the different concentrations needed in tetrachloroauric acid and sodium borohydride were made with MilliQ water.

3.2 Chitosan

3.2.1 Material

Chitosan samples used in gold nanoparticles surface coating were provided by Dr. Sabina P. Strand (Department of Biotechnology, Norwegian University of Science and Technology). Table 3-1 presents some of the properties of chitosan samples.

Table 3-1. Chitosan samples properties. FA: degree of acetylation. DPn: polymerization degree. AAM is a trisaccharide formed by GlcNAc and anhydromannose. SB is a branched structure via Schiff bases.

Chitosan sample	FA	DPn	Intrinsic viscosity (mL/g)	Others
K1	0	200		
K2	0	400		
K3	0.01	800-1000	810	
K4	0.15	300	280	
K5				SB alpha 0.01
K6	0.48			
K7		75-AAM		

Polymerization degree is directly related with the Molecular weight of the polymer. K1, K2, K3, K4 and K5 chitosan samples were provided for the adsorption in the layer between the gold nanoparticle and siRNA. On the other hand, K6 and K7 chitosan were suggested as a final covering when the siRNA and chitosan were attached in several layers.

3.2.2 Chitosan solutions preparation

All chitosans were dissolved in MilliQ water in a concentration 0.2 mg/mL and buffered with equal volume of 50 mM HAc/NaAc buffer pH 5.5. The chitosan samples had a final concentration of 0.1 mg/mL.

Chitosan solutions were stored in a freezer for about a week and after this were frozen.

3.3 siRNA

3.3.1 Materials

siRNA was supplied by Dr. Sabina P. Strand (Department of Biotechnology, Norwegian University of Science and Technology).

3.3.2 siRNA solutions

siRNA was diluted in MilliQ water in a concentration 0.02 mg/mL. After this, the solution was buffered with 50 mM HAc/NaAc buffer pH 5.5 obtaining a final concentration of 0.01 mg/mL

siRNA was directly diluted in 50 mM HAc/NaAc buffer pH 5.5 obtaining a concentration of 0.02 mg/mL.

Sterile pipette tips were used in the experiment due to the easy degradation of the siRNA.

3.4 Coatings

3.4.1 AuNP/Chitosan

The gold nanoparticles covering with chitosan was prepared mixing the same volume of solutions prepared before, chitosan with MilliQ water buffered and the gold nanoparticles obtained.

3.4.2 AuNP/Chitosan/siRNA

For covering the AuNP/Chitosan obtained in the previous step the procedure is only to add the siRNA solution at room temperature.

3.5 Zetasizer

Size and zeta potential measurements of gold nanoparticles were carried out in the Ugelstad laboratory (NTNU, Trondheim) with Nano ZS 3600 from Malvern Instruments.

Following the procedure [59], zeta cells supplied by Malvern were cleaned with ethanol solution, dried with air and filled with the sample for analysing. Regarding the parameters of the instrument: the model used was Smoluchowski, the number of measurement was fixed as 3 and they were reproduced twice.

3.6 UV-vis spectrophotometer

UV-vis spectrophotometer UV-2401 PC from Shimadzu was used to obtain the absorption measurements of gold nanoparticles in the Ugelstad Laboratory (NTNU, Trondheim).

Samples were analysed with quartz cells of 10 and 2 mm supplied by Hellma with MilliQ water as reference. The wavelength range was established between 190-1100 nm and each sample was measured twice. After each use cells were cleaned with MilliQ water and acetone and dried with air.

For analysing data acquired with UV-vis spectrophotometer was necessary to elaborate a calibration curve for obtaining the molar absorption coefficient, ϵ . Solutions of known concentration gold were prepared and measured with the UV-vis spectrophotometer (Table 3-2) determining the value of absorbance at 525 nm. Following Beer-Lambert's, with the lineal representation absorbance vs concentration (mM) the coefficient was estimated with the slope (Figure 3-1).

Table 3-2. Absorbance obtained for determined gold samples concentration.

Sample	Concentration (mM)	Absorbance
1	$3.32108 \cdot 10^{-7}$	1,136
2	$2.65686 \cdot 10^{-7}$	0,924
3	$6.64216 \cdot 10^{-8}$	0,268
4	$2.12549 \cdot 10^{-7}$	0,747
5	$1.70039 \cdot 10^{-7}$	0,609
6	$1.36031 \cdot 10^{-7}$	0,492

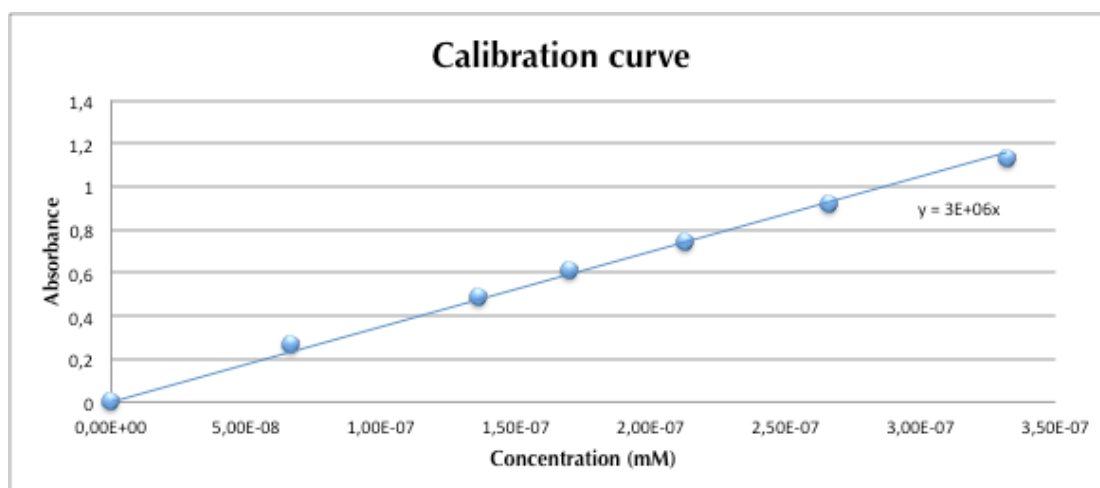


Figure 3-1. Calibration curve for gold samples.

The molar absorption coefficient obtained was:

$$\varepsilon = 300,000 \text{ mM}^{-1} \cdot \text{mm}^{-1}$$

3.7 Quartz Crystal Microbalance

Measurements of Δm in different coatings were obtained with qsense D300 from Qsense Instruments in Ugelstadlab (NTNU, Trondheim).

The Au-coated crystals were cleaned for 20 minutes in a Piranha solution consisting of H_2SO_4 and H_2O_2 in the ratio 3:1. After this, crystals were rinsed with MilliQ water and dried with air. In some experiments it was necessary to cover the Au-coated crystals with MUA introducing the crystals in a solution 10 mM of this chemical reactant for 24 hours. Then, crystals were rinsed with ethanol for removing the MUA excess.

For the measurements, all data were taken from the harmonic $n=3$.

Chapter 4

Results and discussion

This chapter is divided into 4 sections that show the chronological steps followed in the researching. In first place, the study was focused into the synthesis of AuNP/Chitosan/siRNA nanoparticles that was the aim established for this thesis. Nevertheless, with the results obtained was necessary to considerate possible solution to achieve nanoparticles with the most similar characteristics. The following steps considering alternatives was the analysis of AuNP/C₁₆TAB/siRNA nanoparticles, AuNP/PEI/siRNA nanoparticles, and AuNP/Chitosan nanoparticles crosslinked with EDAC

4.1 Synthesis of AuNP/Chitosan/siRNA nanoparticles

This study started with the gold nanoparticles synthesis followed by the coating tests for the obtaining of AuNP/chitosan/siRNA nanoparticles. The last step in each coating was to realise a characterization of results achieved with the aim of prove the accomplishment of the expectations.

4.1.1 Gold nanoparticles synthesis

Firstly, gold nanoparticles were synthetized by two methods: ascorbic acid reduction and sodium borohydride reduction with MUA stabilization. All gold nanoparticles synthesis require the presence of a passivating ligand/stabilizer; ascorbic acid procedure offers reduction and stabilization in a single step, whereas the reduction with NaBH₄ need a separate stabilizer.

For the synthesis, different concentration of chemical reactants such as gold precursor, reducing agent and passivating ligand were used with the objective to check the variation of the properties and optimize conditions in order to continue with the next covering steps.

4.1.1.1 Gold nanoparticles obtained by ascorbic acid reduction

Gold nanoparticles were prepared following the procedure related in chapter 3. For obtaining different size range, various relations of chemical reactants concentration were used. The modification of reducing agent concentration was determinant in the nanoparticles diameter owing to the fact that the less reducer agent is added, the larger the particles will be produced. This is logical since if the reducer concentration is lower is more difficult to reduce the tetrachloroauric acid, and at the same time and stabilize the particle.

Table 4-1 shows different relations tetrachloroauric acid/ascorbic acid used in the synthesis of gold nanoparticles produced in the volume ratio 1:1.

Table 4-1. Relation of tetrachloroauric acid and ascorbic acid for different experiments in gold nanoparticles synthesis with ascorbic acid reduction.

Experiment	Tetrachloroauric acid (mM)	Ascorbic acid (mM)
a	0.1	10
b	1	10
c	1	25
d	1	30
e	1	50
f	1	100

The first indication of gold nanoparticles successfully synthesized was the deep red wine colour obtained (Figure 4-1). This colour is different depending on the sample owing to this characteristic is strongly dependent of the size and the shape of the nanoparticles. To characterise Gold nanoparticles obtained, properties were analysed with UV-vis spectrophotometer and nanosizer.

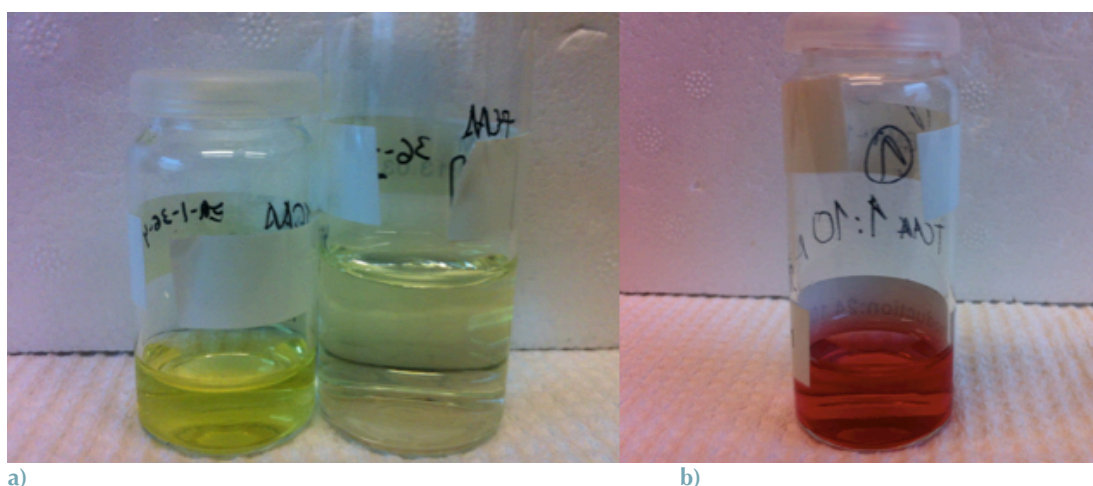


Figure 4-1. a) tetrachloroauric acid 10 mM on the left and 1 mM on the right, gold precursor before the reduction reaction. b) gold nanoparticles obtained with the reduction of tetrachloroauric acid with ascorbic acid with relation 1:10.

Size

The determination of gold nanoparticles size was accomplished using the Zetasizer. The diameters measured were in values between 45.07 ± 3 and 74.55 ± 2 nm (Figure 4-2). These results were approximately hoped since the highest diameter belongs to gold nanoparticles synthesized with the lowest ascorbic acid concentration (TCAA 1mM: ascorbic acid 10 mM). The difference between diameters is not big but it is noticeable, as the ascorbic acid concentration was higher the size decreased.

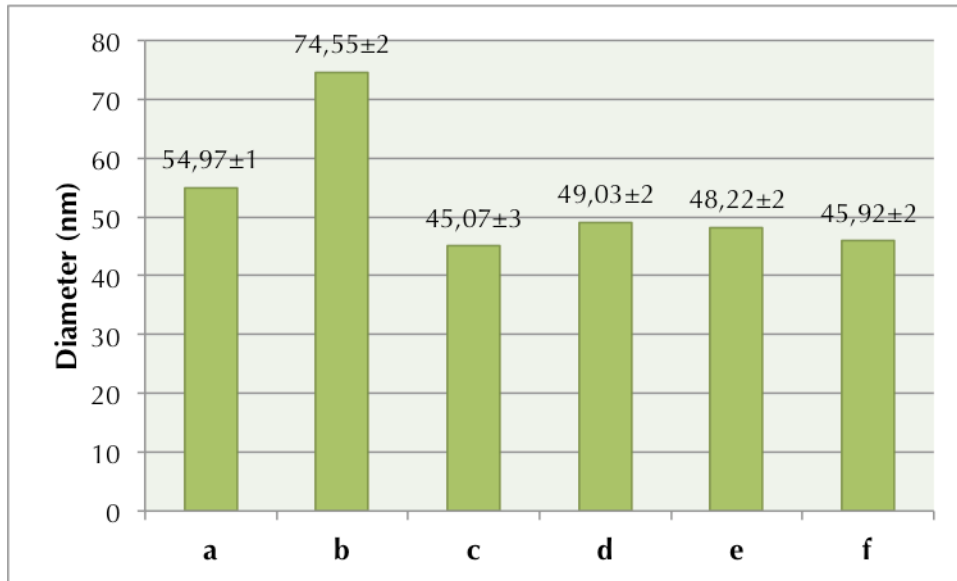


Figure 4-2. Diameters of gold nanoparticles acquired with Nanosizer with the uncertainty associated for the experiment carried out with different concentration ratio tetrachloroauric acid (mM): ascorbic acid (mM) a) 0.1:10, b) 1:10, c) 1:25, d) 1:30, e) 1:50, f) 1:100.

Zeta potential

Zeta potential data was acquired by mean of the Zetasizer instrument. All gold nanoparticles synthesized showed a zeta potential value in a range from -30.15 ± 4 mV to -37.85 ± 2 mV (Figure 4-3). Generally, a suspension can be considered as stable by electrostatic mechanisms if the absolute value of the zeta potential exceeds 25-30 mV, depending on the particle size. Taking this hypothesis as a starting point, all gold nanoparticles obtained can be considered stable and there was not a tendency to form aggregations. These values will be useful subsequently to observe if the deposition of the layer in the coating step was successfully or not.

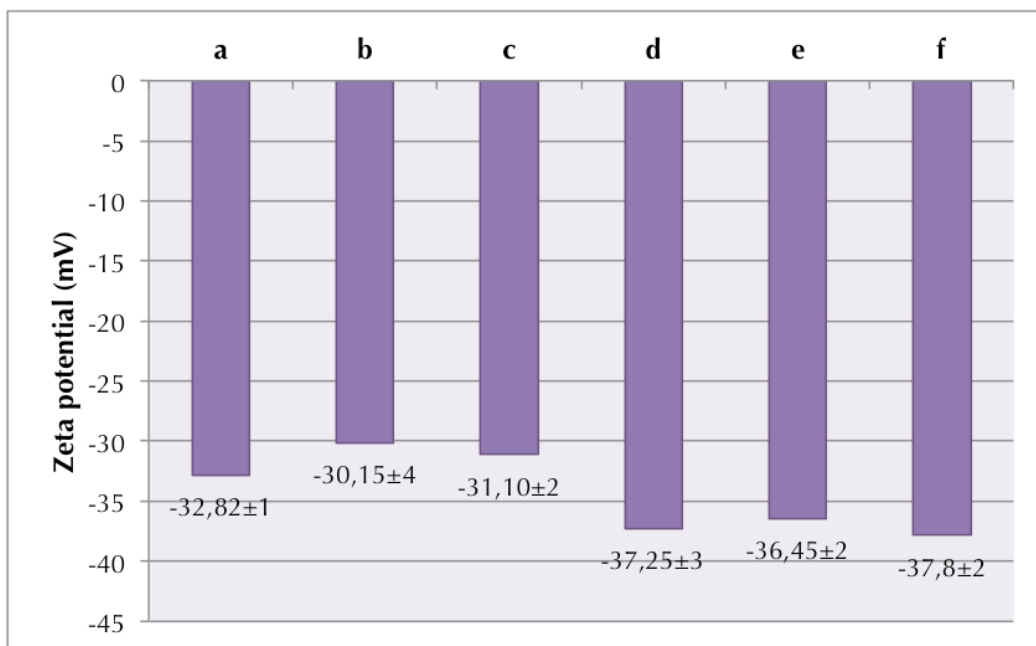


Figure 4-3. Zeta potential obtained with Nanosizer measurements with the uncertainty associated for the gold nanoparticles synthesized by ascorbic acid reduction with ratio tetrachloroauric acid (mM): ascorbic acid (mM) a) 0.1:10, b) 1:10, c) 1:25, d) 1:30, e) 1:50, f) 1:100.

UV-vis spectra

UV-vis spectrophotometer provided absorbance data allowing the concentration calculation applying the Lambert-Beer's law (Table 4-2). Localized Surface Plasmon Resonance, as was defined in chapter 2, is the localization of the electromagnetic field around the metal surface producing electron density oscillation. The extinction spectrum generated allows estimating some parameters due to the dependence on the size, shape, and aggregation level. Regarding the size, the higher LSPR value, the larger the particle diameter. This peak value of surface plasmon resonance was obtained around 525 nm and this indicates the sample can be considered monodispersed and absented of aggregations (Figure 4-4) except in the case of the experiment realized with 0.1:10 ratio with a broad absorption band with no clear maximum at 536 nm. The rest of gold nanoparticles have a similar size and this is the reason why the peak values are between 522-524 nm in all of them. Particularly is remarkable the peak value of particles with 54.97 ± 1 nm that is 535 nm, approximately the same than the particles with bigger size but this can be produced by the fact that the peak of the spectra is not really marked.

Table 4-2. Characterisation with UV-vis spectrophotometer. Concentration calculated with absorbance and wavelength of the peak of plasmon resonance.

Experiment	Tetrachloroauric acid (mM): Ascorbic acid (mM)	Concentration (mM)	Peak value (nm)
a	0.1:10	$7.18 \cdot 10^{-8}$	536
b	1:10	$5.42 \cdot 10^{-7}$	535
c	1:25	$4.68 \cdot 10^{-7}$	522
d	1:30	$6.20 \cdot 10^{-7}$	524
e	1:50	$6.01 \cdot 10^{-7}$	523
f	1:100	$6.19 \cdot 10^{-7}$	522

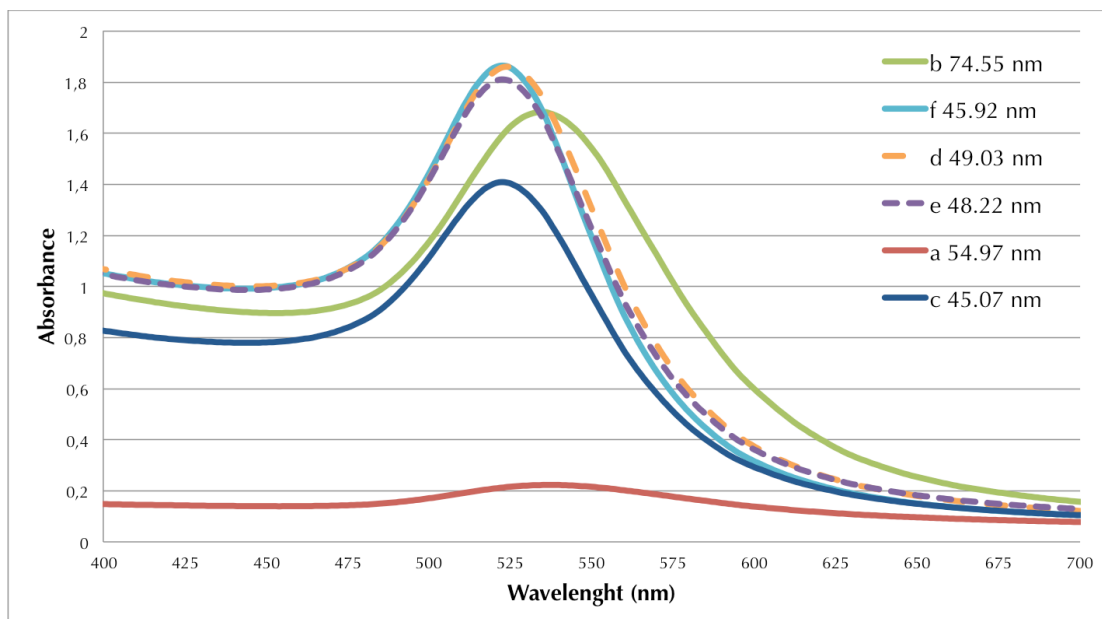


Figure 4-4. UV-vis spectra of gold nanoparticles synthesized by ascorbic acid reduction in a different ratio tetrachloroauric acid (mM):ascorbic acid (mM). a) 0.1:10, b) 1:10, c) 1:25, d) 1:30, e) 1:50, f) 1:100.

4.1.1.2 Gold nanoparticles obtained by sodium borohydride reduction and MUA stabilizing

The reduction of tetrachloroauric acid with sodium borohydride was completed following the methodology explained in chapter 3. The experiments were carried out with diverse chemical reactant concentrations with the purpose of obtaining different gold nanoparticles size, and with a volume ratio in mL of tetrachloroauric acid:MUA:NaOH:NaBH₄ of 1:0.1:0.1:0.1 (Table 4-3). Tetrachloroauric acid concentration was adjusted between 1-5mM after trying a higher concentration. Gold precursor concentration of 10mM was experimented and the nanoparticles formed aggregations probably caused by the acid character of the medium. NaOH added increase the pH stabilizing the particle dispersion deprotonating the carboxylic acid groups of MUA but probably in some case this amount was not enough [33].

Table 4-3. Concentration of chemical reactants for different experiments in gold nanoparticles synthesis with sodium borohydride reduction and MUA stabilization.

Experiment	Tetrachloroauric acid (mM)	MUA (mM)	NaOH (M)	NaBH ₄ (mM)
g	1	10	0.25	10
h	1	10	0.25	1
i	5	10	0.25	10
j	5	10	0.25	1

After 5 months, it was possible to observe directly with the human eye the aggregations formed in all experiments Figure 4-5.

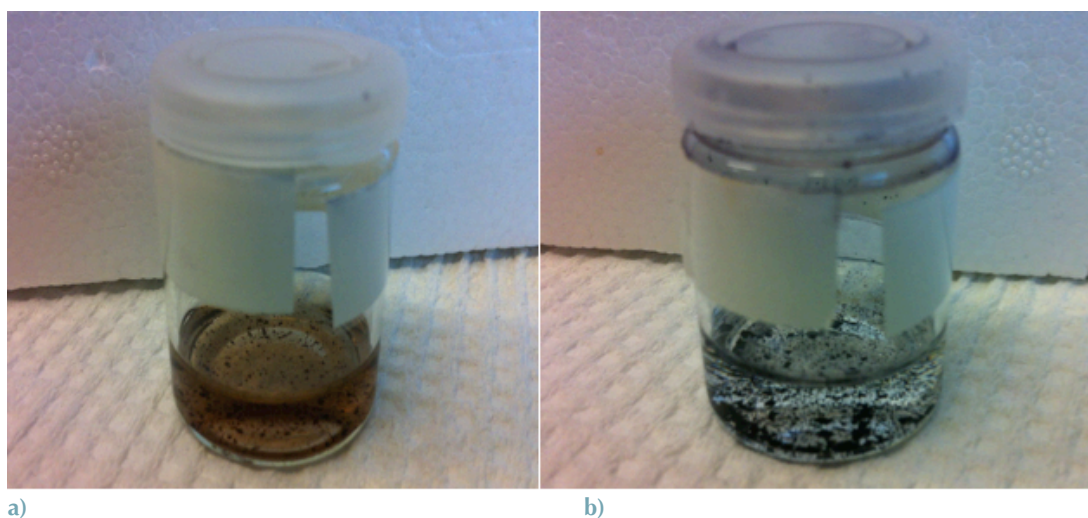


Figure 4-5. Gold nanoparticles precipitated out 5 months after the synthesis realized with the relations showed for a) experiments g and h b) experiments i and j.

Size

For gold nanoparticles produced with TCAA concentration of 5 mM the finally size is around 610 ± 142 nm, 618.17 ± 260 nm when the sodium borohydride concentration is 1 mM and 610.50 ± 142 nm when it is 10 mM (Figure 4-6). Nevertheless, when a TCAA concentration of 1mM was used the nanoparticles had a size measurement of

159.50±12 nm with 10 mM sodium borohydride and 127.67±22 nm with 1 mM. Consequently, the gold precursor concentration used affects strongly to the final size of gold nanoparticles being the sodium borohydride concentration important but not in the same magnitude.

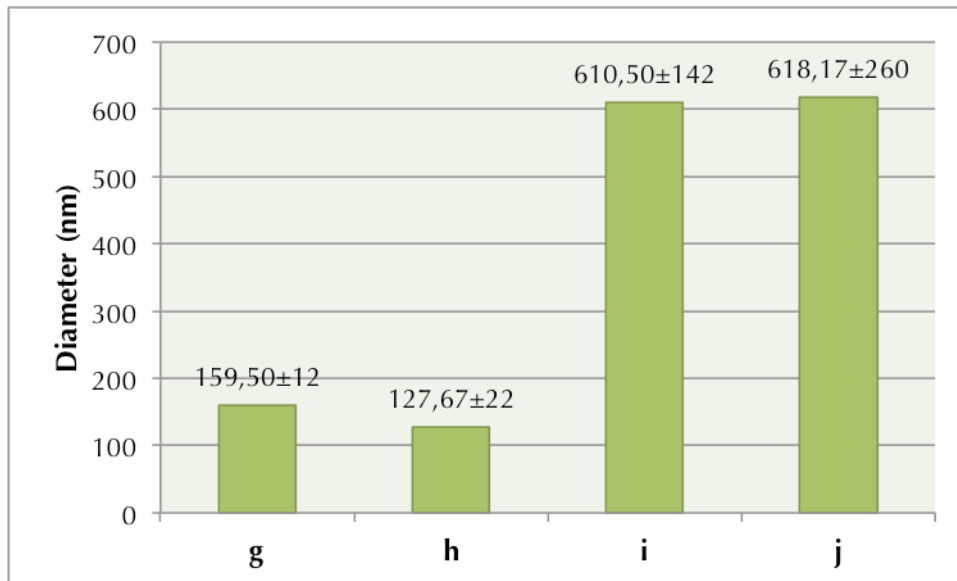


Figure 4-6. Different diameters (nm) with the associated uncertainties associated for gold nanoparticles obtained by synthesis with sodium borohydride as reducer agent. The relation TCAA (mM): NaBH₄(mM) in the experiment was g) 1:10, h) 1:1, i) 5:10, j) 5:1.

Zeta potential

Zeta potential estimated with Zetasizer resulted in a range from -30.60±4 to -39.18±4 mV (Figure 4-7). This parameter is not size dependent [22] and this is the reason that there is a big difference in size depending on the concentration of gold precursor but this is not noticeable in zeta potential measurement. Moreover, the values of zeta potential are more negative than -30 mV hence the solutions are considered stable.

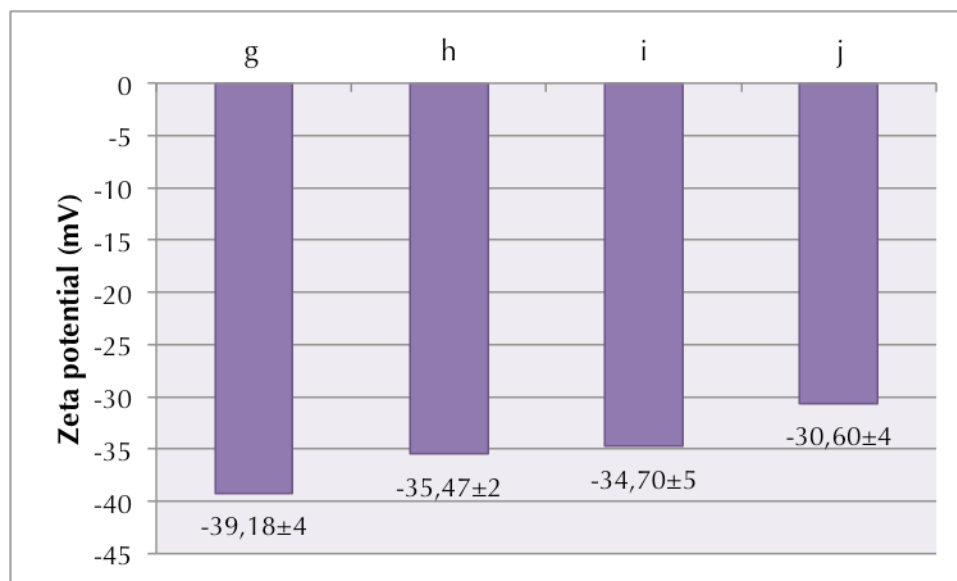


Figure 4-7. Zeta potential (mV) with associated uncertainty measured in gold nanoparticles synthesized with the relation TCAA (mM): NaBH₄ (mM) g)1:10, h) 1:1, i) 5:10, j)5:1.

UV-vis spectra

UV-vis spectrophotometer allowed the acquirement of absorbance data for the concentration calculating (Table 4-4). The UV-vis spectra (Figure 4-8) shows the peak value of surface plasmon resonance for the different gold nanoparticles obtained. It is remarkable the fact that the gold nanoparticles obtained starting with the tetrachloroauric acid concentration 1mM did not present a peak in the UV-vis spectra due to the formation of aggregations leaving only the small particles not representatives of the sample. In experiments "i" and "j" there was a broad absorption band and a no clear maximum due to the progressively aggregations produced.

Table 4-4. Concentration calculated for the gold nanoparticles synthesized in TCAA(mM): NaBH₄ (mM) g)1:10, h) 1:1, i) 5:10, j)5:1.

Experiment	Tetrachloroauric acid (mM): Sodium borohydride (mM)	Concentration (mM)	Peak value (nm)
g	1:10	$2.78 \cdot 10^{-7}$	-
h	1:1	$1.66 \cdot 10^{-7}$	-
i	5:10	$2.73 \cdot 10^{-6}$	510
j	5:1	$2.70 \cdot 10^{-6}$	510

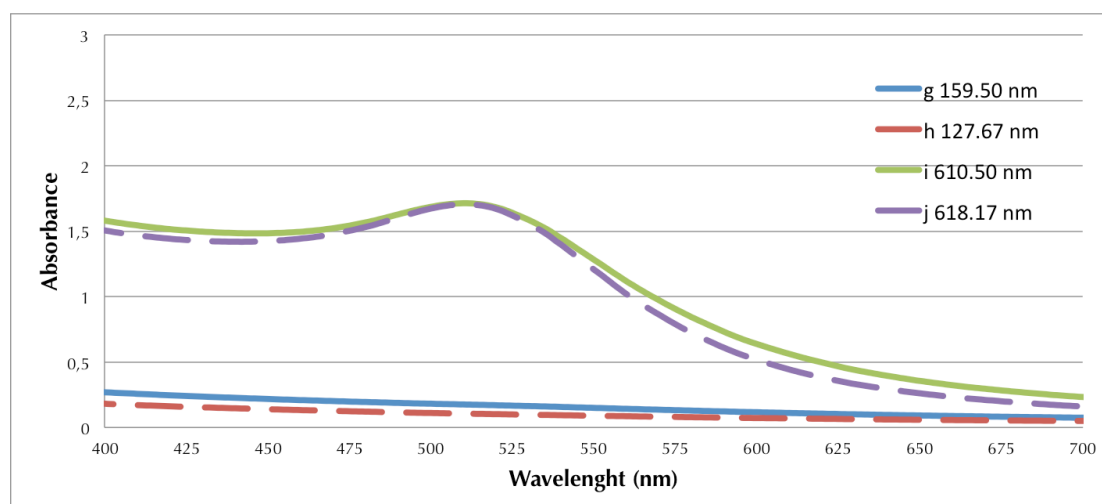


Figure 4-8. UV-vis spectra of gold nanoparticles synthesized with the relation TCAA (mM): NaBH₄ (mM) g)1:10, h) 1:1, i) 5:10, j)5:1.

4.1.2 Coating of gold nanoparticles with chitosan (AuNP/Chitosan nanoparticles)

On completion of gold nanoparticles synthesis and characterisation, the next step to consider was the coating of gold nanoparticles with chitosan. For this coating, the starting point was to analyse with the Quartz Crystal Microbalance if the chitosan is successful attached to gold surface and how fast and how strong depending on the different chitosan sample. After this analysis, it was necessary to cover the gold nanoparticles with the chitosan to characterize them.

4.1.2.1 QCM analysis simulating chitosan coating in a gold surface covered with MUA.

The first analysis realised was the coating of chitosan into a gold surface covered with MUA. Thiolated chitosan has been widely studied in drug delivery applications [60] [61] and because of this, it can be supposed that they have a good interaction. For quantifying the amount of chitosan that could be bound to the nanoparticle, the Quartz Crystal Microbalance was determinant.

The procedure applied has to be a representation the most similar to the process that is the object of study. For the exactly reproduction in the instrument, the Au-coated crystals were covered before the use with MUA 10 mM following the procedure related in chapter 3. MilliQ water was injected firstly into the instrument to establish the base line. When this line could be considered stable, the chitosan sample (0.1 mg/mL, preparation in chapter 3) was introduced into the chamber through a 0.2 µm filter. This last addition was reproduced 3 times because the concentration of chitosan required was not known when the measurement is carried out. This repetition guaranteed that the amount of chitosan adsorbed is the maximum possible. To finish, acetic acid HAC/ sodium acetate NaAc buffer 50 mM was injected twice. This last step was realized to check the irreversibility of chitosan adsorption. Hence, the buffer was flushed trough the chamber because chitosan samples were buffered after the preparation of the solutions.

Quartz Crystal Microbalance provided data about the oscillating frequency changes when a substance was added. In this case, the object of the study was the chitosan and the knowledge of the mass attached was possible applying the Sauerbrey equation:

$$\Delta m = - \frac{C \cdot \Delta f}{n}$$

This equation had to be study to check the validity for thickness layer due to the fact that mass changes have to be related with the viscoelasticity of the layer. This validation is developed in chapter 3. The aim is not only to adsorb the chitosan into gold nanoparticle surface, but also the knowledge of how fast and how strong is the coating with the different chitosan samples. Hence, time and mass adsorbed was evaluated for each chitosan sample (Table 4-5).

The oscillating frequency progress could be evaluated following a chart that provides information not only about important points to calculate the adsorbed/desorbed mass but also how is the process evolution. In this case, Figure 4-9 and Figure 4-10 show this information about chitosan samples K1 and K2. In both charts, the frequency changes are very fast and strong and are followed by a flat line indicating the instantaneous adsorption and irreversibility; proved with the last addition of buffer and frequency stability observed.

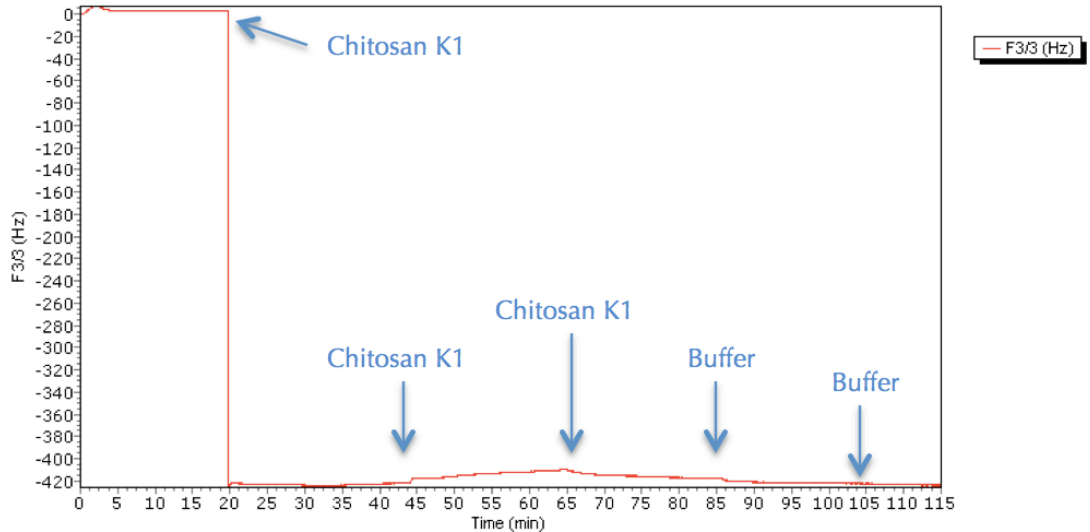


Figure 4-9. Data obtained from simulating with QCM: Au-coated crystal covered with MUA/chitosan K1/buffer.

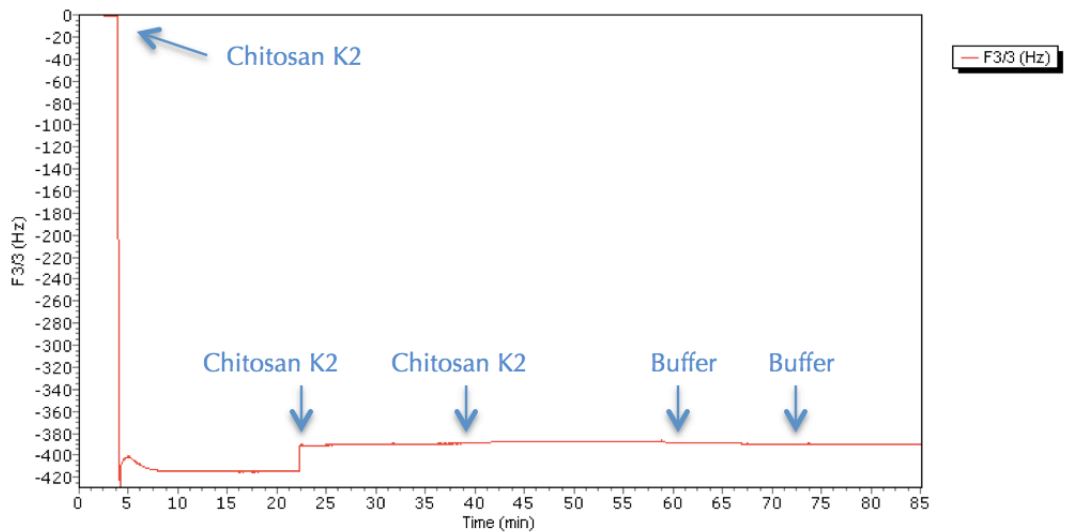


Figure 4-10. Data acquired with QCM for Au-coated crystal covered with MUA/chitosan K2/buffer.

Table 4-5. Quartz Crystal Microbalance data for K1, K2 chitosan samples acquired the third harmonic, $n=3$. The Δt (min) is the time from the beginning of frequency changes to the stabilisation of the frequency after the change, Δf (Hz) is the change in crystal oscillating frequency and Δm (ng/cm^2) is the mass adsorbed calculate.

Chitosan sample	Δt (min)	Δf (Hz)	Δm (ng/cm^2)
K1	1.18	424.51	7556.28
K2	3.71	411.95	7351.87

For both chitosan samples the frequency shift obtained was large, 424.51 Hz for chitosan K1 and 411.95 Hz for chitosan K2. These values involve a large amount of chitosan wrapped on the gold surface, $7556.28 \text{ ng}/\text{cm}^2$ for K1 and $7351.87 \text{ ng}/\text{cm}^2$.

In the matter of time, both chitosan were adsorbed very quickly due to the fact that in only 1.18 and 3.71 minutes, for K1 and K2 respectively, they were totally covering the surface and the oscillating frequency was stable again. These samples have an acetylation degree of 0 but the difference lies in the polymerization degree (DPn). This

characteristic is directly related with the molecular weight, chitosan K1 has a DPn of 200 whereas chitosan K2 is 400. According to this, chitosan K1 had a higher adsorption because of mass attached calculated is bigger and has a lower molecular weight.

As the QCM results exhibit, the attachment of chitosan samples K1 and K2 to gold surface covered with MUA is quickly and apparently successful. Before the testing of the rest of chitosan samples, gold nanoparticles achieved by ascorbic acid reduction were chosen as the most proper for continuing with the covering. This choice was realized because of the size range between 45.07 ± 3 and 74.55 ± 2 nm and the stability checked with zeta potential values. To continue with these nanoparticles was necessary the displacement of ascorbic acid with MUA and the accomplishment was attained adding directly MUA 10 mM solution in a volume proportion of 10%.

The displacement was not successful due to the aggregations that were formed in gold nanoparticles solutions. After trying with all particles samples obtained with ascorbic acid reduction, the same phenomenon happened and was necessary to prepare new gold nanoparticles. It was considered the possibility of a strong linking between the gold surface and ascorbic acid resulting in difficult the accomplishment of this displacement.

4.1.2.2 Synthesis of new gold nanoparticles by ascorbic acid reduction

In the preparation of the new gold nanoparticles, ascorbic acid was used as reducing agent following the procedure shown in chapter 3. The relation of chemical reactants (Table 4-6) used in this new elaboration was the same then in the first try (related in 4.1.1.1) to obtain approximately the same size and stability.

Table 4-6. Relation of tetrachloroauric acid and ascorbic acid in different experiments for the synthesis of gold nanoparticles.

Experiment	Tetrachloroauric acid	Ascorbic acid
a	0.1mM	10mM
b	1mM	10mM
c	1mM	25mM
d	1mM	30mM
e	1mM	50mM
f	1mM	100mM

Visual results of samples after 5 months from the synthesis are shown in (Figure 4-11). Obviously, in case of concentration ratio (mM) 0.1:10 and 1:10 the gold nanoparticles exhibited aggregations.

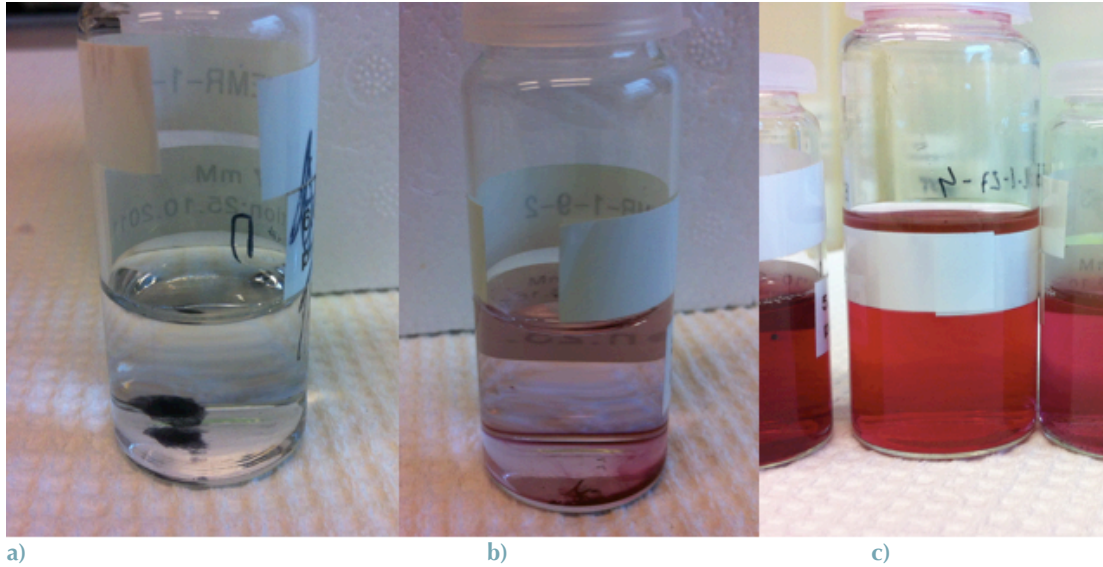


Figure 4-11. Gold nanoparticles obtained reducing the tetrachloroauric acid with ascorbic acid with the concentration ratio (mM) a) 0.1:10, b) 1:10, c) 1:50 after 5 months.

Size

The size range achieved was from 38.08 ± 1 to 128.52 ± 100 nm (Figure 4-12). These particles keep the relation between the quantity of reducer added and the final size being the smallest the nanoparticles synthesized in a ratio 1:100. Only in the case of 1:30 this hypothesis is not fulfilled because the size was expected smaller than 100 nm. The size resulted was bigger compared with the first gold nanoparticles synthesized. The pH was not measured and it is not sure that this is a parameter changing between methodologies. The other factor varied was the volume added, it followed the volume ratio 1:1 but the starting amount was bigger than in the first made. It can be possible that in the moment to add the ascorbic acid, it started to reduce the particles stronger and the size resulted is bigger. Nevertheless, the gold nanoparticles were considered apt to continue with the research.

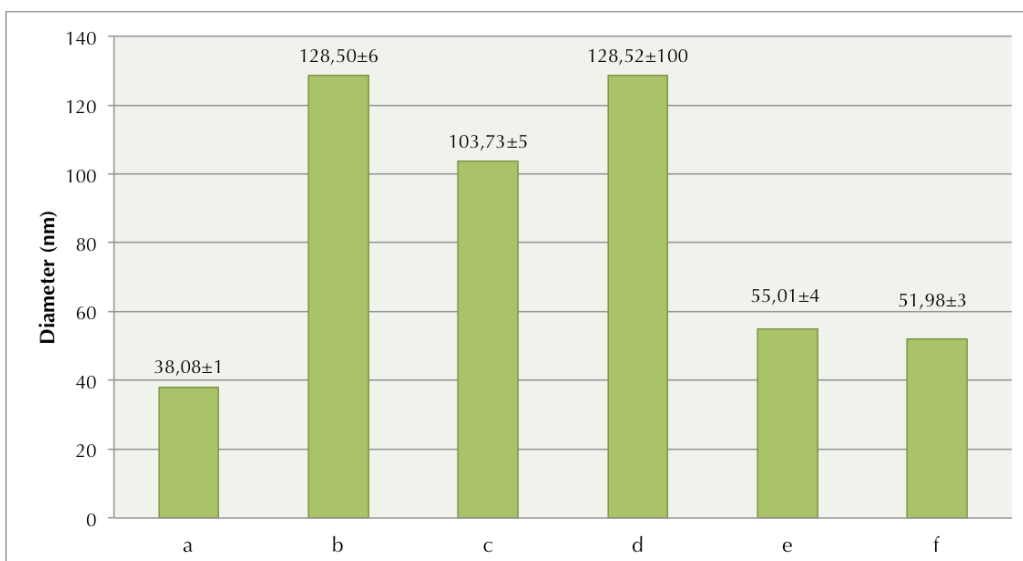


Figure 4-12. Diameter (nm) with uncertainties of new gold nanoparticles obtained by ascorbic acid reduction with different ratio TCAA (mM) : ascorbic acid (mM) a) 0.1:10, b) 1:10, c) 1:25, d) 1:30, e) 1:50, f) 1:100.

Zeta potential

Data acquired with Zetasizer showed Zeta potential values from -24.13 ± 2 to -34.83 ± 2 mV for the gold nanoparticles (Figure 4-13). The common value of zeta potential that is consider to establish if one particle is stable or not is more positive or negative than 30mV but is not a fix value and depending on the referents consulted this limit can be ± 20 mV. Accordingly with this, all gold nanoparticles obtained can be considered stable.

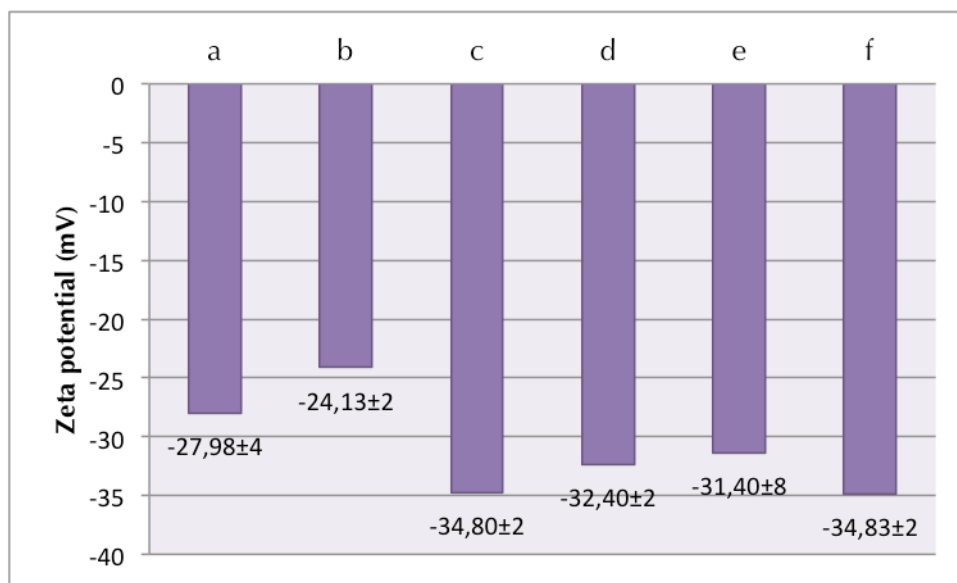


Figure 4-13. Zeta potential (mV) with uncertainties of new gold nanoparticles obtained by ascorbic acid reduction with different ratio TCAA(mM):ascorbic acid (mM) a) 0.1:10, b) 1:10, c) 1:25, d) 1:30, e) 1:50, f) 1:100.

UV-vis spectra

Concentration could be calculated with the absorbance data obtained with the UV-vis spectrophotometer (Table 4-7). The peak value of surface plasmon resonance is around 525 nm and it reveals gold nanoparticles remained as single colloids. Nevertheless, according to the spectra, experiments "a" and "b" present a broad absorption band and the maximum of the plasmon peak is not clear. These results are logic due to the aggregations formed and observed in Figure 4-14.

Table 4-7. Characterisation with UV-vis spectrophotometer. Concentration calculated with absorbance and wavelength of the peak plasmon resonance. Experiments in ratio TCAA(mM):ascorbic acid (mM) a) 0.1:10, b) 1:10, c) 1:25, d) 1:30, e) 1:50, f) 1:100.

Experiment	Tetrachloroauric acid (mM): Ascorbic acid (mM)	Concentration (mM)	Peak value (nm)
a	0.1:10	$6.63 \cdot 10^{-8}$	529
b	1:10	$2.95 \cdot 10^{-7}$	536
c	1:25	$4.73 \cdot 10^{-7}$	536
d	1:30	$4.59 \cdot 10^{-7}$	521
e	1:50	$5.68 \cdot 10^{-7}$	522
f	1:100	$2.84 \cdot 10^{-7}$	522

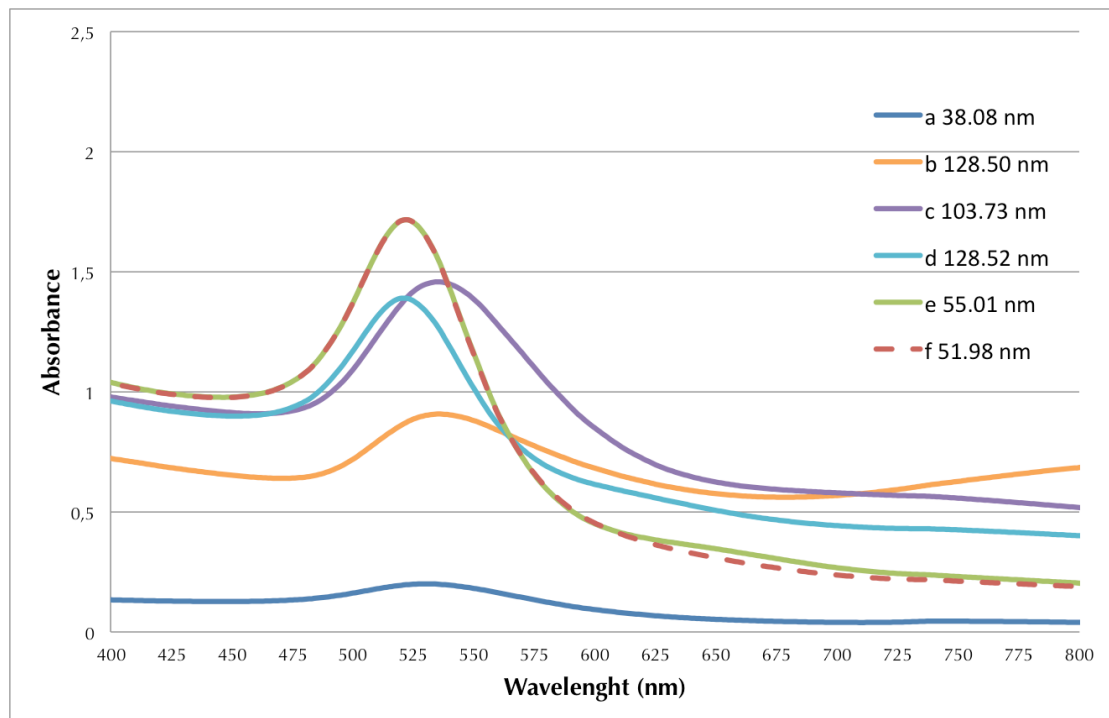


Figure 4-14. UV-vis spectra of gold nanoparticles obtained with ascorbic acid reduction. Different ratio experiments TCAA (mM): ascorbic acid (mM) a) 0.1:10, b) 1:10, c) 1:25, d) 1:30, e) 1:50, f) 1:100.

4.1.2.3 QCM analysis simulating chitosan coating in a gold surface covered with ascorbic acid

As a consequence of the results obtained trying to displace the ascorbic acid with MUA from the surface of gold nanoparticles, a new experiment with the Quartz Crystal Microbalance was accomplished. The objective of this was to observe the adsorption of chitosan into gold surface covered with ascorbic acid acting as the passivating ligand on the gold nanoparticles.

The procedure set in this case, MilliQ water was injected firstly into the instrument to establish the base line. Once the base line was considered stable, ascorbic acid was added to represent the cover of the gold nanoparticles. After this, when the covering with ascorbic acid was succeed, the chitosan sample was introduced through a 0.2 μm filter into the chamber 3 times as in the procedure effectuated with MUA. The last step in this method was to inject acetic acid HAc/ sodium acetate NaAc buffer 50 mM to check the irreversibility.

This procedure was carried out with all the different chitosan samples (K1 to K5) to observe the quantity of each type adsorbed into gold surface and how fast was the adsorption. Oscillating frequency changes were followed visually due to the fact that the evolution gives information about how the process studied is happening. Hence the graphs obtained with each chitosan sample are included. Nevertheless, the visual information is not enough to obtain satisfactory conclusions and the calculations are attached after the charts.

In the case of chitosan K1 (Figure 4-15), the oscillating frequency decreased when the chitosan was injected around 17 minutes after starting due to the deposition experimented. The consecutive additions did not cause another remarkable change, only allowed to reach the equilibrium. After this, the buffer exhibited a linearity considering the system irreversible. The little instantaneous changes observed, for example in minute 5 or 15, were produced when the sample was injected in the loop or in the chamber of the instrument due to the mechanical crash in the injection. These changes will be observed practically in all QCM graphs in the following points.

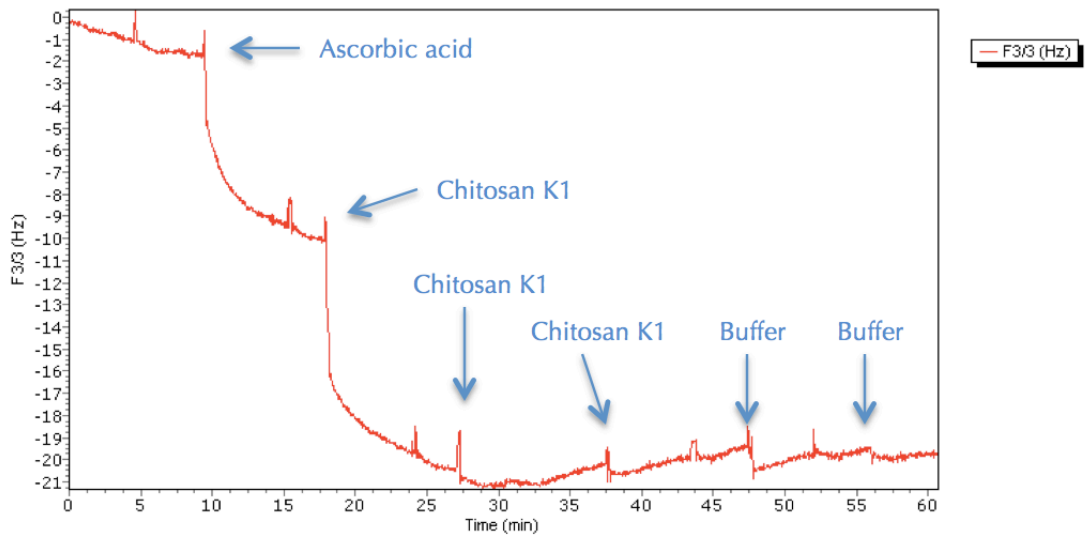


Figure 4-15. Oscillating frequency variation obtained for the simulation Au-coated crystal/Ascorbic acid/Chitosan K1/Buffer.

Data obtained in QCM for the chitosan K2 can be followed in (Figure 4-16). The results were quite similar to the ones obtained for the chitosan K1. After the covering of the surface with ascorbic acid, chitosan K2 injection caused a decrease in the oscillating frequency produced by the adsorption of the polymer into the surface. The next additions of chitosan realized allowed proving that the system had reached the equilibrium. Last step was the flushing of buffer verifying the irreversibility achieved.

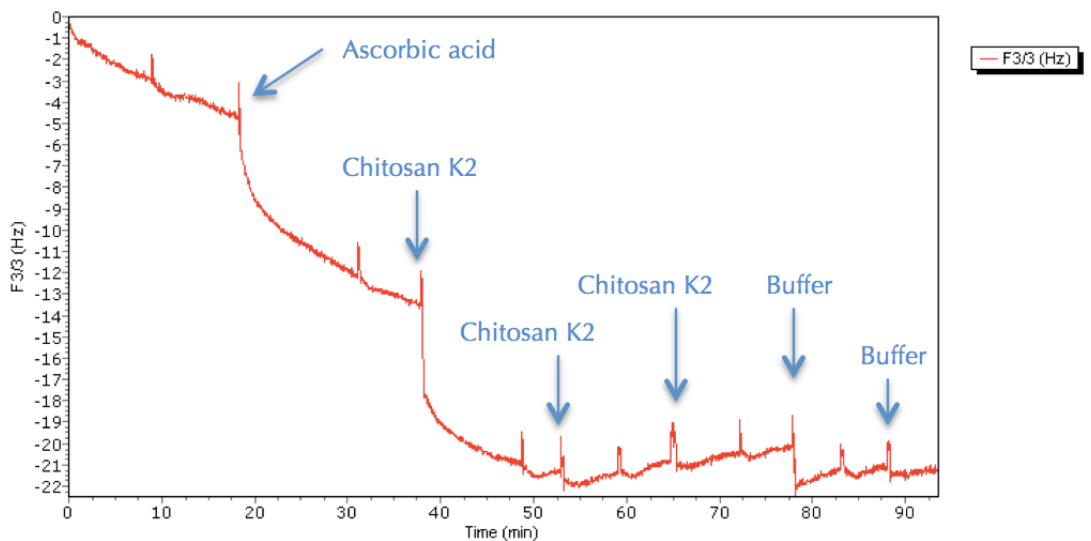


Figure 4-16. QCM analysis of oscillating frequency acquired for the simulation Au-coated crystal/Ascorbic acid/Chitosan K2/Buffer

Chitosan K3 analysis in QCM shows (Figure 4-17) the frequency evolution throughout the experiment. The first addition of chitosan K3 produced a decrease in frequency value owing to the mass adsorbed, as in the experiments realized with K1 and K2 types. Nevertheless, in the second injection, the frequency did not remain stable such in K1 and K2 chitosan; the frequency decreased again because more chitosan was attached into the surface. The third addition exhibited the equilibrium reaches. Afterwards the buffer was flushed into the chamber, there was a little desorption of the chitosan attached in the anterior step.

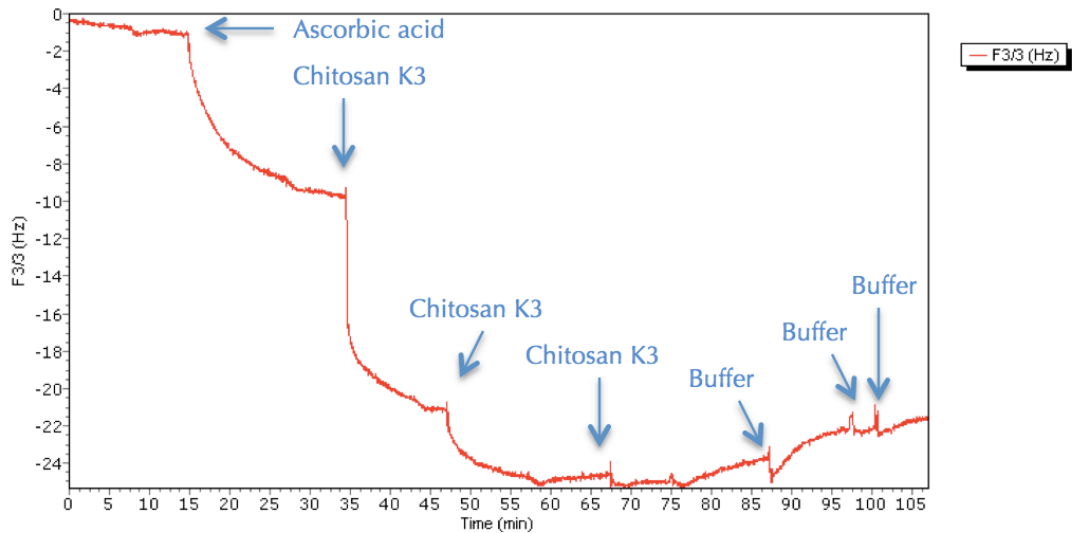


Figure 4-17. Oscillating frequency evolution obtained with QCM for the system Au-coated crystal/Ascorbic acid/Chitosan K3/Buffer.

K4 chitosan exhibited (Figure 4-18) a different behaviour regarding the other samples analyzed. When the chitosan sample K4 was injected the first time, the oscillation frequency started to decrease progressively and after some minutes the tendency was to increase. This could be an indication of surface modification that is not the main goal of this study but it can be interesting for another future studies about AuNP/chitosan particles. The characteristic that differences this chitosan from the other is a higher acetylation degree, 0.15 and maybe this is the reason to explain this comportment. *N*-acetyl groups leads the creation of more expand structures allowing the creation of loops in local zones [62].

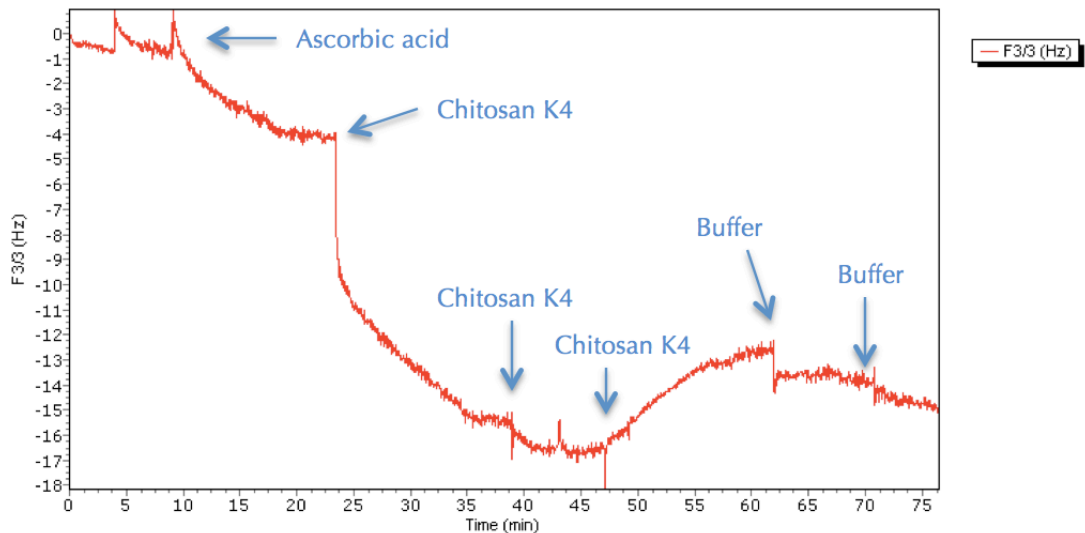


Figure 4-18. QCM analysis of oscillating frequency in system simulation composed by Au-coated crystal/Ascorbic acid/Chitosan K4/Buffer.

Evolution of oscillating frequency for chitosan K5 (Figure 4-19) shows a similar behaviour to the chitosan K1 and K2 samples. Frequency decreased in the first addition of chitosan and remained stable with the consecutive additions. The first injection of buffer produced a change in frequency that probably means a deposition of chitosan that could be over the surface but not totally attached. The next buffer flushing proved the irreversibility.

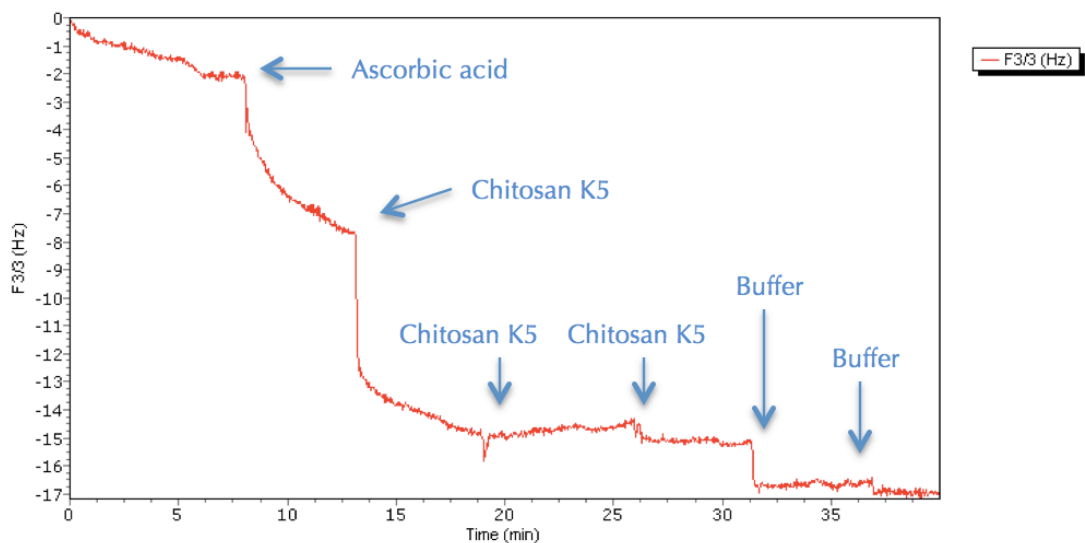


Figure 4-19. Oscillating frequency evolution obtained by means of the QCM for the system Au-coated crystal/Ascorbic acid/Chitosan K5/Buffer.

Frequency changes were the data provided by Quartz Crystal Microbalance instrument and it was related to the mass changes with the Sauerbrey equation explained in chapter 3 (Table 4-8).

Table 4-8. Quartz Crystal Microbalance data for K1, K2, K3, K4 and K5 chitosan samples. The Δt (min) is the time from the beginning of frequency changes to the stabilisation of the frequency after the change, Δf (Hz) is the change in crystal oscillating frequency and Δm (ng/cm²) is the mass adsorbed calculate.

Methodology		Δt (min)	Δf (Hz)	Δm (ng/cm ²)
	Ascorbic acid	8.49	9.40	167.32
Chitosan K1		11.96	8.36	148.81
	Ascorbic acid	19.96	10.44	185.77
Chitosan K2		10.39	7.72	137.48
	Ascorbic acid	18.01	8.75	155.81
Chitosan K3		17.68	15.61	277.86
	Buffer	24.94	-2.87	-51.15
	Ascorbic acid	13.09	3.15	56.13
Chitosan K4		18.70	12.45	221.67
	Ascorbic acid	4.96	5.60	99.62
Chitosan K5		6.05	7.99	142.16

According to the time, chitosan sample in adsorption onto gold surface, K5 provided the best result with 6.05 minutes, followed by K1 and K2 with 11.96 and 10.39 minutes respectively. Compared to these, K3 and K4 required about 18 minutes to obtain a stable frequency value after the shift. Time calculated is an approximation because it is difficult to determine exactly the stabilization in some cases, hence these times values include the change in frequency and the time needed to stabilize the oscillating frequency in the crystal.

Regarding the mass attached to the surface, K3 and K4 gave good results with 277.86 and 221.67 ng/cm² adsorbed respectively but this is not strange because of the long time they needed to be stable. Furthermore, K3 has a higher molecular weight than the other chitosan samples due to the polymerization degree (DP_n) is higher. DP_n is directly related with the molecular weight [63] and it can be the reason about the high value of mass adsorbed. Compared to this, K1 with 148.81 ng/cm², K2 with 137.48 ng/cm² and K5 with 142.16 ng/cm² exhibited a better relation between time of adsorption and mass attached.

Considering the two factors commented before, time to finish the covering and quantity of mass adsorbed, K1 and K2 chitosan samples were chosen as the better combination.

The results garnered with the binding of Au/MUA surface with chitosan were excellent and better than the ascorbic acid results (Table 4-9) but the problems arisen forced the try with the binding of Au/ascorbic acid surface. Nonetheless, the results were positive and it was possible to continue with the analysis of this coating.

Table 4-9. Comparison with results obtained with QCM instrument for MUA or ascorbic acid with K1 and K2 chitosan samples.

Chitosan	MUA		Ascorbic acid	
	Δt (min)	Δm (ng/cm ²)	Δt (min)	Δm (ng/cm ²)
K1	1.18	7556.28	11.96	148.81
K2	3.71	7351.87	10.39	137.48

4.1.2.4 AuNP/chitosan nanoparticles obtaining and characterization

Selected the two chitosan types most promising with the QCM analysis, gold nanoparticles were covered with these to measure different properties and characterize them. The gold nanoparticles were chosen according to the parameters obtained before in the characterization. The particles selected were the ones synthesized with the ratio of tetrachloroauric acid (mM): ascorbic acid (mM) of 1:50, with 55.01 ± 4 nm diameter and zeta potential -31.40 ± 8 mV. Data of mass attached provided by QCM was useful to know the minimum necessary concentration of chitosan prior the covering of gold nanoparticles. The surface available in the particles was known by means of the diameter obtained with the Nanosizer (Table 4-10).

Table 4-10. Surface available for covering in gold nanoparticles. Minimum chitosan K1 and K2 concentration necessary for nanoparticles covering. K1 and K2 chitosan concentration chosen considering the spherical shape.

Chitosan sample	Gold nanoparticle surface (nm ² /particle)	Minimum m_{chitosan} (mg/mL AuNP solution)	Chitosan concentration for AuNP coating (mg/mL)
K1	9507.12	0.00484	0.09
K2		0.00447	0.1

Au-coated crystals used in QCM analysis has a flat surface where the coatings studied are deposited. This surface has to be considered in this study due to the spherical shape of nanoparticles because the covering is carried out in a different way depending on the form. To prevent this factor, the concentration of the chitosan added to the gold nanoparticles was higher than the minimum calculated before.

The gold nanoparticles were covered adding the amount of chitosan samples K1 and K2 mentioned (Table 4-10) with the gold nanoparticles selected before in a volume ratio 1:1. After one hour, different parameters were measured to characterise the chitosan coated gold nanoparticles. All analysis were realised before and after filtering the solutions with 0.2 μm filter to observe the effect of removing chitosan excess.

Size

Size of gold nanoparticles after coating with K1 and K2 chitosan samples was measured with Zetasizer (Figure 4-20). These results presented an increase in diameter that confirms the successful deposition of chitosan into de gold surface. This growth is very similar for both types of chitosan, K1 with a diameter of 162.83 ± 13 nm and K2 with 160.83 ± 24 nm, and after filtering (0.2 μm filter), 149 ± 6 nm for K1 and 144.17 ± 16 nm for K2.

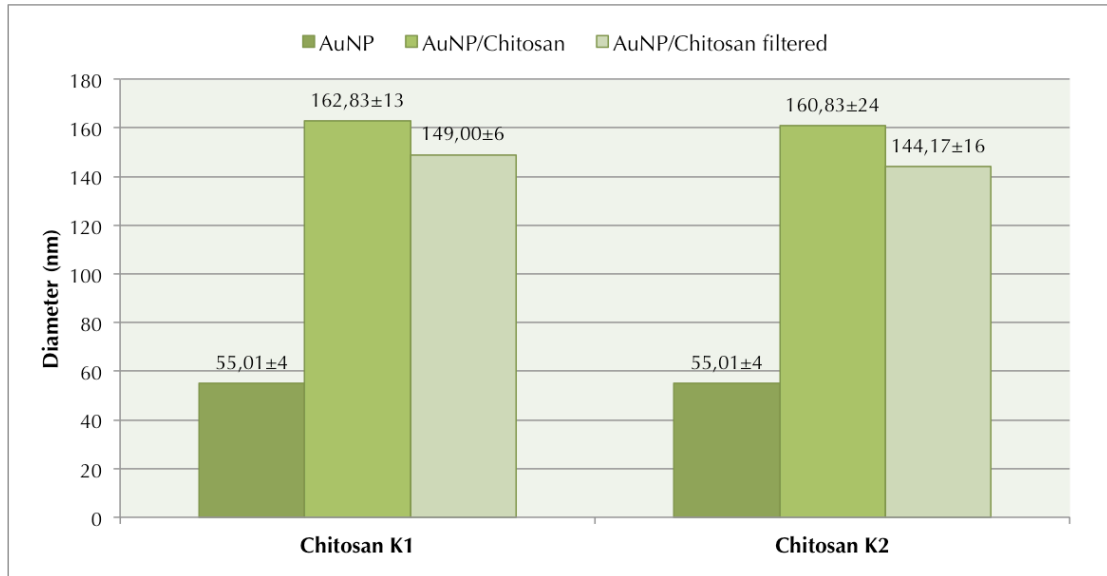


Figure 4-20. Comparison of gold nanoparticles diameter (nm) with uncertainties associated before and after the coating with the chitosan samples K1 and K2. The data is compared after filtering the covered particles AuNP/chitosan.

Thickness of the layer (nm) obtained for each chitosan sample is obtained by difference of diameters from the initial size of the gold nanoparticles to the size after the covering with the chitosan (Table 4-11).

Table 4-11. Results obtained for the thickness of the layer (nm) with the uncertainties associated to chitosan samples K1 and K2.

AuNP/Chitosan	Thickness layer (nm)
K1	107.82±19
filtered	93.99±10
K2	105.82±28
filtered	89.16±20

Zeta potential

The measurement of reversal zeta potential is an indication of the success achieved in the deposition of chitosan after the coating step. The value of zeta potential of gold nanoparticles before the covering was -31.40 ± 8 mV and the change to 49.98 ± 2 mV for K1 and 49.05 ± 2 mV proves the fulfilment of the deposition (Figure 4-21). Moreover, the fact that the zeta potential in both cases is more than 30 mV determines the stability of the nanoparticles.

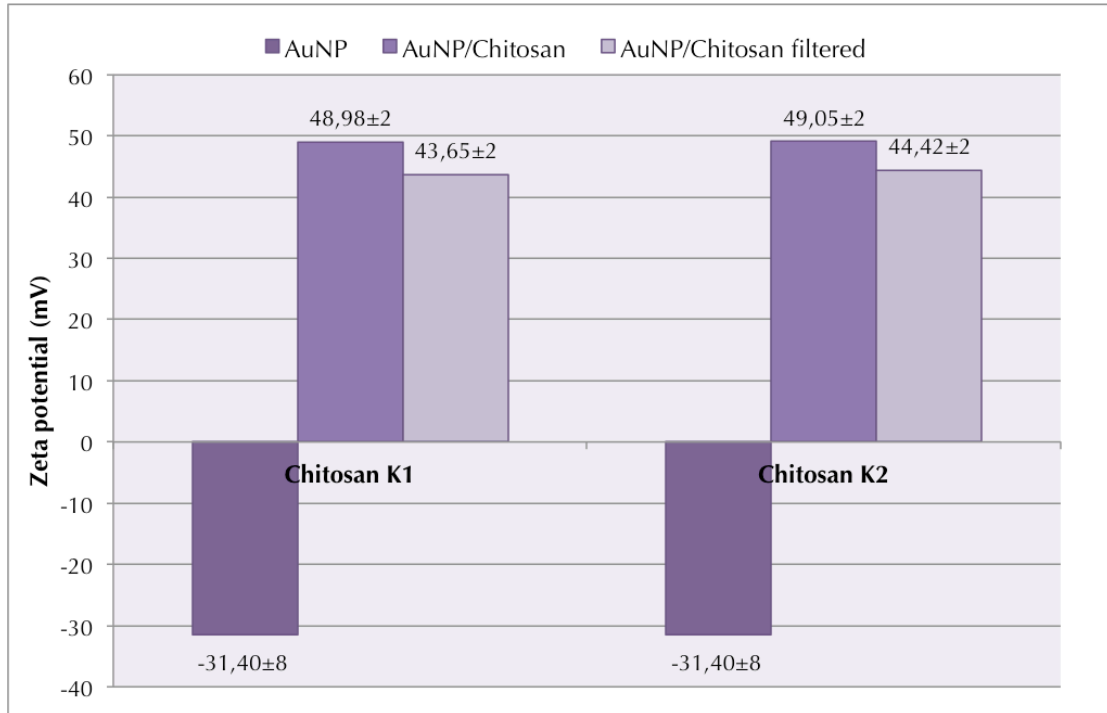


Figure 4-21. Zeta potential (mV) with associated uncertainties obtained from gold nanoparticles before and after the adsorption of chitosan sample K1 and K2.

UV-vis spectra

The analysis of the AuNP/chitosan with the UV-vis spectrophotometer provided the data of absorbance allowing the calculation of the concentration (Table 4-12) and the value of the peak plasmon resonance. The unique surface plasmon resonance around 523-524 nm (Figure 4-22) confirms that the nanoparticles exhibit low aggregation and high stability. The peak of the uncoated gold nanoparticle was established before in 522 nm. Owing to this, the values obtained are logic because of the higher size, the higher plasmon resonance peak wavelength and the gold nanoparticles has increased the size with the chitosan covering.

Table 4-12. Characterisation with UV-vis spectrophotometer. Concentration calculated with absorbance and wavelength of the peak plasmon resonance. The data was obtained for AuNP/chitosan before and after the filtering with 0.2µm filter and for both chitosan samples, K1 and K2.

Chitosan sample	Concentration (mM)	Peak value (nm)
K1	$2.87 \cdot 10^{-7}$	523
	filtered $1.99 \cdot 10^{-7}$	524
K2	$2.89 \cdot 10^{-7}$	523
	filtered $2.03 \cdot 10^{-7}$	524

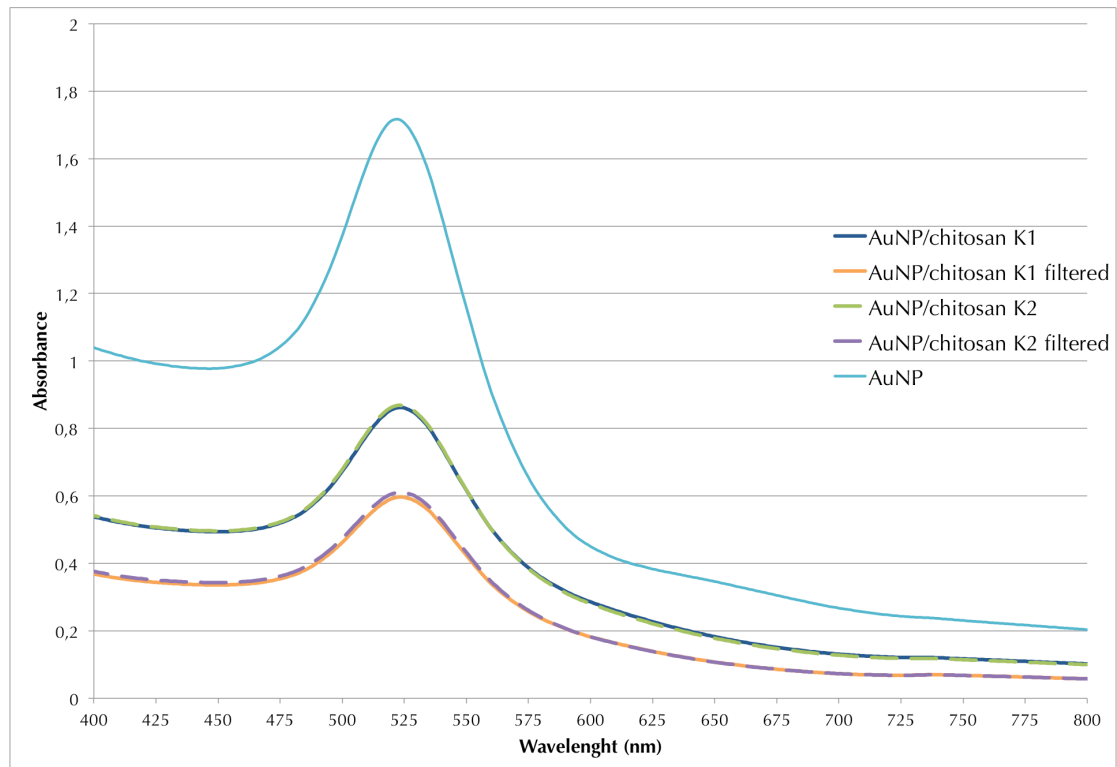


Figure 4-22. UV-vis spectra of gold nanoparticles covered with chitosan samples K1 and K2 and uncoated AuNP. The measurements were realized before and after the nanoparticles filtering (filter 0.2 μm).

UV-vis spectra of gold nanoparticles covered with chitosan samples K1 and K2. The measurements were realized before and after the nanoparticles filtering (filter 0.2 μm). This characterization of AuNP/chitosan nanoparticles verifies the effective accomplishment achieved with the binding and determines the properties for the subsequent step. Gold nanoparticles selected for following with the research were the filtered samples.

4.1.2.5 Coating of AuNP/chitosan nanoparticles with siRNA (AuNP/Chitosan/siRNA nanoparticles)

Once the chitosan was bound to the gold nanoparticles, the next layer in the study was the siRNA covering. This is an important part in this research due to the aim of this vector that is the targeted delivery of siRNA.

4.1.2.6 QCM analysis simulating the siRNA deposition into a gold surface covered with ascorbic acid and chitosan

The experiment in Quartz Crystal Microbalance was realized with the two chitosan samples selected before as the best types (K1 and K2). First, MilliQ water was introduced establishing the base. Afterwards, the ascorbic acid was added and then the chitosan sample, as it was made in the procedure to analyse the covering of gold nanoparticles with chitosan. After the chitosan, the acetic acid HAC/ sodium acetate NaAc buffer 50 mM to check the irreversibility and reject the influence of this in later

additions. Once these steps were reproduced to reach the level researched before, the siRNA was injected into the instrument. siRNA solution (0.01 mg/mL) was prepared following the method described in chapter 3. Thereafter, buffer was flushed into the chamber to exclude the effect of the siRNA stripping produced by the flow of a new substance. Chitosan sample was introduced again to complete the reproduction of the layer-by-layer assembly and finally the buffer to check the irreversibility of the system.

Charts with frequency evolution are showed in Figure 4-23 and Figure 4-24, for chitosan K1 and K2 respectively. For both samples of chitosan, K1 and K2, the behaviour is similar. The adsorption of chitosan into gold surface was studied before and in this case the compartment was the same; chitosan produced a decrease in frequency value due to the mass attachment. When the siRNA was introduced to the system AuNP/chitosan, the shift in frequency was not the expected result. The siRNA not only was not attached to the surface covered with chitosan, but also it stripped off part of this and this fact is reflected in a decrease of frequency.

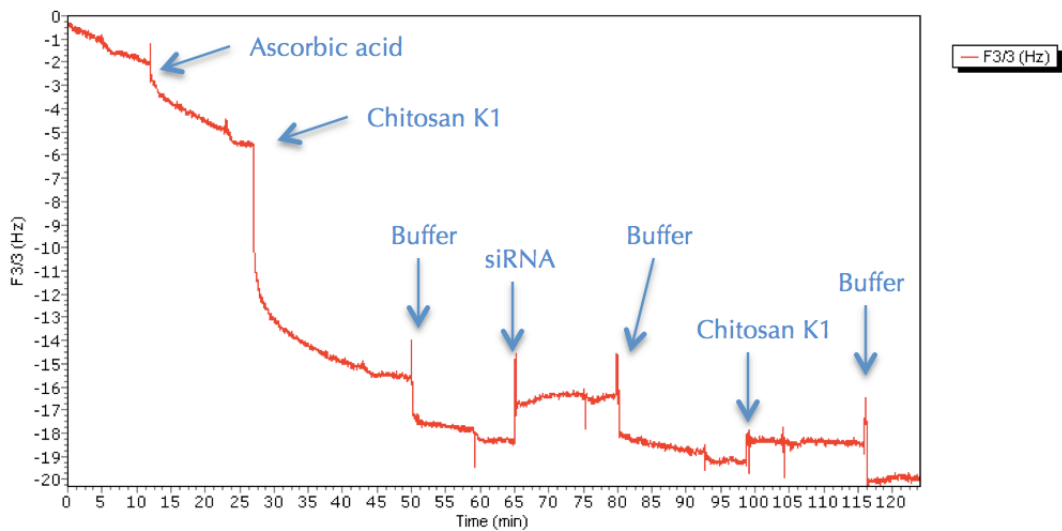


Figure 4-23. Oscillating frequency acquired with QCM for the system Au-coated crystal/Ascorbic acid/ChitosanK1/Buffer/siRNA/Buffer/ChitosanK1/Buffer.

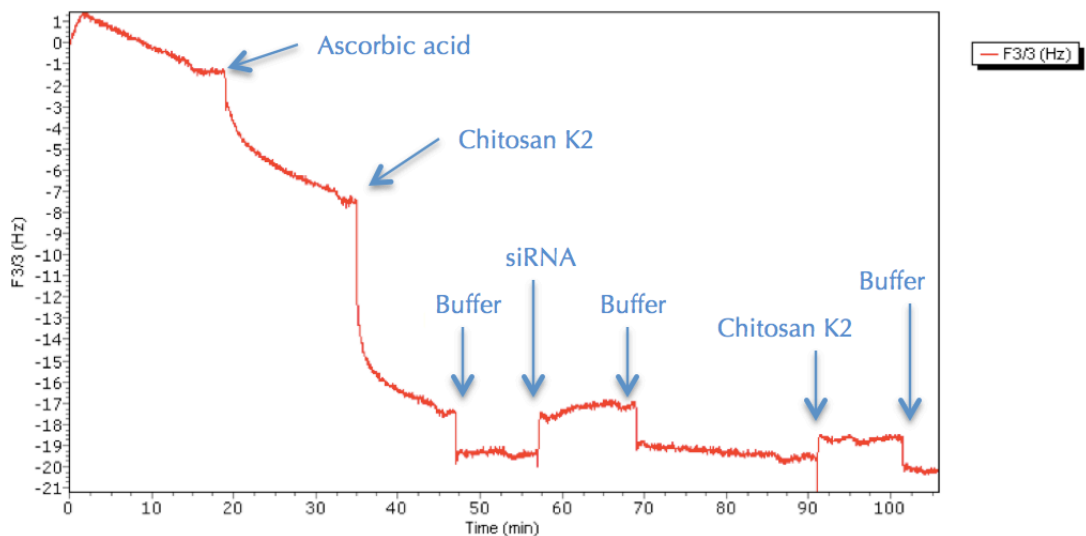


Figure 4-24. QCM analysis of frequency changes obtained for the simulation Au-coated crystal/Ascorbic acid/ChitosanK2/Buffer/siRNA/Buffer/Chitosan K2/Buffer.

Data collected with the QCM is exposed in Table 4-13. With the changes of oscillating frequency the mass attached was calculated with the Sauerbrey equation.

Table 4-13. Quartz Crystal Microbalance data for K1 and K2 chitosan samples in the reproduce of the coating AuNP/chitosan/siRNA. The Δt (min) is the time from the beginning of frequency changes to the stabilisation of the frequency after the change, Δf (Hz) is the change in crystal oscillating frequency and Δm (ng/cm²) is the mass adsorbed calculate.

Methodology		Δt (min)	Δf (Hz)	Δm (ng/cm ²)
	Ascorbic acid	14.15	4.33	77.01
Chitosan K1		16.99	9.89	176.04
	Buffer	0.80	1.88	33.46
siRNA		4.08	-1.87	-33.35
	Buffer	0.26	2.87	51.03
Chitosan K1		0.66	-0.98	-17.44
	Buffer	0.51	1.11	19.76
	Ascorbic acid	15.57	5.86	104.37
Chitosan K2		9.95	9.95	177.11
	Buffer	0.18	1.94	34.53
siRNA		5.40	-2.25	-40.11
	Buffer	1.35	1.87	33.29
Chitosan K2		0.95	-1.09	-19.40
	Buffer	0.95	1.34	23.85

Chitosan adsorbed was the expected quantity for both samples according with the experiment realized before only coating the gold surface with chitosan, 176.04 ng/cm² for K1 and 177.11 ng/cm². After the chitosan, the buffer flushed experimented a decrease in frequency that can be considered as a settlement of the chitosan, not an adsorption of buffer. In this point, where the siRNA was injected, the frequency increases, reflecting the chitosan stripping off. Nevertheless, this stripping only was produced with certain amount of chitosan from the layer formed over the gold surface. This fact was probably produced because when the chitosan layer is adsorbed, there are some molecules that remain over the layer but are not adsorbed. Then, when the next addition is made, these chitosan molecules are swept and this is showed in mass results.

This measurement in QCM was the first sign of the failure in the synthesis of the AuNP/Chitosan/siRNA nanoparticles but it is not possible to conclude the study only with this data. According to this, the study continued with the trial on real synthesis to measure other parameters and observe these results. After this, the conclusions will be taken observing the overview of data collected and analysed.

4.1.2.7 Characterization of AuNP/chitosan /siRNA nanoparticles

The data garnered with QCM reveal the problems in the AuNP/chitosan nanoparticles coating with siRNA. However these results, it was indispensable to contrast these results. With this purpose, the next proof was adding the siRNA to the nanoparticles AuNP/chitosan obtained and characterized before (4.1.3.2.). This addition was made in a volume ratio of 1:1.

Size

Gold nanoparticles size estimated after addition of siRNA not only did not remain constant, but it also decreased (Figure 4-25) from 149 ± 6 nm to 144.83 ± 7 nm in case of chitosan K1 and from 144.17 ± 16 nm to 130.83 ± 10 nm in the case of chitosan K2. Thickness of the layer before and after the addition of the siRNA to the AuNP/Chitosan is calculated in Table 4-14.

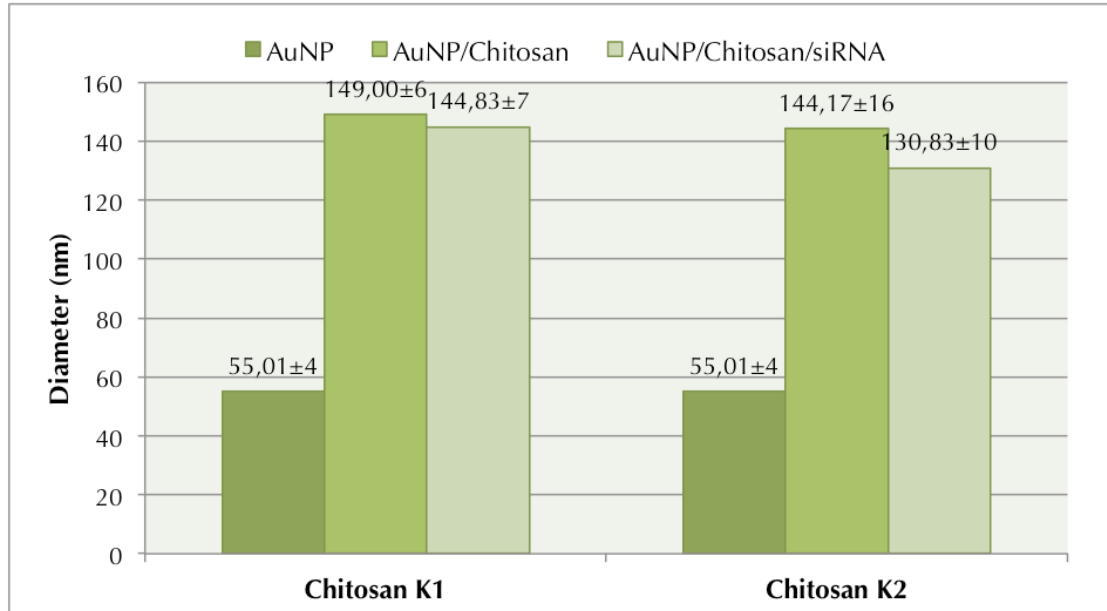


Figure 4-25. Comparison of gold nanoparticles diameter (nm) with associated uncertainties before the coating, AuNP/chitosan and AuNP/chitosan/siRNA. The experiments were carried out with K1 and K2 chitosan samples.

Table 4-14. Results obtained for the thickness of the layer (nm) with the uncertainties associated to AuNP/chitosan samples K1 and K2 and AuNP/Chitosan/siRNA.

AuNP/Chitosan	Thickness layer (nm)
K1	93.99±10
siRNA	89.82±11
K2	89.16±20
siRNA	75.82±14

Zeta potential

Zeta potential acquired with Zetasizer revealed the failure in siRNA deposition into AuNP/chitosan nanoparticles (Figure 4-26). If the siRNA is attached correctly it is supposed to reverse the zeta potential, in other words, the value has to become negative. Not only AuNP/chitosan/siRNA did not show a reverse in zeta potential but also the zeta potential decreased and this was produced by the chitosan stripping off, decreasing the stability. Nevertheless, the solutions can be considered stable anyway because of the value in both chitosan samples are higher than 30 mV.

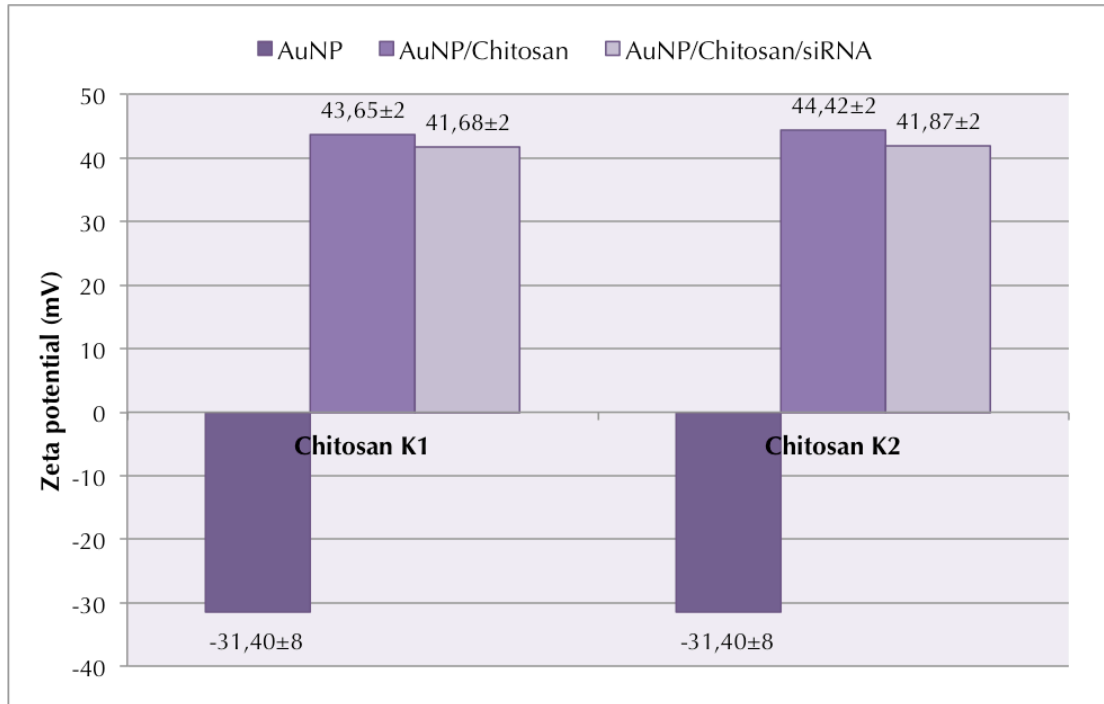


Figure 4-26. Comparison of gold nanoparticles zeta potential (mV) values with associated uncertainties before the coating, AuNP/chitosan and AuNP/chitosan/siRNA. The experiments were carried out with K1 and K2 chitosan samples.

UV-vis spectra

Absorbance data acquired with UV-vis spectrophotometer allowed the calculation of samples concentrations (Table 4-15). The plasmon resonance peak is around 525 nm (Figure 4-27) in both samples and it is an evidence of monodispersity and stability.

Table 4-15. Characterisation of AuNP/chitosan/siRNA nanoparticles with UV-vis spectrophotometer. Concentration calculated with absorbance and wavelength of the peak plasmon resonance. Data obtained for both chitosan samples, K1 and K2.

Chitosan sample/siRNA	Concentration (mM)	Peak value (nm)
K1	$1.50 \cdot 10^{-7}$	524
K2	$1.47 \cdot 10^{-7}$	524

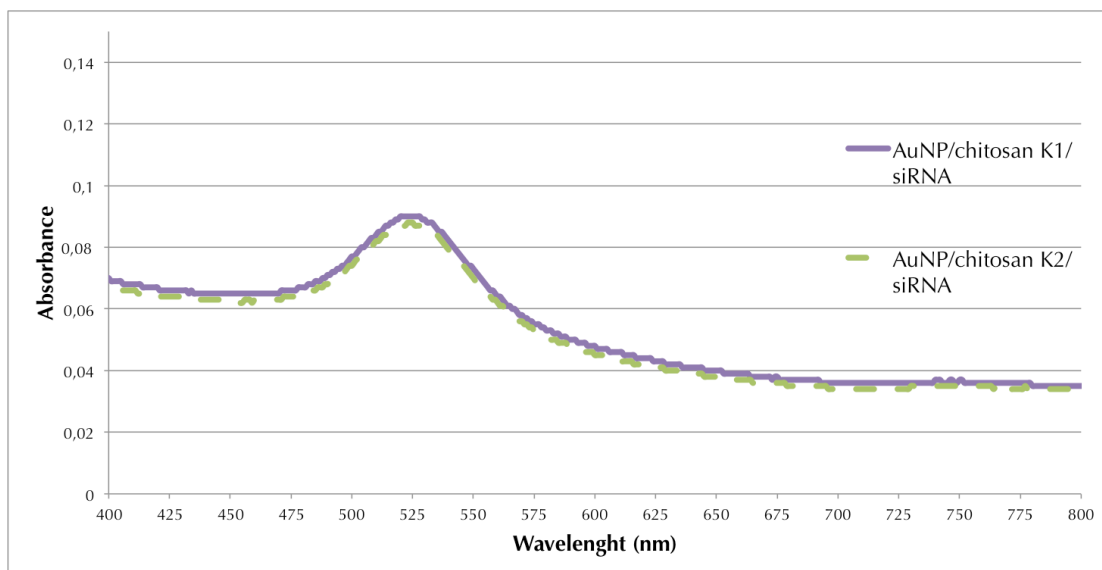


Figure 4-27. UV-vis spectra of gold nanoparticles covered with chitosan samples K1 and K2 and siRNA.

According to the values of size and zeta potential, the failure of the process showed in QCM analysis is proved. Furthermore, size and zeta potential decrease revealing the possibility hypothesized of not only the siRNA did not cover successful the AuNP/chitosan but also it stripped of part of the chitosan.

Regarding the results obtained and the problems arose, in this point was considered the possibility to change the drug delivery vector to find another way to build it keeping the premise established in objectives.

4.2 Synthesis of AuNP/C₁₆TAB/siRNA nanoparticles

The failure in the accomplishment of the AuNP/Chitosan/siRNA supposed the new design of a nanocarrier. In this case, C₁₆TAB was selected to produce the reversal charge between the gold nanoparticle and the siRNA and produce the adsorption layer-by-layer.

4.2.1 Theory

C₁₆TAB is a cationic surfactant widely used in the synthesis of nanorods. This substance is commonly added with the reducer agent to produce the complex of gold ions [64]. The surfactants have a very large polar head and a small chain forming a cone shape. The chain tends to self-associate to form a spherical aggregated called a normal micelle. On the other hand, if the surfactant has a small polar head and branched hydrocarbon chains, spherical reverse micelles are formed. These reverse micelles were discovered as a excellent candidate for templates [65].

4.2.2 Material and methods

Hexadecyltrimethylammonium bromide (C₁₆TAB ≥ 99%), was purchased from Sigma-Aldrich. Sodium citrate solution was provided by Ugelstad Laboratory of NTNU (Trondheim, Norway).

10 mM C₁₆TAB solution was prepared dissolving the chemical reactant in MilliQ water. Sodium citrate solution used in the researching had a concentration of 10mM

4.2.3 QCM analysis simulating the siRNA deposition into a gold surface covered with C16TAB and a final layer of chitosan

This analysis in Quartz Crystal Microbalance was realised to check the possibility of binding the gold nanoparticles with a first layer of C₁₆TAB and adsorb the siRNA into this layer. Once the siRNA is attached, then was proposed a chitosan layer to observe the interaction produced if the siRNA is successfully attached to the C₁₆TAB.

The research was realised with chitosan sample K1 since it was only a trial suggested after the conclusions drawn with the failed synthesis of AuNP/chitosan/siRNA nanoparticles.

The measurement was performed as follows: first a stable base line was established with MilliQ water. After this, a sodium citrate solution 10 mM was flushed following the protocol of analysis. The next component introduced was C₁₆TAB 10 mM 3 times to be sure that the adsorption is complete and a possible low concentration is not a parameter affecting. When the frequency value was considered stable, acetic acid HAc/ sodium acetate NaAc buffer 50 mM was flushed through the chamber to check the irreversibility of this adsorption. The next step was the addition of siRNA (0.01mg/mL) and was necessary to wait until no further change in frequency could be observed. Following on from the procedure buffer was flushed again to prove the irreversibility and after a while the chitosan sample K1 (0.1 mg/mL) was introduced into the chamber. Finally, the analysis was finished with a last addition of buffer.

Data obtained from the instrument is shown in Table 4-16, the changes in frequency allow the calculation of mass attached to the surface. First changed in frequency produced by C₁₆TAB was very fast but after this the value began to decrease progressively until a second addition stabilised the oscillating frequency. The third one did not produce a change in frequency proving the effectivity of the possible adsorption. In the next step, siRNA was not attached to the system not only because the frequency did not decrease but it also increased the value. This type of shift shows that probably part of the C₁₆TAB was stripped off with the pass of siRNA through the chamber. The last addition of chitosan had no sense after the failure with the siRNA.

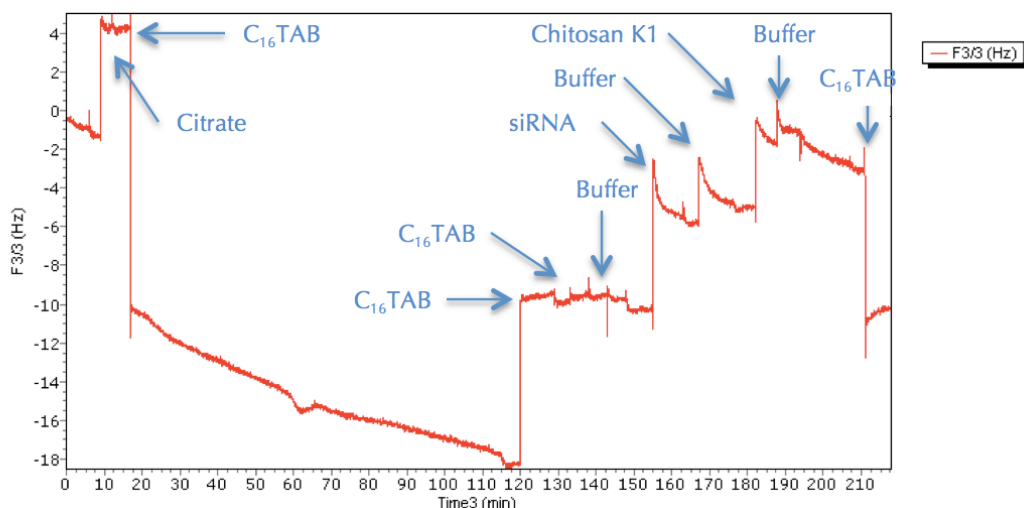


Figure 4-28. Evolution of oscillating frequency obtained in the Au-coated/Citrate/C₁₆TAB/Buffer/siRNA/Buffer/ChitosanK1/Buffer/C₁₆TAB system simulation.

Regarding Figure 4-28, when the first addition of C₁₆TAB was made, oscillating frequency decreased due to the deposition of C₁₆TAB into the surface. After this, the frequency value started to decrease progressively until C₁₆TAB was injected again and then the oscillation achieved a stable level. The third addition confirmed that this level of frequency is the correct value for the frequency and the decrease produced in the first step was not considered in calculations. In calculations buffer was not considered because the instantaneous change in frequency was due to the mechanical crash in the injection but in a few minutes the value was stabilized in the chamber.

Table 4-16. Quartz Crystal Microbalance data for K1 chitosan samples in the reproduce of the coating AuNP/C₁₆TAB/siRNA/chitosan. The Δt (min) is the time from the beginning of frequency changes to the stabilisation of the frequency after the change, Δf (Hz) is the change in crystal oscillating frequency and Δm (ng/cm²) is the mass adsorbed calculate.

Methodology	Δt (min)	Δf (Hz)	Δm (ng/cm ²)
C ₁₆ TAB	0.15	14.95	266.11
siRNA	3.83	-4.66	-82.89
Chitosan K1	1.57	-3.97	-70.61

Results obtained for AuNP/C₁₆TAB/siRNA/Chitosan show the failure in the deposition of a siRNA layer covering the C₁₆TAB attached before. When siRNA was introduced into the chamber, oscillating frequency increased exhibiting the same behaviour as the study realized before where the first layer was chitosan. The most probably cause of this increase in frequency is because not only the siRNA was not attached, but also part of the C₁₆TAB was stripped off the layer formatted into gold surface.

4.3 Synthesis of AuNP/Chitosan nanoparticles crosslinked with EDAC

The last trial in this study was considering the possibility of crosslink the chitosan to the MUA covering the gold nanoparticle by means of a carbodiimide called EDAC. This crosslinker have been used in diverse chitosan complexes formation such as the

crosslinking of thioglycolic acid with chitosan for scaffold engineering [66]. The synthesis of thermosensitive nanoparticles with PNIPAAm core and chitosan shell crosslinked with EDAC is a new challenge for drug delivery applications owing to the release of drug is made when it is necessary [67]. Other example of EDAC use was reported some years ago, with the sequestration of liposomes in chitosan gel crosslinking with this carbodiimide [68]

1.1.1. Theory considerations

N-(3-Dimethylaminopropyl)-N-ethylcarbodiimide hydrochloride (EDAC) is a cross-linker generally used as a carboxyl-activating agent for amide bonding with primary amines. Cross linkers have become important tools for the preparation of conjugates used in a lot of immunotechnologies, and for protein studies (structure, interactions, activity, and degradation). Heterobifunctional crosslinkers are the most interesting because of the presence of 2 reactivities that allow the determinate conjugation of molecules, avoiding the formation of dimers and polymers. EDAC has been used in peptide synthesis, crosslinking proteins to nucleic acids, and preparation of immunoconjugates as examples [69] [70].

4.3.1 Material and methods

N-(3-Dimethylaminopropyl)-N-ethylcarbodiimide hydrochloride (EDAC) was purchased from Sigma-Aldrich.

EDAC solutions were made freshly for each experiment carried out. The EDAC was dissolved in 50 mM HAC/NaAc buffer pH 5.5 due to the fact that chitosan were buffered with this.

Magnetic gold nanoparticles were provided by PhDS Gurvinder Singh, whereas gold nanoparticles obtained by citrate reduction were purchased in BBInternational (Gold colloidal, 30 nm).

4.3.2 QCM analysis simulating the chitosan coating crosslinked with EDAC into a gold surface covered with MUA.

This essay tried to reproduce the crosslinker reaction between the MUA and chitosan with EDAC. This simulation was supposed to be complicated due to the difficulty to reproduce the crosslinking with the Quartz Crystal Microbalance.

This simulation was realised with the MUA covering into the crystals to achieve a reliable process. The method was accomplished as follows: first, a stable line of MilliQ water was fixed before starting with the injection of the objective compounds. Afterwards, 3 consecutives additions of chitosan solution (0.2mg/mL) were made to be sure the adsorption capacity is covered, as in the experiments realised before with this instrument. Once the chitosan could be considered completely adsorbed, EDAC solution (0.5 mg/mL) was introduced into the chamber 3 times for the same reason

considered before with the chitosan. Finally, acetic acid HAC/ sodium acetate NaAc buffer 50 mM was flushed to check the irreversibility.

Results for chitosan K1 are shown in Figure 4-29 and Figure 4-30 for chitosan K2. In both cases the evolution of the chitosan when was added to the chamber was quite fast due to the frequency value was stabilized again quickly. After the chitosan, the EDAC was adsorbed showing the same behaviour than chitosan with a quick adsorption. In the last addition made with buffer, the value of frequency increases due to the EDAC that can remain in the surface of the EDAC layer adsorbed. The fact that this last change un frequency was very low gives a proof of the irreversibility of the system.

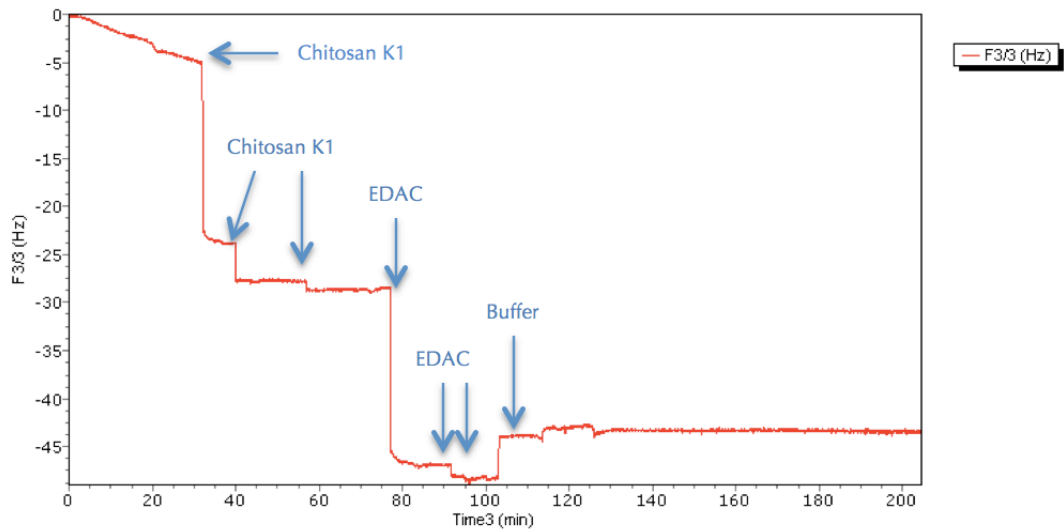


Figure 4-29. Oscillating frequency data acquired with QCM for the simulation of Au-coated crystal covered with MUA/Chitosan K1/EDAC/Buffer.

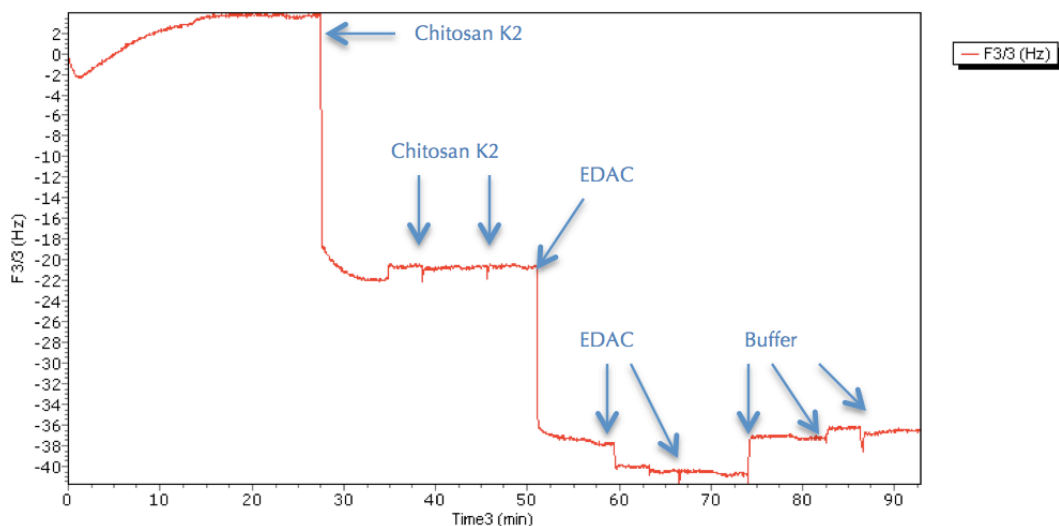


Figure 4-30. Data obtained from QCM about oscillating frequency for the system Au-coated crystal covered with MUA/Chitosan K2/EDAC/Buffer.

Data acquired with the instrument (Table 4-17) about changes in frequency allow the calculation of mass adsorbed or desorbed by means of the Sauerbrey equation.

Table 4-17. Quartz Crystal Microbalance data for K1 and K2 chitosan samples in the reproduce of the coating AuNP/Chitosan crosslinked with EDAC. The Δt (min) is the time from the beginning of frequency changes to the stabilisation of the frequency after the change, Δf (Hz) is the change in crystal oscillating frequency and Δm (ng/cm²) is the mass adsorbed calculate.

Chitosan sample		Δt (min)	Δf (Hz)	Δm (ng/cm ²)
K1		1,88	23,54	418,95
	EDAC	2,97	19,46	346,33
	Buffer	0,96	-5,49	-97,72
K2		4,59	25,63	456,27
	EDAC	3,81	18,90	336,48
	Buffer	5,43	-4,06	-72,27

The results show the successful attachment of chitosan to the gold surface due to the high changes decreasing the oscillating frequency. Mass adsorbed was calculated for samples resulting, 418.95 ng/cm² for K1 chitosan and 456.27 ng/cm² for K2 type. With the addition of EDAC other shift was observed, decreasing the frequency again. This variation means the correct adsorption of EDAC, and it is supposed to be a signal that the crosslinking was produced between the chitosan and the gold surface. Values for the EDAC adsorption were 346.33 ng/cm² for K1 chitosan and 456.27 ng/cm² for K2. The last addition of buffer to the system for checking the irreversibility exhibited a little desorption of the system built but it can be considered irreversible because of the consecutive addition did not show any changes in frequency.

After this experiment was considered the possibility of this reproduction were not exactly the required in the methodology. According to this, another simulating with the Quartz Crystal Microbalance was realised to find the differences. Regarding these considerations the experimentation was reproduced as follows: first, a stable line of MilliQ water was fixed before starting with the injection of the objective compounds. Afterwards, 3 consecutives additions of EDAC solution (0.5mg/mL) were made to be sure the adsorption capacity is covered, as in the experiments realised before with this instrument. Once the EDAC was completely adsorbed, chitosan solution (0.2 mg/mL) was introduced into the chamber. Finally, acetic acid HAc/ sodium acetate NaAc buffer 50 mM was flushed to check the irreversibility.

In the Table 4-18 results are showed following the order of the acquirement from QCM. Data of frequency changes allow the calculation of variation in mass on the gold surface. This experiments was realised only with K1 chitosan because it was only a proof about the procedure followed.

Frequency experimented a large change when the EDAC was added Figure 4-31, decreasing the value owing to the mass adsorbed into the gold surface. When the chitosan was introduced into the chamber, the oscillating frequency increased again. The rest of additions after this were made only for observing the variation of frequency.

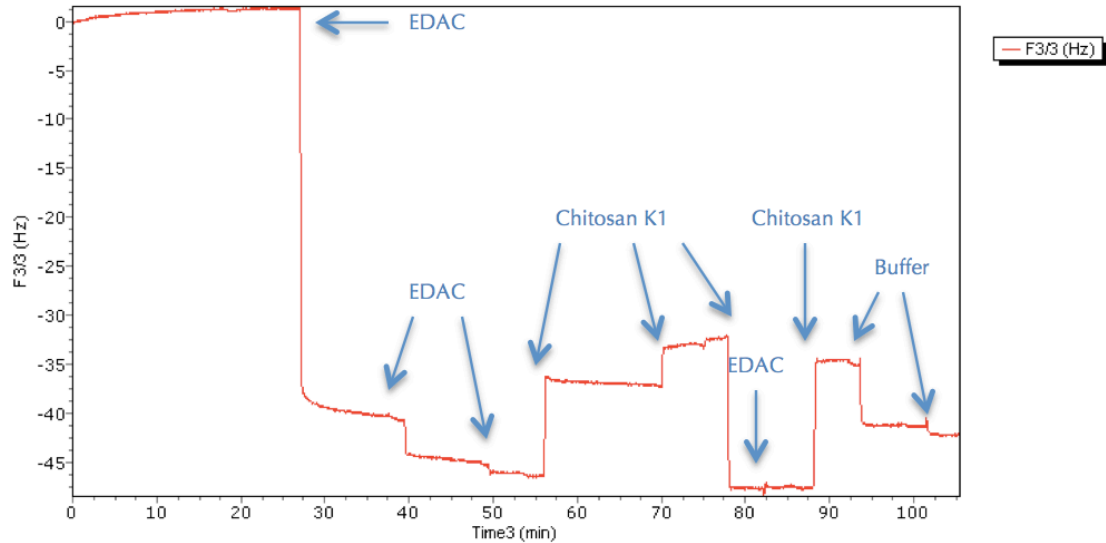


Figure 4-31. Oscillating frequency obtained in QCM for the simulation Au-coated crystal covered with MUA/EDAC/Chitosan/Buffer. A second step of EDAC is added after chitosan to check if it would be adsorbed again.

Table 4-18. Quart Crystal Microbalance data for K1 chitosan sample in the reproduce of the coating AuNP/Chitosan crosslinked with EDAC considering the procedure adding first EDAC. The Δt (min) is the time from the beginning of frequency changes to the stabilisation of the frequency after the change, Δf (Hz) is the change in crystal oscillating frequency and Δm (ng/cm^2) is the mass adsorbed calculate.

Methodology	Δt (min)	Δf (Hz)	Δm (ng/cm^2)
EDAC	7,10	45,56	811,03
Chitosan K1	2,45	-13,92	-247,84
Buffer	1,49	7,00	124,60

As it was predicted before, the order followed injecting the reactants into the chamber affects to the results. In this case, the EDAC was deposited into the surface successful with a high value of mass attached, $811.03 \text{ ng}/\text{cm}^2$. However, when chitosan was introduced into the chamber the value of frequency decreased again representing not only the failure in the chitosan adsorption, but also an EDAC stripping off, at least, one part of this component adsorbed before.

According to the data garnered in these two tests, the interaction between MUA, chitosan and EDAC is positive but the results were very different depending on the order the components were introduced. This is logical but the problem was to consider the most exact reproduction of the crosslinking process. The last test proposed is exactly that the last carried out but flushing buffer between the additions of different components. The motivation of this was to reject the effect of a new reactant flowing into the chamber for considering only the adsorption/desorption. Then, the procedure was to establish the MilliQ water base line, inject the EDAC ($0.5 \text{ mg}/\text{mL}$) solution 3 times and flush with acetic acid HAc/ sodium acetate NaAc buffer 50 mM to check the irreversibility of this layer. The next steps were the addition of chitosan sample ($0.2 \text{ mg}/\text{mL}$) 3 times and flush with buffer again. This procedure tried to reject the effect of the samples injection into the chamber for considering only the knowledge about interactions.

Observing the Figure 4-32, the oscillating frequency evolution was the same than in the case the experiment was carried out without flushing buffer.

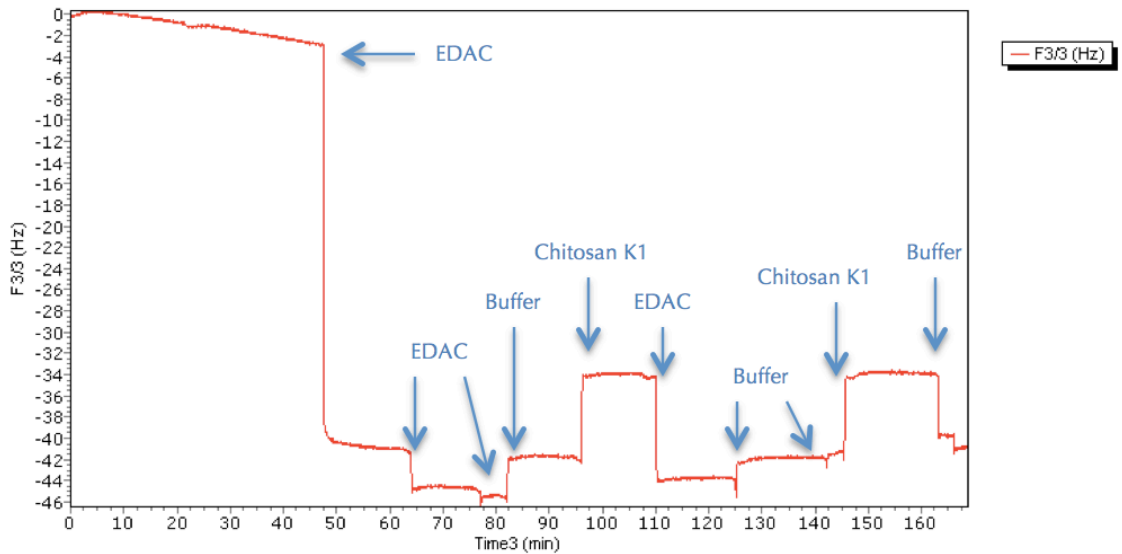


Figure 4-32. Data obtained with QCM about oscillating frequency in the simulation Au-coated covered with MUA/EDAC/Buffer/ChitosanK1/Buffer

QCM data obtained and calculations about mass adsorption are exhibited in Table 4-19.

Table 4-19. Quartz Crystal Microbalance data for K1 chitosan sample in the reproduce of the coating AuNP/Chitosan crosslinked with EDAC considering the procedure adding first EDAC and buffer between compounds. The Δt (min) is the time from the beginning of frequency changes to the stabilisation of the frequency after the change, Δf (Hz) is the change in crystal oscillating frequency and Δm (ng/cm^2) is the mass adsorbed calculate.

Chitosan sample		Δt (min)	Δf (Hz)	Δm (ng/cm^2)
	EDAC	5,18	40,65	723,51
	Buffer	0,92	-3,73	-66,39
K1		0,53	-8,30	-147,74
	Buffer	3,33	6,87	122,23

EDAC addition to the chamber produced an adsorption onto the gold surface. This attachment caused the decreasing in oscillating frequency of the crystal due to the mass covering this surface, $723.51 \text{ ng}/\text{cm}^2$. The buffer flushed after this addition increased the frequency but only in several hertz and the adsorption of EDAC could be considered as irreversible. The next step was the covering with chitosan and the results show the same behaviour as the experiment where buffer was not flushed. According to this, the possibility of the chitosan was not adsorbed because the system created before was not irreversible was rejected. This experiment confirmed the results obtained previously and was verified the failure in chitosan attachment adding the EDAC crosslinker firstly.

As a result of this, the continuing with the AuNP/chitosan nanoparticles crosslinked with EDAC synthesis was decided because of the not certain information acquired to consider the successful or failure of the technique.

4.3.3 Obtaining and characterization of AuNP/chitosan crosslinked with EDAC

4.3.3.1 Magnetic gold nanoparticles 7.3nm

Gold nanoparticles selected to procedure with the synthesis of AuNP/chitosan nanoparticles crosslinked with EDAC were magnetic gold nanoparticles covered with MUA. The starting parameters of these particles were a diameter of 7.3 nm and zeta potential value of -46.43 ± 2 mV. This tests were only made with a few samples of chitosan, in some cases with only one, due to the fact that is only an experiment about the possibility of carrying out this. If the results were positive the possibility of study the different chitosan samples has to be considerate.

Synthesis without chitosan preadsorption

The synthesis was carried out adding a solution of EDAC (0.5mg/mL) to the gold nanoparticles under mechanical stirring. After this, the chitosan sample (0.2 mg/mL) was introduced in the beaker where the reaction was accomplishing. It is considered significant the fact that after the addition of EDAC to the solution, some aggregations could be observed, disappearing when the chitosan was introduced.

Synthesis with preadsorbed chitosan

The other synthesis was accomplished with a preadsorption of chitosan sample (0.2mg/mL) for 2h at room temperature in a beaker with the magnetic gold nanoparticles under stirring. After this 2h, the EDAC solution (0.5 mg/mL) was added to produce the crosslinking and waited for 4h under the same conditions to complete the reaction.

Synthesis with filtered chitosan without preadsorption

The characterisation of these samples obtained with the two procedures was made before and after the filtering (with 0.2 μ m filter) but a third synthesis was accomplished to study the effect of chitosan filtering and discard the influence of this factor. In this case, EDAC was added to the solution firstly and after this, the chitosan sample was filtered (filter 0.2 μ m) before starting the reaction.

Size

Size of different AuNP/chitosan nanoparticles was acquired with Zetasizer instrument (Figure 4-33).

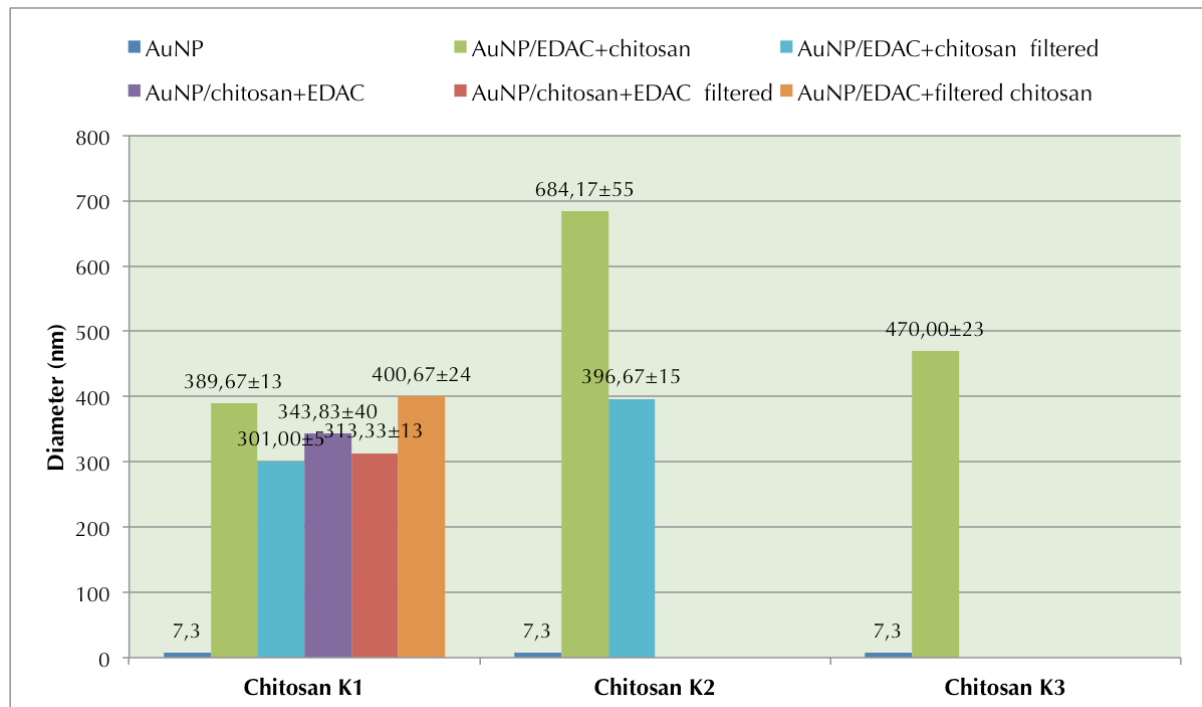


Figure 4-33. Diameter (nm) for different nanoparticles synthesized with the associated uncertainties. AuNP/EDAC+chitosan is referred to synthesis produced adding first the EDAC to AuNP and after the chitosan, before and after filtering. AuNP/chitosan+EDAC are the nanoparticles conjugated with a preadsorption of chitosan and the addition of EDAC to crosslink it after, before and after filtering. AuNP/EDAC + filtered chitosan is the label for nanoparticles with the addition of chitosan previously filtered.

Firstly, the most remarkable fact is that all AuNP/chitosan nanoparticles had huge increase in their size. In the case of AuNP/chitosan nanoparticles with the previous addition of EDAC for the crosslinking, the different of size is from 7.3 nm to 389.67±13 nm for chitosan K1, 684.17±55 nm in K2 and to 470 nm to K3. For AuNP/chitosan nanoparticles obtained with preadsorption of chitosan, size is very similar to the particles achieved without this step. Finally, the experiment accomplished with filtered chitosan provided nanoparticles with a size of 400.67±24 nm evidencing that this is a factor not considered essential in this case.

Zeta potential

Zeta potential data was obtained with the Zetasizer instrument for all AuNP/chitosan synthesized. Results are presented in Figure 4-34.

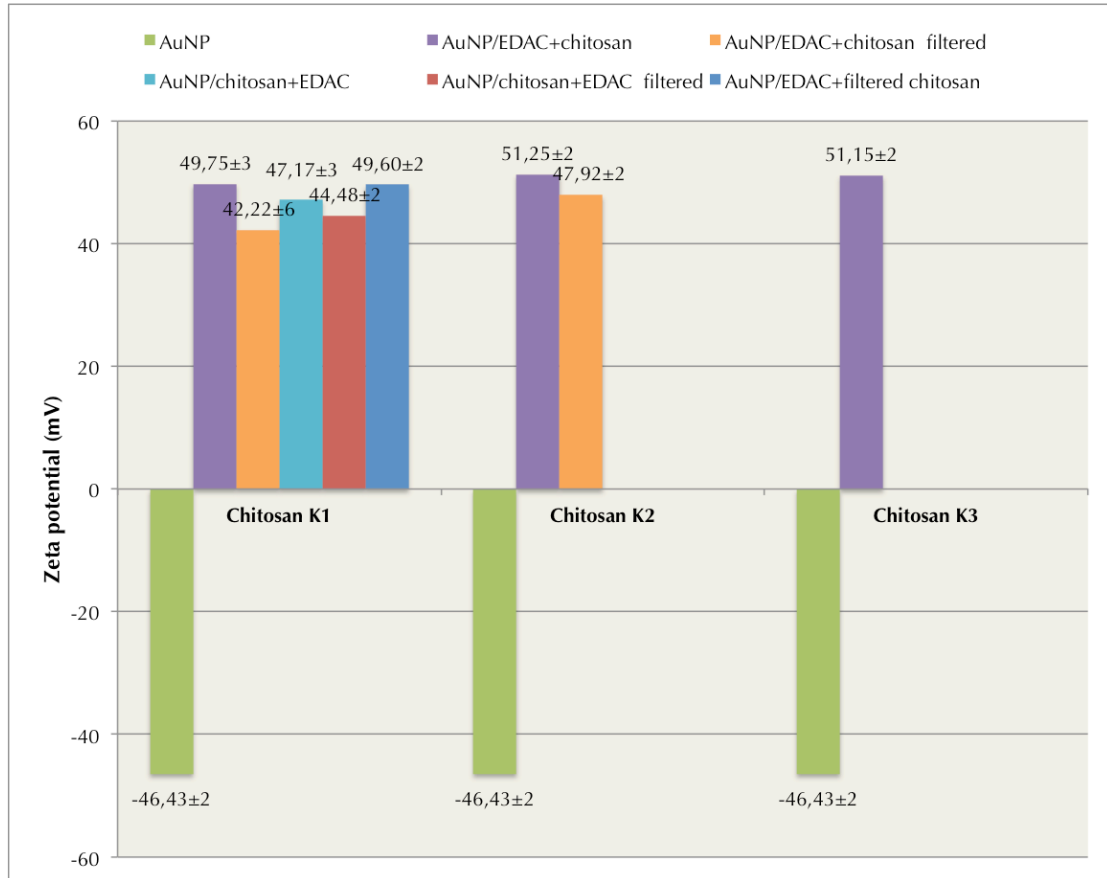


Figure 4-34. Zeta potential (mV) for different nanoparticles synthesized with the associated uncertainties. AuNP/EDAC+chitosan is referred to synthesis produced adding first the EDAC to AuNP and after the chitosan, before and after filtering. AuNP/chitosan+EDAC are the nanoparticles conjugated with a preadsorption of chitosan and the addition of EDAC to crosslink it after, before and after filtering. AuNP/EDAC + filtered chitosan is the label for nanoparticles with the addition of chitosan previously filtered.

Zeta potential value for magnetic gold nanoparticles before the covering was measuring to have the possibility of checking the successful deposition of chitosan. This value resulted -46.43 ± 2 mV. All samples of AuNP/chitosan created in the different ways exposed exhibited a positive zeta potential in the range from 42.22 ± 6 to 51.25 ± 2 mV. Hence, these nanoparticles can be considered stable because the value is higher than 30 mV. Moreover, the different steps carried out in the nanoparticles are not considering relevant to the zeta potential owing to these values are very similar.

UV-vis spectra

UV-vis spectroscopy provided data of absorbance for calculating the concentration of different nanoparticles obtained (Table 4-20). The unique peak of plasmon resonance is located between 529-531 nm that evidence high stability and low aggregations in the nanoparticles produced (Figure 4-35). The highest value of plasmon resonance peak is for the chitosan K2 (531nm) and it is logic due to the fact that these particles have the biggest size 684 nm, followed by chitosan K3 (530 nm) with a diameter of 470 nm. The rest of the size values are around 530 nm because of the similar size registered.

Table 4-20. Characterisation with UV-vis spectrophotometer for AuNP/chitosan crosslinked with EDAC. Concentration calculated with absorbance and wavelength of the peak plasmon resonance. AuNP/EDAC+chitosan before and after the filtering with 0.2µm filter. AuNP/chitosan+EDAC, the addition of chitosan was made first for preadsorbing, measured before and after the filtering with 0.2µm filter. AuNP/EDAC+filtered chitosan, the chitosan was filtered before the reaction.

Sample		Concentration (mM)	Peak value (nm)
AuNP		$3.56 \cdot 10^{-6}$	524
AuNP/EDAC+chitosan	K1	$1.59 \cdot 10^{-6}$	529
	K2	$1.51 \cdot 10^{-6}$	531
	K3	$1.52 \cdot 10^{-6}$	530
	K1 filtered	$1.34 \cdot 10^{-6}$	530
	K2 filtered	$8.52 \cdot 10^{-7}$	530
AuNP/chitosan+EDAC	K1	$1.69 \cdot 10^{-6}$	529
	K1 filtered	$1.11 \cdot 10^{-6}$	530
AuNP/EDAC+filtered chitosan	K1	$1.52 \cdot 10^{-6}$	530

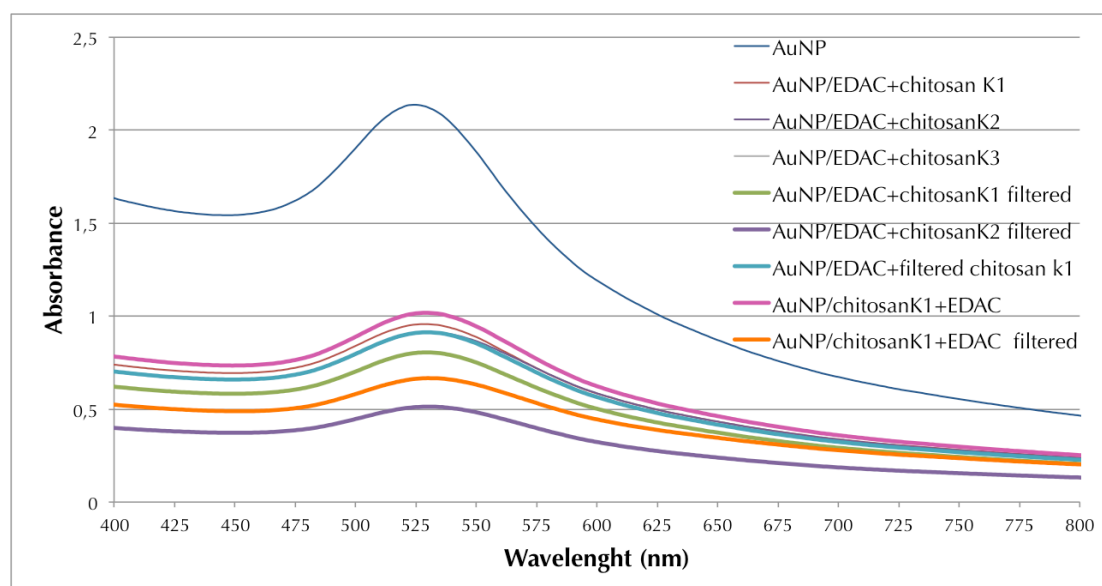


Figure 4-35. UV-vis spectra for different AuNP/chitosan nanoparticles crosslinked with EDAC. AuNP/EDAC+chitosan before and after filtering, In AuNP/chitosan+EDAC, a preadsorption of chitosan was made, measured before and after filtering. In AuNP/EDAC+chitosan filtered, the chitosan was filtered before use.

After the characterisation is obviously that the result obtained with the size are not considered positives because the change between the AuNP diameter before and after the covering is huge, from 7.3 nm to around 400 nm or 600 nm in some cases (e.g. with chitosan K2). Chitosan is a big molecule and it suggests the hypothesis that there is a possibility of not only chitosan is not covering these AuNP but also the nanoparticles are encrusted in the chitosan strand. Thus, it was proposed to use AuNP with a size around 40 nm to observe if the little size of starting AuNP was affecting to the results.

4.3.3.2 Gold nanoparticles 40 nm

It was necessary to synthesize new gold nanoparticles to continue with the study. For this, the procedure followed was the same than with the gold nanoparticles used before with the other experiments. Briefly, tetrachloroauric acid was reduced by ascorbic acid in a ratio concentration 1:50 (mM). Moreover, the nanoparticles were characterized before their use obtaining a size of 61.97 ± 3 nm and a zeta potential of -23.1 ± 2 mV.

To continue with the work carried out before, the gold nanoparticles were supposed to be covered with MUA. For this accomplishment, some experiences different to ones related in 4.2.1.2 were tested to displace the ascorbic acid with MUA (Table 4-21).

The variations in the displacement procedure are referred to changes in MUA concentration and volume ratio. In some cases, it is added NaOH increase the pH stabilizing the particle dispersion deprotonating the carboxylic acid groups of MUA [33]. A little amount of gold nanoparticles conserved of the production made in 4.2.1.2. was also tested to make a comparison between the old and new particles and refuse the hypothesis of a problem with the new gold nanoparticles. Finally, commercial gold nanoparticles obtained by sodium citrate reduction with a diameter of 30 nm was tested.

Table 4-21. Experiments carried out for the displacement of ascorbic acid or citrate with MUA. The volume ratio is referred in mL.

AuNP origin	MUA (mM)	NaOH (M)	Volume ratio AuNP:MUA:NaOH	Result
New	10		1:0.1	Agglomerations
New	10		1:0.05	Agglomerations
New	10		1:0.01	Agglomerations
Old	10		1:0.01	Agglomerations
New	5		1:0.01	Agglomerations
New	10	0.25	1:0.1:0.1	Agglomerations
New	10	0.25	1:0.01:0.1	Agglomerations
New	10	0.25	1:0.1:0.2	Agglomerations
New	10	0.25	1:0.01:0.2	Agglomerations
Commercial (30nm)	10		1:0.1	Stable dispersion
Commercial (30 nm)	10		1:0.01	Stable dispersion

The intention of displace the ascorbic acid was failed in all cases tried, decreasing the MUA concentration, increasing the pH and decreasing the volume of MUA. Hence, is concluded the ascorbic acid linking with the gold surface is strong and this way of displacement is difficult to carry out. On the contrary, the commercial gold nanoparticles were successfully covered with MUA, displacing the citrate. Thus, these commercial gold nanoparticles were selected to continue with the experimentation.

Commercial gold nanoparticles with a size of 30 nm diameter were characterized after the displacement of the citrate with MUA. The size and zeta potential was measured with Zetasizer and resulted in 49 ± 9 nm diameter and zeta potential of -47.93 ± 5 mV. The UV-vis spectra showed a strong peak plasmon resonance at 527 nm.

To study how affects the EDAC concentration to the final properties of the nanoparticles synthesized, different concentrations were analysed in the same

conditions; 0.5, 0.1, 0.05, and 0.01 mg/mL. According to this, synthesis were realized in a volume ratio (mL) of 3:1 (AuNP : EDAC) under stirring and adding the chitosan K1 sample (0.2 mg/mL) to this mixture in a ratio volume 1:1. The reaction was carried out for 4 h and after this the appropriate characterisation was accomplished. For this, AuNP first were covered with MUA, after the EDAC was added to the solution and the last step consisted on the addition of the chitosan.

Size

All nanoparticles size was measured with Zetasizer. Data obtained with the software for gold nanoparticles covered with MUA informed about the monodispersity of the solution, only one peak was observed in the size distribution, whereas in the case of gold nanoparticles with chitosan bound by means of the EDAC showed very different results. All solutions can be considered polydispersed because of all of them have at two remarkable peaks in a size distribution in some cases near 50%-45%.

Data showed in Figure 4-36 is the data considering the value of the peak most noticeable but in most of the cases is not a complete reliable data due to the polydispersity commented before.

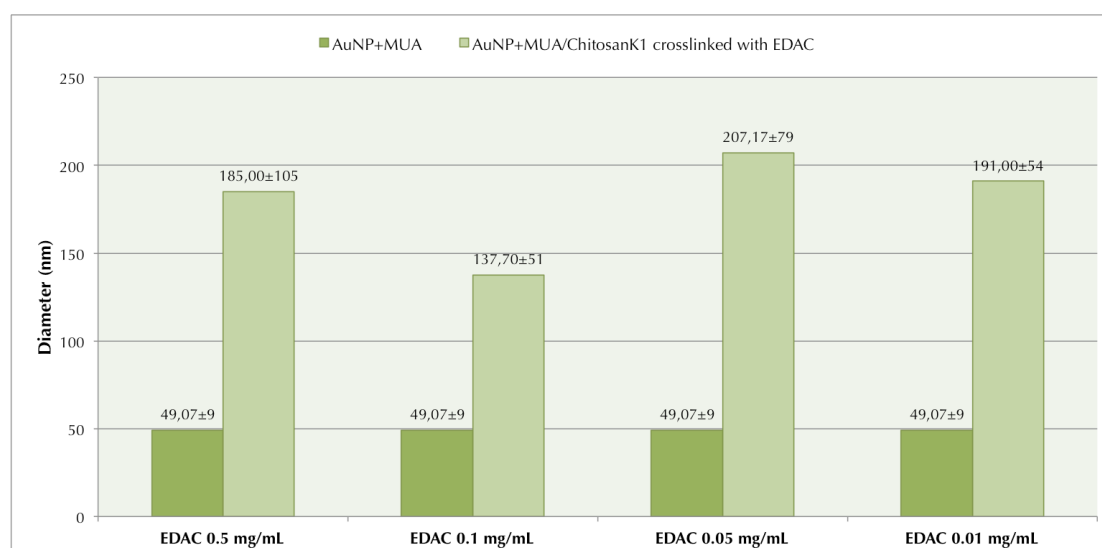


Figure 4-36. Diameter (nm) measured with Zetasizer with the associated uncertainties for the gold nanoparticle covered with MUA and the synthesis AuNp covered with MUA/ChitosanK1 crosslinked with EDAC in different concentrations: 0.5, 0.1, 0.05, and 0.01 mg/mL

Zeta potential

Zeta potential was measured with Zetasizer instrument. In Figure 4-37, value obtained for the uncoated gold nanoparticles is represented in comparison with the zeta potential for the AuNP/chitosanK1 crosslinked with EDAC. This crosslinker was added in different concentrations to observe if this quantity is an affecting parameter regarding the stability of the solution.

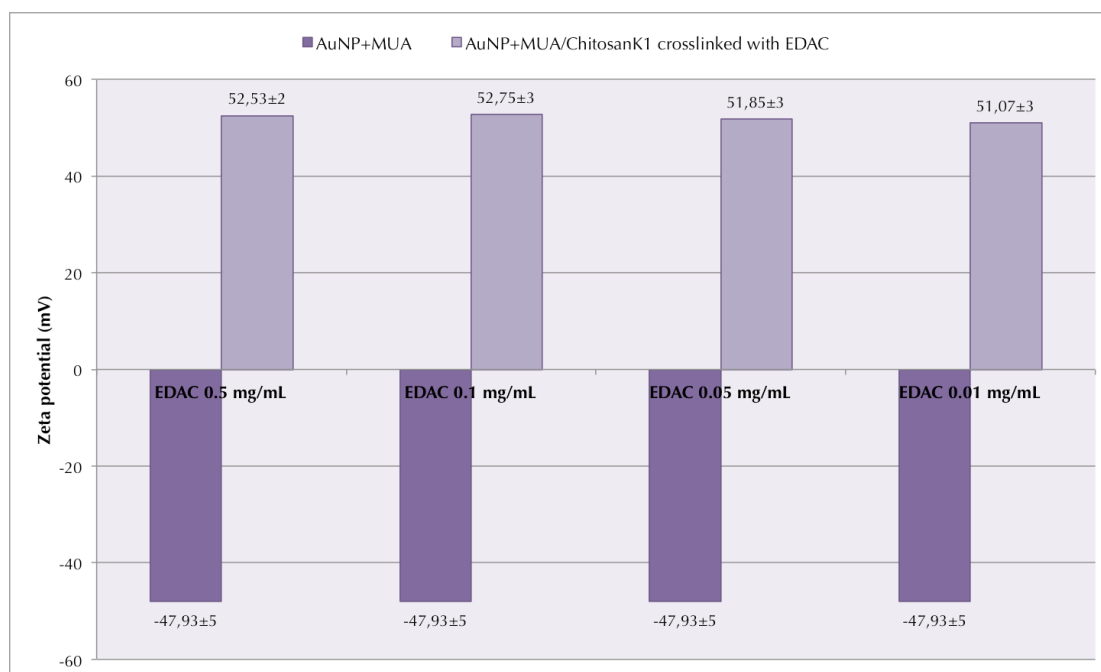


Figure 4-37. Comparison of zeta potential (mV) measured with Zetasizer with the associated uncertainties for AuNP covered with MUA and for the AuNP covered with MUA/ChitosanK1 crosslinked with EDAC in different concentrations; 0.5, 0.1, 0.05, and 0.01 mg/mL.

Results show a similar zeta potential value around 52 mV proving that solutions are stable and the chitosan was attached correctly to the gold nanoparticle. Conclusion extracted with this analysis is the lower EDAC concentration, the lower zeta potential and less stability. Nevertheless, the lower value is 51.07 ± 3 mV that is a quite good result regarding the stability of a solution.

UV-vis spectra

UV-vis spectrometry provided the information about absorbance necessary to calculate the concentration by means of Beer-Lambert's law (Table 4-22). Plasmon resonance peak (Figure 4-38) is located around 529 nm, sign that gold nanoparticles remain disaggregated in solution. According to the size, the higher are the gold nanoparticles, the higher is the peak wavelength of plasmon resonance. Apparently, these values follow this hypothesis because the peak of 526 nm pertains to the gold nanoparticles with the smallest diameter, 137 nm, but as mentioned above, the size average data cannot be totally considered.

Table 4-22. Data of absorbance obtained with UV-Vis spectrophotometer, calculations of concentration and plasmon resonance peak wavelength (nm).

EDAC (mg/mL)	Concentration (mM)	Peak value (nm)
0.5	$2.45 \cdot 10^{-7}$	529
0.1	$2.43 \cdot 10^{-7}$	526
0.05	$2.42 \cdot 10^{-7}$	529
0.01	$2.52 \cdot 10^{-7}$	529

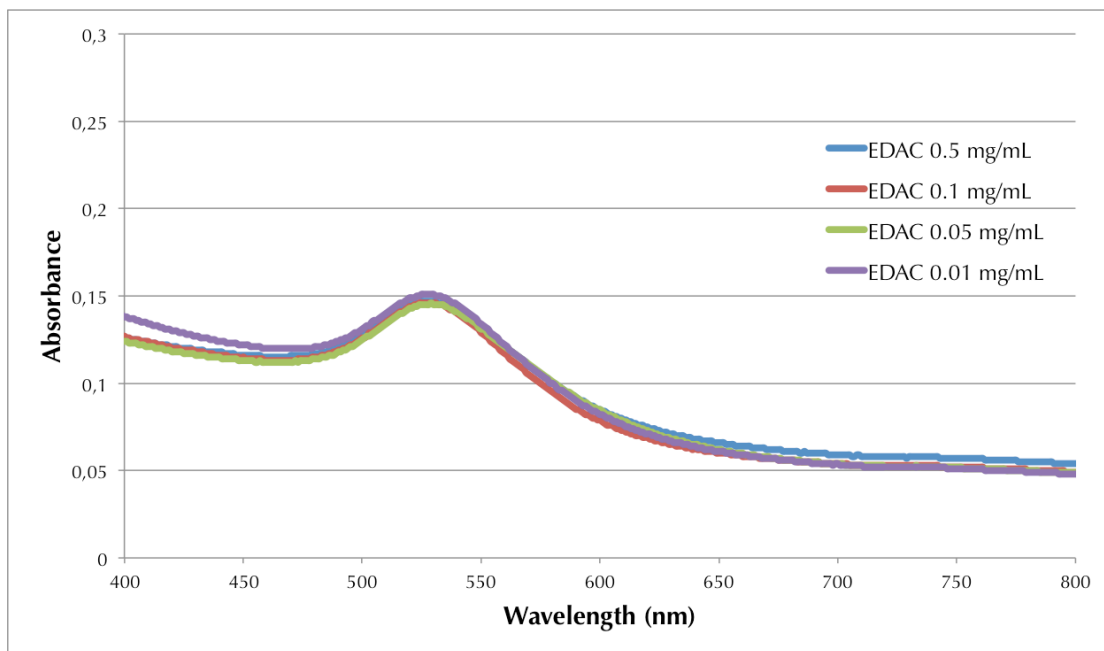


Figure 4-38. UV-vis spectra for AuNP/Chitosan nanoparticles prepared by crosslinking with EDAC in different concentrations: 0.5, 0.1, 0.05, and 0.01 mg/mL.

Chapter 5

Conclusion

The main aim considered for this work was the accomplishment of AuNP/Chitosan/siRNA nanoparticles and characterisation. The gold nanoparticles were successfully covered with the chitosan strongly and quickly, being the chitosan K1 and K2 selected as the best considering time to be adsorbed, mass attached to the gold surface, and stability. The next step to assembly the next layer of siRNA to the AuNP/chitosan nanoparticles was not achieved. This was predicted with QCM study and verified with the analysis of the attempt of synthesis AuNP/Chitosan/siRNA. The failure in the purpose was properly demonstrated.

According to the results obtained it was necessary to consider a solution for obtaining the vector desired. The next attempt was to synthesize AuNP/C₁₆TAB/siRNA nanoparticles. The C₁₆TAB binding of gold nanoparticles was fast accomplished but the next step of adsorbing siRNA resulted in a failed attempt. This was predicted and characterized with the same techniques than before.

Regarding the conclusions obtained in this point, the possibility of AuNP/Chitosan crosslinked with EDAC was tried. Gold nanoparticles covered with MUA had a good interaction with the chitosan considering the crosslinking with the EDAC but the nanoparticles resulted in a big size that in the AuNP/Chitosan produced in the first synthesis trial. For solve this, different concentrations of EDAC and sizes of gold nanoparticles were used to prove that the AuNP around 7 nm showed more aggregations that in the case of diameters of 50 nm, but the last were considered polydispersed. The effect of concentration using nanoparticles of 50 nm was difficult to evaluate because of the polydispersity obtained before but seems that is not a principal parameter affecting.

Chapter 6

Future work

Regarding the results obtained is a good option to consider the possibility of continuing with the researching of the AuNP/Chitosan/siRNA nanoparticles. Owing to the research for the thesis has to be carried out in a limited time, the experiments realized as a possible solution to the failure in the synthesis of AuNP/Chitosan/siRNA could not be finished. The last option of AuNP/Chitosan crosslinked with EDAC has to be investigated to try to adjust the correct gold nanoparticles, between 7-50 nm and analyse the size obtained in this case. At the same time it could be very interesting try to adjust the quantity of EDAC necessary to achieve monodisperse nanoparticles.

Once the chitosan is correctly attached and the size adjusted, different chitosan samples attachments would have to be tested to conclude if there are differences between chitosan samples. The interesting parameters would be, as in this research, how fast and how strong they cover the gold surface. It was proved the difficulty to reproduce the synthesis process in QCM; hence this simulation would have to be improved because of the importance for obtaining the behaviour of the process and the knowledge of the mass that can be adsorbed into the surface.

Finally, when all these parameters have been adjusted and proved as successfully the siRNA covering has to be carried out to check the accomplishment of the main objective. If this goal is achieved, the next step has to be considered; continue with the layer by layer assembly AuNP/Chitosan/siRNA/Chitosan to validate the opportunity to create a multilayer vector.

Chapter 7

References



- [1] A.G. Rad, H. Abbasi, and M.H. Afzali, "Gold Nanoparticles: Synthesising, Characterizing and Reviewing Novel Application in Recent Yeas," *Physics Procedia*, vol. 22, pp. 203-208, 2011.
- [2] S. Al-Qadi and C. Remuñán-López, "Nanopartículas metálicas: oro," Department of Pharmacy and Pharmaceutical Technology, Santiago de Compostela University, Monograph.
- [3] P. Guo et al., "Engineering RNA for Targeted siRNA Delivery and Medical Application," *Advanced Drug Delivery Reviews*, vol. 62, pp. 650-666, 2010.
- [4] T.M. Rana, "Illuminating the silence: understanding the structure and function of small RNAs," *Natural Reviews|Molecular Cell Biology*, vol. 8, pp. 24-36, 2007.
- [5] M. Sioud, Ed., *Ribosymes and siRNA protocols*, 2nd ed. USA: Humana Press.
- [6] S. Guo et al., "Enhanced Gene Delivery and siRNA Silencing by Gold Nanoparticles Coated with Charge-Reversal Polyelectrolyte," *ACS Nano*, vol. 4, pp. 5505-5511, 2010.
- [8] J.H., Saravanakumar, G., Kim, K., Kwon, I.C Park, "Targeted delivery of low molecular drugs using chitosan and its derivatives," *Advanced Drug Delivery Reviews*, vol. 62, pp. 28-41, 2010.
- [7] N.M., Mano, J.F. Alves, "Chitosan derivatives obtained by chemical modifications for biomedical and environmental applications," *International Journal of Biological Macromolecules*, vol. 43, pp. 401-414, 2008.
- [9] S. Eustis and M.A. El-Sayed, "Why gold nanoparticles are more precious than pretty gold: Noble metal surface plasmon resonance and its enhancement of the radiative and nonradiative properties of nanocrystals of different shapes," *Chemical Society Reviews*, vol. 35, pp. 209-217, 2006.
- [10] A. Elbakry et al., "Layer-by-Layer Assembled Gold Nanoparticles for siRNA Delivery," *Nano Letters*, vol. 9, pp. 2059-2064, 2009.
- [11] F. Caruso, Ed., *Colloids and Colloids Assemblies.*: WILEY-VCH.
- [12] J. Turkevich, G. Garton, and P.C. Stevenson, "The color of colloidal gold," *Journal of Colloid Science*, vol. 9, pp. 26-35, 1954.
- [13] F.J. García Vidal and Martín Moreno L., "Plasmones superficiales," *Investigación y ciencia*, pp. 66-76, October 2008.
- [14] E. Hutter and J.H Fendler, "Exploitation of Localized Surface Plasmon Resonance," *Advanced Materials*, vol. 19, pp. 1685-1706, 2004.
- [15] K.L. Kelly, E. Coronado, L.L. Zhao, and G.C. Schatz, "The Optical Properties of Metal Nanoparticles: The Influence of Size, Shape, and Dielectric Environment.," *Journal of Physical Chemistry*, vol. 107, pp. 668-677, 2003.
- [16] V. Amendola and M. Meneghetti, "Size Evaluation of Gold Nanoparticles by UV-vis Spectroscopy," *The Journal of Physical Chemistry*, vol. 113, pp. 4277-4285, 2009.
- [17] H Jans and Q. Huo, "Gold nanoparticle-enabled biological and chemical detection and analysis," *Chemical Society Review*, vol. 41, pp. 2849-2866, 2012.

- [18] Resham Bhattacharya and P. Mukherjee, "Biological properties of "naked" metal nanoparticles," *Advanced Drug Delivery Reviews*, vol. 60, pp. 1289-1306, 2008.
- [19] W.R. Glomm, "Functionalized Gold Nanoparticles for Applications in Bionanotechnology," *Journal of Dispersion Science and Technology*, vol. 26, pp. 389-414, 2005.
- [20] Malvern instruments. [Online]. HYPERLINK
"[http://www.malvern.com/malvern/kbase.nsf/allbyno/KB000734/\\$file/MRK654-01%20An%20Introduction%20to%20Zeta%20Potential%20v3.pdf](http://www.malvern.com/malvern/kbase.nsf/allbyno/KB000734/$file/MRK654-01%20An%20Introduction%20to%20Zeta%20Potential%20v3.pdf)"
[http://www.malvern.com/malvern/kbase.nsf/allbyno/KB000734/\\$file/MRK654-01%20An%20Introduction%20to%20Zeta%20Potential%20v3.pdf](http://www.malvern.com/malvern/kbase.nsf/allbyno/KB000734/$file/MRK654-01%20An%20Introduction%20to%20Zeta%20Potential%20v3.pdf)
- [21] Malvern Instruments. [Online]. HYPERLINK
"http://www.malvern.com/LabEng/industry/colloids/colloids_stability.htm"
http://www.malvern.com/LabEng/industry/colloids/colloids_stability.htm
- [22] Nanobiotechnology Center (NBTC). [Online]. HYPERLINK
"<http://www.nbtc.cornell.edu/facilities/downloads/Zetasizer%20chapter%2016.pdf>"
<http://www.nbtc.cornell.edu/facilities/downloads/Zetasizer%20chapter%2016.pdf>
- [23] G. Schmid, "Larger Clusters and Colloids. Metals in the Embryonic State," *Chemical Reviews*, vol. 92, pp. 1709-1727, 1992.
- [24] T.C. Prathna, L. Mathew, N. Chandrasekaran, A.M. Raichur, and A. Mukherjee, "Biomimetic Synthesis of Nanoparticles: Science, Technology & Applicability," *INTECH*.
- [25] V. Rotello, Ed., *Nanoparticles. Building Blocks for Nanotechnology*, 1st ed. New York: KluwerAcademic/Plenum Publishers, 2004.
- [26] Chemistry Department of National Taiwan University. National Taiwan University. [Online]. HYPERLINK
"http://www.ch.ntu.edu.tw/-genchem99/doc/T26_gold%20nanoparticle.pdf"
http://www.ch.ntu.edu.tw/-genchem99/doc/T26_gold%20nanoparticle.pdf
- [27] K.C. Grabar, R.G. Freeman, M.B. Hommer, and M.J. Natan, "Preparation and Characterization of Au Colloid Monolayers," *Analytical Chemistry*, vol. 67, pp. 735-743, 1995.
- [28] G. Frens, "Controlled Nucleation for the Regulation of the Particle Size in Monodisperse Gold Suspensions," *Nature Physical Science*, vol. 241, pp. 20-22, 1973.
- [29] M. Brust, M. Walker, D. Bethell, D.J. Schiffrin, and R. Whyman, "Synthesis of Thiol-derivatised Gold Nanoparticles in a Two-phase Liquid-Liquid System," *Journal of the Chemical Society, Chemical Communications*, vol. 7, pp. 801-802, 1994.
- [30] A. Balinski, "Improved synthesis of tetraethylene glycol-derived thiol for monolayer-protected gold nanoparticles," Department of Chemistry, Graduate School of Vanderbilt University, Nashville, Master Thesis 2010.
- [31] D. Andreescu, T.K. Sau, and D.V. Goia, "Stabilizer-free nanosized gold sols," *Journal of Colloidal and Interface Science*, vol. 298, pp. 742-751, 2006.
- [32] W. Shi, Y. Sahoo, and M.T. Swihart, "Gold nanoparticles surface terminated with bifunctional ligands," *Colloids and Surfaces*, vol. 246, pp. 109-113, 2004.
- [33] T. Laaksonen, P. Ahonen, C. Johans, and K.K. Prof, "Stability and Electrostatics of Mercatoundecanoid Acid-Copper Gold Nanoparticles with Varying Counterion Size," *Chemical Physics and Physical Chemistry*, vol. 7, pp. 2143-2149, 2006.
- [34] S.D. Perrault and W.C.W. Chan, "Synthesis and Surface Modification of Highly Monodispersed, Spherical Gold Nanoparticles of 50-200 nm," *Journal of American Chemical Society*, vol. 131, pp. 17042-17043, 2009.
- [35] J. Li et al., "Controllable Synthesis of Stable Urchin-like Gold Nanoparticles Using Hydroquinone to Tune the Reactivity of Gold Chloride," *The Journal of Physical Chemistry*, vol. 115, pp. 3630-3637, 2011.

- [36] COSMOS (California State Summer School for Mathematics and Science). COSMOS Cluster 2 Nanotechnology. [Online]. HYPERLINK
["http://.clustertwo.org/ShaoWei%20Chen%20lectures/Cluster%20%20lecture%202.pdf"](http://.clustertwo.org/ShaoWei%20Chen%20lectures/Cluster%20%20lecture%202.pdf)
<http://.clustertwo.org/ShaoWei%20Chen%20lectures/Cluster%20%20lecture%202.pdf>
- [37] R.A. Sperling, P. Rivera, F. Zhang, M. Zanella, and W.J. Parak, "Biological applications of gold nanoparticles," *Chemical Society Review*, vol. 37, pp. 1745-2140, 2008.
- [38] S. Rana, A. Bajaj, R. Mout, and V.M. Rotello, "Monolayer coated gold nanoparticles for delivery applications," *Advanced Drug Delivery Reviews*, vol. 64, pp. 200-216, 2012.
- [39] V.P. Torchilin, "Passive and Active Drug Targeting: Drug Delivery to Tumors as an Example," *Handbook of Experimental Pharmacology*, vol. 197, pp. 3-53, 2012.
- [40] D. Reischl and A. Zimmer, "Drug delivery of siRNA therapeutics: potentials and limits of nanosystems," *Nanomedicine: Nanotechnology, Biology, and Medicine*, vol. 5, pp. 8-20, 2009.
- [41] P.K. Jain, K.S. Lee, I. El-Sayed, and M.A. El-Sayed, "Calculated Absorption and Scattering properties of Gold Nanoparticles of Different Size, Shape, and Composition: Applications in Biological Imaging and Biomedicine.," *Journal of Physical Chemistry*, vol. 110, pp. 7238-7248, 2006.
- [42] D. Pissuwan, S.M. Valenzuela, and M.B Cortie, "Therapeutic possibilities of plasmonically heated gold nanoparticles," *TRENDS in Biotechnology*, vol. 24, pp. 62-67, 2006.
- [43] V.K., Inamdar, N.N. Mourya, "Chitosan-modifications and applications: Opportunities galore," *Reactive & Functional Polymers*, vol. 68, pp. 1013-1051, 2008.
- [44] V., Vilivalam, V.D. Dodane, "Pharmaceutical applications of chitosan," *Pharmaceutical Science & Technology*, vol. 1, pp. 246-253, 1998.
- [45] M. Rinaudo, "Chitin and chitosan: Properties and applications," *ScienceDirect*, vol. 31, pp. 603-632, 2006.
- [46] M., Chiellini, F., Ottenbrite, R.M., Chiellini, E. Dash, "Chitosan- A versatile semi-synthetic polymer in biomedical applications," *Progress in Polymer Science*, vol. 36, pp. 981-1014, 2011.
- [47] T.A., Sharma, C.P. Sonia, "Chitosan and Its Derivatives for Drug Delivery Perspective," *Advances in Polymer Science*, vol. 243, pp. 23-54, 2011.
- [48] M.N.V. Ravi Kumar, "A review of chitin and chitosan applications," *Reactive & Functional Polymers*, vol. 46, pp. 1-27, 2000.
- [49] R. Oliva Virgili and J.M. Vidal-Taboada, *Genoma Humano: nuevos avances en investigación, diagnóstico y tratamiento*. Barcelona: Publicacions i edicions de la Universitat de barcelona, 2006.
- [50] Alnylam Pharmaceuticlas. [Online]. HYPERLINK "http://www.alnylam.com/rnai_primer/rna-interference-pg3.htm" http://www.alnylam.com/rnai_primer/rna-interference-pg3.htm
- [51] I.P. Stoleran, Ed., *Encyclopedic of Psychopharmacology, Volume 2*. London: Springer.
- [52] Microbiologybytes. [Online]. HYPERLINK
["http://www.microbiologybytes.com/virology/3035Imunopath.html"](http://www.microbiologybytes.com/virology/3035Imunopath.html)
<http://www.microbiologybytes.com/virology/3035Imunopath.html>
- [53] S.H. Lee and P.J. Sinko, "siRNA- Getting the message out," *European Journal of Pharmaceutical Sciences*, vol. 27, pp. 401-410, 2006.
- [54] M.J.K. Thomas, *Ultraviolet and Visible Spectroscopy*, 2nd ed., D.J. Ando, Ed. Greenwich, UK: John Wiley & sons, 1996.
- [55] D.A., Holler, F.J., Nieman, T.A. Skoog, *Principles of Instrumental Analysis*, 5th ed., A.,

- Sherman, M., Bortel, J. Mc Donald, Ed.: Saunders Golden Sunbrust Series, 1997.
- [56] D. C. Harris, *Quantitative Chemical Analysis*, 8th ed., W. H. Freeman and company, Ed. New York.
- [57] qsense. [Online]. HYPERLINK "[http://www.q-sense.com/\\$2/qcm-d.swf](http://www.q-sense.com/$2/qcm-d.swf)" [http://www.q-sense.com/\\$2/qcm-d.swf](http://www.q-sense.com/$2/qcm-d.swf)
- [58] B.D. Vogt, E.K. Lin, W. Wu, and C.C. White, "Effect of Film Thickness on the Validity of the Sauerbrey Equation for Hydrated Polyelectrolyte filmF," *Journal of Physical Chemistry*, vol. 108, pp. 12685-12690, 2004.
- [59] S. Håkonsen, "Determination of solid particle by Malvern Nanosizer," Department of Chemical Engineering, NTNU, Trondheim, Procedure 2010.
- [60] D. Lee et al., "Thiolated Chitosan/DNA Nanocomplexes Exhibit Enhanced and Sustained Gene Delivery," *Pharmaceutical Research*, vol. 24, pp. 157-167, 2007.
- [61] A. Bernkop-Schnürch, M. Hornof, and T. Zoidl, "Thiolated polymers-thiomers: synthesis and in vitro evaluation of chitosan-2-iminothiolane conjugates," *International Journal of Pharmaceutics*, vol. 260, pp. 229-237, 2003.
- [62] F.M. Goycoolea et al. Effect of Molecular weight and degree of acetylation on the physicochemical characteristics of chitosan nanoparticles. [Online]. HYPERLINK "http://www.nanobiosaccharides.org/Documents/EUCHIS_paper_FM_Goycoolea_et_al.pdf" http://www.nanobiosaccharides.org/Documents/EUCHIS_paper_FM_Goycoolea_et_al.pdf
- [63] D.R. Askeland, P.P. Fulay, and W.J. Wright, *The science and engineering of materials*, 6th ed. USA: Global Engineering.
- [64] J. Kimling et al., "Turkevich Method for Gold Nanoparticles Synthesis Revisited," *Journal of Physical Chemistry*, vol. 110, pp. 15700-15707, 2006.
- [65] M.P. Pileni, "The role of soft colloidal templates in controlling the size and shape of inorganic nanocrystals.," *Nature materials*, vol. 2, pp. 145-150, 2003.
- [66] C.E. Kast, W. Frick, U. Losert, and A. Bernkop-Schnürch, "Chitosan-thioglycolic acid conjugate: a new scaffold material for tissue engineering," *International Journal of Pharmaceutics*, vol. 256, pp. 183-189, 2003.
- [67] H. Jung, M. Jang, and J. Nah, "Synthesis and Characterization of Thermosensitive Nanoparticles Based on PNIPAAm Core and Chitosan Shell Structure," *Macromolecular Research*, vol. 17, pp. 265-270, 2009.
- [68] S. Alamelu and R. Panduranga, "Liposomes sequestered in chitosan gel as a delivery device for dapson," *Carbohydrate Polymers*, vol. 24, pp. 215-221, 1994.
- [69] Interchim. [Online]. HYPERLINK "<http://www.interchim.fr/ft/5/52005D.pdf>" <http://www.interchim.fr/ft/5/52005D.pdf>
- [70] Sigma-Aldrich. [Online]. HYPERLINK "<http://www.sigmaaldrich.com/catalog/product/sial/e6383?lang=en®ion=NO>" <http://www.sigmaaldrich.com/catalog/product/sial/e6383?lang=en®ion=NO>
- [71] J. Handley, "Product review: Quartz Crystal Microbalances. Some new innovations alongside the standard, reliable workhorse," *Analytical chemistry*, vol. 73, pp. 225-229, 2001.
- [72] R. Van Duyne, "Biosensing with plasmonic nanosensors," *Nature*, vol. 7, pp. 442-453, 2008.
- [73] J.S. Lee et al., "Gold, Poly(B-amino ester) Nanoparticles for Small Interfering RNA Delivery," *Nano Letters*, vol. 9, pp. 2402-2406, 2009.

APPENDIX

NTNU	Risk assessment			Utarbeidet av	Nummer	Dato	
				HMS-avd.	HMSRV/2603	04/02/11	
HMS/KS	Godkjent av	Side	Erstatter				

Unit:

Kjemisk prosesseteknologi

Date:

20/09/11

Line manager:


Øyvind Gregersen

Participants in the identification process (including their function):

Wilhelm R. Glomm, supervisor

Signatures:

ID no.	Activity from the identification process form	Potential undesirable incident/strain	Likelihood:				Consequence:				Risk value	Comments/status Suggested measures
			Likelihood (1-5)	Human (A-E)	Environment (A-E)	Economy/ material (A-E)	Reputation (A-E)	Human				
1	Chemicals	Health hazard if spilled or consumed	1	B	B	B	A	A	1B	Follow HES guidelines		
2	UV-vis	Radiation risk, exposure to eyes	1	A	A	A	A	A	1A	See instrument folder		
3	Piranha solution (preparation, handling and disposal)	Accidental release. Corrosive, causes severe	1	B/C	A	B	B	B	1B	Follow HES guidelines		
4	Piranha solution (preparation, handling and disposal)	Potentially explosive in contact with organic	1	B/C	A	B	B	B	1B	Disposal in appropriate, clearly labeled waste		
5	Nanosizer	Short-circuiting instrument	1	A	A	B	A	A	1A	Avoid spillage		
6	Sodium borohydride (NaBH ₄)	Accidental release. Strong reducing agent,	1	B	A	A	A	A	1B	Allow solution to deactivate before		
7	BAM	Exposure to laser beam	1	B	A	A	A	A	1B	Wear laser goggles		

NTNU	Hazardous activity identification process			Risikovurdering	Nummer	Dato
 HMS				HMS-avd.	HMSRV2601	
		Godkjent av	Side	Erstatler		

Unit: Kjemisk prosesseteknologi Date: 20/09/11

Line manager: Øyvind Gregersen

Participants in the identification process (including their function): Wilhelm R. Glomm, supervisor

Short description of the main activity/main process:

ID no.	Activity/process	Responsible person	Laws, regulations etc.	Existing documentation	Existing safety measures	Comment
1	Syntheses of nanoparticles	Elena	General lab precautions	HES guidelines	HES guidelines	Appropriate use and disposal of chemicals
2	Characterization of nanoparticles	Elena	General and instrument-specific precautions	Instrument folder	Instrument folder	See instrument-specific comments
3	Modification of surfaces	Elena	General lab precautions	HES guidelines	HES guidelines	Appropriate use and disposal of chemicals
4	QCM	Sina/Elena		Instrument folder	Instrument folder	Caution if using Piranha solution
5	Nanosizer	Signe/Elena		Instrument folder	Instrument folder	Safe
6	Langmuir / BAM	Andreas/Elena		Instrument folder	Instrument folder	Use of laser
7	UV-vis	Sina/Elena				Safe